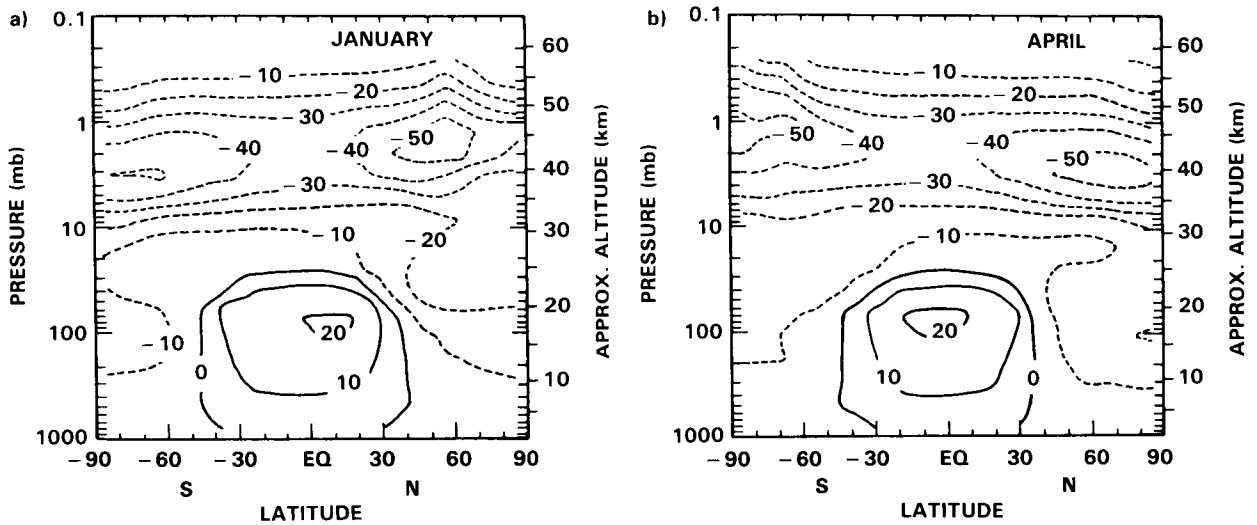


# MODEL PREDICTIONS OF OZONE CHANGES



## Panel Members

H.S. Johnston and F. Kaufman, Co-Chairmen

R.J. Cicerone  
 C.E. Kolb  
 M. Prather  
 U. Schmailzl

S. Solomon  
 N.D. Sze  
 D.J. Wuebbles

## CHAPTER 13

### MODEL PREDICTIONS OF OZONE CHANGES

#### TABLE OF CONTENTS

13.0 INTRODUCTION .....	721
13.1 RESULTS OF MODEL CALCULATIONS .....	722
13.1.1 Scenarios for a Perturbed Atmosphere .....	722
13.1.2 Assessment Calculations with 1-D Models .....	724
13.1.2.1 Steady-State Perturbations .....	725
13.1.2.2 Time-Dependent Perturbations .....	740
13.1.3 Assessment Calculations with 2-D Models .....	744
13.1.4 Comparison of 1-D and 2-D Results .....	762
13.2 DISCUSSION OF CURRENT MODEL PREDICTIONS AND ASSESSMENT OF RECOGNIZED UNCERTAINTIES .....	771
13.2.1 Uncertainties in Model Predictions .....	771
13.2.2 History of Model Predictions for Assumed Perturbations .....	772
13.2.3 Sensitivity to Chemistry and Photochemistry .....	772
13.2.3.1 Ensemble Sensitivity to Uncertainty in Rate Parameters .....	773
13.2.3.2 Sensitivity to Uncertainty in Individual Rate Parameters .....	776
13.2.3.3 Uncertainties Due to Chemistry Omitted From the Models .....	780
13.2.4 Uncertainty of Model Predictions to Choice of Boundary Conditions .....	782
13.2.5 Sensitivity to Trends of Trace Gas Species .....	783
13.2.6 Ozone Changes Calculated to Occur in the Troposphere .....	783
13.2.7 Some Dynamical Uncertainties in Assessment Calculations .....	784
13.2.8 A Recently Published Article .....	785
13.2.9 Discussion of Total Uncertainty .....	785
13.3 SUMMARY AND CONCLUSIONS .....	786
13.3.1 Future Research .....	788

**PRECEDING PAGE BLANK NOT FILMED**

### 13.0 INTRODUCTION

For more than a dozen years, the present and future stratosphere has been modeled in increasing detail in order to estimate the effects of human activity on the composition of the atmosphere and particularly of the ozone layer. In chronological order, potential perturbations have included stratospheric flight, that is, injection of nitrogen oxides (CIAP, 1974; NRC, 1975), chlorofluoromethane release (NRC, 1976), halocarbon release in general (NRC, 1979; NASA, 1979), and the increased use of fertilizers which may increase the release of nitrous oxide from the soil and thereby increase  $\text{NO}_x$  in the stratosphere. This report is regarded as the update of the WMO Report No. 11 (1981). Among the threats to stratospheric ozone, the halocarbons, particularly CFC-11 ( $\text{CFCl}_3$ ) and CFC-12 ( $\text{CF}_2\text{Cl}_2$ ), have remained the principal ones, both because of their inertness in the troposphere and lower stratosphere and their continued usage as shown by their measured build-up over the past 15 years. Their ultimate photolysis in the mid-to-upper stratosphere (Rowland and Molina, 1975), where their chlorine atoms are released and take part in the catalytic cycle  $\text{Cl} + \text{O}_3 = \text{ClO} + \text{O}_2$  and  $\text{ClO} + \text{O} = \text{Cl} + \text{O}_2$  that removes odd oxygen,  $\text{O} + \text{O}_3$ , has been established.

Considering this simple outline of the  $\text{Cl}_x$  problem, it is perhaps surprising that model predictions of ozone-column changes have varied so widely since 1974 (NRC, 1984, p. 101) from high values of 15% to 20% depletion to low values of 3% to 5%. These model calculations all used one-dimensional eddy-diffusion to represent transport. Their variations were largely due to chemical and photochemical rate parameters, both from improved laboratory measurements and from inclusion of reactions in the mechanism that had earlier been overlooked. One might reasonably hope that the uncertainty of laboratory measurements has been reduced and that omission of critical steps is now less likely. Section 13.1 discusses these questions.

Since the 1981 WMO report, increased emphasis has been given to two important ideas, which are points of focus in this chapter: (a) The one-dimensional model predictions of ozone-column changes as a result of CFC increases are strongly dependent on concurrent increases of other trace gases, methane, nitrous oxide, and carbon dioxide (Wuebbles *et al.*, 1983; Callis *et al.*, 1983a; Sze *et al.*, 1983; DeRudder and Brasseur, 1984; Owens *et al.*, 1985a,b). Methane and nitrous oxide interact chemically with various processes that affect ozone. Carbon dioxide and also the CFCs, nitrous oxide, and methane are active in the "greenhouse effect", which (in addition to increasing surface temperature) reduces stratospheric temperatures (Chapter 15), slowing down chemical reactions that destroy ozone, and thus increasing ozone. Some combinations of increasing trace gases (Chapter 3) along with continued use of CFCs lead to ozone-column increases, instead of decreases, in the one-dimensional models. (b) Some two-dimensional models predict strong latitude gradients for ozone-column reductions as a result of increasing CFCs (Pyle, 1980; Haigh and Pyle, 1982; Haigh, 1984; Ko *et al.*, 1985; Solomon *et al.*, 1985b), in the sense of larger ozone reductions in temperate and polar regions than the global average of the two-dimensional result or of the one-dimensional result. The formulation used for atmospheric dynamics (Chapter 12) affects the strength of this latitude gradient.

This chapter could have been written as a review of all articles published on this subject during the past four years, but a different approach was taken to avoid the wide variety of specific scenarios and input parameters used by the different authors. On the basis of model studies in the recent literature, a series of standard scenarios was set up for both one-dimensional and two-dimensional models. A group of modelers was invited to calculate ozone changes (and temperature changes in some cases) using these scenarios, using NASA 1985 recommendations for chemical and photochemical rate coefficients (Appendix 1) and solar spectral irradiances (Chapter 7) but otherwise using their own treatment of atmospheric motions, boundary values, and numerical methods. It is the purpose of this chapter: (a) to examine the predictions of several one-dimensional models for a number of prescribed scenarios (Section 13.1.1) in steady-state

## MODEL PREDICTIONS

or time-dependent approximations; (b) to examine a small number of two-dimensional steady-state calculations for a limited number of scenarios, to compare the results of the various two-dimensional models with one another, and to compare these results with those of one-dimensional models; and (c) to examine in various ways the sensitivity of the calculated predictions to the values of input parameters in order to assess recognized uncertainties in these predictions.

Most of the model calculations presented in this chapter are new and represent the generous input of modelers, listed below, both within and outside of the Chapter panel membership. We are most grateful for their help.

Panel members: R.J. Cicerone, H.S. Johnston (co-chair), F. Kaufman (co-chair), C.E. Kolb, M. Prather, U. Schmailzl, S. Solomon, N.D. Sze, D.J. Wuebbles.

Other contributors: G. Brasseur, C. Bruehl, P. Connell, P.J. Crutzen, A. Owens, R. Stolarski.

### 13.1 RESULTS OF MODEL CALCULATIONS

#### 13.1.1 Scenarios For a Perturbed Atmosphere

A set of scenarios for the future evolution of the atmosphere has been selected for the 1-D and 2-D model simulations of stratospheric ozone. They are restricted in number by necessity and have been chosen to represent typical, but not necessarily most likely, scenarios. For those gases with dominant industrial sources such as the halocarbons, a range in the growth of emissions is considered. For those species with natural or uncertain sources, there is the choice of assuming that concentrations remain fixed or of extrapolating the currently observed rates of increase into the next century. Both steady-state and time-dependent scenarios have been selected and are listed in Table 13-1.

The chlorofluorocarbons are the centerpiece of chemical modeling studies for the perturbed atmosphere because (1) increases in chlorine (from halocarbons) are expected to deplete stratospheric ozone, and (2) the CFC's are known industrial pollutants with the most rapidly increasing concentrations observed among atmospheric trace gases. Chapter 3 discusses the manufacture, use, and release of halocarbons to the atmosphere. Calculated increases in the atmospheric burden of CFC's during the next 80 years range over a factor of three, depending on estimates for growth in industrial production of these compounds. The scenarios selected have a 0%, 1.5%, and 3% annual compounded growth in emissions of CFC-11 and CFC-12 as reasonable cases. It is important to note that in the modeled atmosphere, CFC-11 and -12 act as surrogates for all chlorocarbon growth in the atmosphere; growth in other industrial sources of stratospheric chlorine—such as CFC-113, CFC-22,  $\text{CCl}_4$ , and  $\text{CH}_3\text{CCl}_3$ —has not been explicitly included. Estimates of long-term growth for CFC-11 and -12 rarely exceed 3%, but inclusion of the diversity of halocarbons might lead to "effective" rates greater than this (see Quinn *et al.*, 1985). For specific effects of related CFC's see Wuebbles (1983a). Some model calculations of ozone perturbations will be presented as a function of total chlorine content of the stratosphere; results are then relatively insensitive to the specific source of stratospheric chlorine.

Bromine is also recognized as a catalytic agent leading to depletion of stratospheric ozone (Wofsy *et al.*, 1975). The halons 1211 and 1301 are expected to lead to increases in stratospheric bromine (see Chapter 3). No time-dependent scenario specific to these bromocarbons has been considered here: only the steady-state impact of a general increase in stratospheric bromine is examined (Prather *et al.*, 1984).

Table 13-1. Scenarios

## STEADY-STATE SCENARIOS

\*S0: Definition of 1980 reference, ambient atmosphere:

CO <sub>2</sub>	= 340 ppmv,	N <sub>2</sub> O	= 300 ppbv,	CH <sub>4</sub>	= 1.6 ppmv,
CO	= 100 ppbv,	CH <sub>3</sub> Cl	= 0.7 ppbv,	CCl <sub>4</sub>	= 100 pptv,
CFC-11	= 170 pptv,	CFC-12	= 285 pptv,	CH <sub>3</sub> CCl <sub>3</sub>	= 100 pptv,
CH <sub>3</sub> Br	= 20 pptv (assumed only stratospheric source of bromine),				
CFC-11 flux	= 309 Gg/yr = 8.4E6 /cm <sup>2</sup> /sec,				
CFC-12 flux	= 433 Gg/yr = 1.34E7/cm <sup>2</sup> /sec.				

S0A: Definition of background chlorine, circa 1960 atmosphere:  
Same as above without CFC-11, CFC-12, CH<sub>3</sub>CCl<sub>3</sub>.

S1A: CFC-11 and -12 in steady state at 1980 fluxes.

\*S2A: Cl<sub>x</sub> = 8 ppbv (approx: from CFC-11 = 0.8 ppbv, CFC-12 = 2.2 ppbv).

\*S2B: Cl<sub>x</sub> = 8 ppbv plus 2 × CH<sub>4</sub> (concentration), 1.2 × N<sub>2</sub>O.

S2C: Cl<sub>x</sub> = 8 ppbv plus 2 × CH<sub>4</sub>, 1.2 N<sub>2</sub>O and 2 × CO<sub>2</sub>.

\*S3A: Cl<sub>x</sub> = 15 ppbv (approx: from CFC-11 = 1.6 ppbv, CFC-12 = 4.4 ppbv).

\*S3B: Cl<sub>x</sub> = 15 ppbv plus 2 × CH<sub>4</sub> (concentration), 1.2 × N<sub>2</sub>O.

S3C: Cl<sub>x</sub> = 15 ppbv plus 2 × CH<sub>4</sub>, 1.2 × N<sub>2</sub>O, and 2 × CO<sub>2</sub>.

S4: 1980 with 2 × CH<sub>4</sub> concentration.

S5: 1.2 × N<sub>2</sub>O.

S6: 2 × CO.

S7: 2 × CO<sub>2</sub>.

S8: NO<sub>x</sub> injection from stratospheric aircraft 1000 molec cm<sup>-3</sup>s<sup>-1</sup> or 2000 molec cm<sup>-3</sup>s<sup>-1</sup> at 17 km and 20 km.

S9: Bromine increase from 20 pptv to 100 pptv.

## TIME-DEPENDENT SCENARIOS (Based on 1980 Start-up Atmosphere Above)

T1A: CFC emissions at 1980 production rates, others (N<sub>2</sub>O, CH<sub>4</sub>, CO, CO<sub>2</sub>) at fixed concentrations.

T1B: Time-dependent CFC's (fixed flux) plus increasing concentrations of CH<sub>4</sub> (1% per yr), N<sub>2</sub>O, (0.25% per yr), and CO<sub>2</sub> (DOE scenario).

T1C: Same as T1B, but without increase in CH<sub>4</sub> and N<sub>2</sub>O.

T2A: CFC emissions begin at 1980 rates and grow 1.5% per yr. (compounded), others fixed.

T2B: Same as T2A but with increasing CH<sub>4</sub> (1% per yr), N<sub>2</sub>O (0.25% per yr), and CO<sub>2</sub> (DOE scenario).

T3A: CFC emissions grow at 3% per yr (compounded), others fixed.

T3B: Time-dependent CFC's (3% per yr) plus increasing concentrations of CH<sub>4</sub> (1% per yr), N<sub>2</sub>O (0.25% per yr), and CO<sub>2</sub> (DOE scenario).

\*Also used as 2-D model scenario

## MODEL PREDICTIONS

Other trace gases are strongly coupled with stratospheric photochemistry involving ozone. A prerequisite to predicting ozone in the future is an understanding of how the concentrations of stratospheric  $\text{H}_2\text{O}$ ,  $\text{CH}_4$ ,  $\text{N}_2\text{O}$ , and  $\text{NO}_x$  will evolve. Radiatively active trace gases, dominated by  $\text{CO}_2$ , further impact ozone directly by reducing stratospheric temperatures and indirectly through changes in global climate (see Chapter 15). There is insufficient information on stratospheric water vapor to characterize trends on a global basis (Mastenbrook and Oltmans, 1983). Possibly, water vapor may be altered with changing climate as  $\text{CO}_2$  increases, but no global models are currently able to predict the distribution and physical processes controlling water vapor in today's stratosphere (see Chapter 5). The concentrations of methane and nitrous oxide are currently observed to be increasing at annual rates of approximately 1% and 0.25%, respectively. Sources of these gases and the cause of their increases are not well defined. Theories differ as to the causes of the current change (see Chapter 3). Without a model of the evolution of the fluxes of these gases, the scenarios here consider the two possibilities of continued growth at these rates or of constant abundance. Two anthropogenic sources of odd-nitrogen that may lead to ozone perturbations are considered: (1) fleet of stratospheric aircraft that is mainly of interest for historical comparison with previous calculations; (2) the  $\text{NO}_x$  emitted in the upper troposphere by commercial aviation in the 1990's that may lead to significant increase in tropospheric ozone (Wuebbles *et al.*, 1983).

The scenarios for time-dependent change in atmospheric composition are summarized in Table 13-1 and focus on those gases which directly affect the stratosphere: CFC's,  $\text{N}_2\text{O}$ ,  $\text{CH}_4$ , and  $\text{CO}_2$ . For CFC's, growth is in terms of emissions; these gases do not approach steady-state in the next 100 years. For the others, concentrations are specified as discussed above. Increases in  $\text{CO}_2$  (DOE scenario, Wuebbles *et al.*, 1984) are assumed to affect only stratospheric temperatures.

The use of steady-state scenarios allows for a simple examination of the effects of a perturbing influence on the atmosphere. In this case, only the initial and final states need be specified, not the complete history of the system. A steady-state scenario can therefore never refer to a specific time in the future, but it may be chosen to have conditions typical of a future time. The baseline case (0) for the steady-state scenarios listed in Table 13-1 is selected from observed atmospheric concentrations circa 1980, and a background chlorine atmosphere is defined simply as the 1980 atmosphere without CFC's and  $\text{CH}_3\text{CCl}_3$ . Three types of chlorine perturbations are considered for the steady-state scenarios: (1) CFC-11 and -12 emissions at 1980 (estimated) rates; (2) CFC-11 and -12 concentrations fixed at levels resulting in approximately 8 ppbv total chlorine ( $\text{Cl}_x$ ); and (3) CFC-11 and -12 concentrations fixed to yield 15 ppbv of  $\text{Cl}_x$ . Other scenarios examine the specific effects of increased levels of  $\text{CH}_4(\times 2)$ ,  $\text{N}_2\text{O}(\times 1.2)$ , and  $\text{CO}_2(\times 2)$  which might be expected if current growth were extrapolated approximately 75 years. These increased concentrations are also coupled with the chlorine perturbations (2) and (3) above, in an attempt to consider a likely condition for the atmosphere in the middle of the next century. As such, these coupled, steady-state scenarios are the focus of the 2-D model calculations. Steady-state scenarios include additional perturbations due to CO, tropospheric  $\text{NO}_x$ ,  $\text{NO}_x$  from stratospheric aircraft, and bromine which are analyzed by 1-D models. These cases are regarded as sensitivity studies for hypothetically isolated parameters, even though interactions in the real atmosphere make it impossible to change these quantities one at a time.

### 13.1.2 Assessment Calculations with 1-D Models

For the scenarios given in Table 13-1, the calculated ozone changes according to one-dimensional models are given in Tables 13-2, 3, and 4. Steady-state calculations for hypothetical single species scenarios are discussed first. There is a long record of diagnostic calculations for such scenarios with which to compare model results. In addition to historical purposes, steady-state analyses of individual perturbations are useful for interpreting the mechanisms that influence a given species effects on atmospheric ozone. For analysis

of their nonlinear interactions and for comparison with 2-D model results, steady-state calculations with coupling of several assumed species perturbations are discussed. Steady-state multiple species perturbations provide a means for interpreting the effects on ozone from complex time-dependent scenarios to be discussed later.

**13.1.2.1 Steady-State Perturbations**

For the purpose of this report, six groups using one-dimensional models of the troposphere and stratosphere calculated the steady-state perturbations to be discussed here. Included are results from models

**Table 13-2.** Change in Total Ozone from Representative One-Dimensional Models for Steady State Scenarios Containing Cl<sub>x</sub> Perturbations. Numbers in Parentheses Refer to Calculated Changes when Including Temperature Feedback.

Scenario	Change in Total Ozone (%)					
	LLNL (Wuebbles)	Harvard (Prather)	AER (Sze)	DuPont (Owens)	IAS (Brasseur)	MPIC (Bruehl)
S1A CFC 1980 Flux only	-7.0 (-7.2)	-5.3	-5.3	-4.9 (-6.1)	(-7.9)	(-9.4)
S2A 8 ppbv Cl <sub>x</sub> only	-5.1 (-5.7)	-2.9	-4.6		(-4.1)	(-9.1)
S2B 8 ppbv Cl <sub>x</sub> + 2 × CH <sub>4</sub> + 1.2 × N <sub>2</sub> O	-3.4 (-2.8)	-3.0	-3.3	-3.1	(-2.3)	(-6.0)
S2C 8 ppbv Cl <sub>x</sub> + 2 × CH <sub>4</sub> + 1.2 × N <sub>2</sub> O + 2 × CO <sub>2</sub>	(+0.2)			(-1.4)	(0.0)	(-5.2)
S3A 15 ppbv Cl <sub>x</sub> only	-12.2 (-12.4)	-17.8	-15.		(-8.8)	(-22.0)
S3B 15 ppbv Cl <sub>x</sub> + 2 × CH <sub>4</sub> + 1.2 × N <sub>2</sub> O	-7.8 (-7.2)	-8.2	-8.8	-7.2	(-5.6)	(-13.7)
S3C 15 ppbv Cl <sub>x</sub> + 2 × CH <sub>4</sub> + 1.2 × N <sub>2</sub> O + 2 × CO <sub>2</sub>	(-4.6)				(-3.5)	(-13.6)

Relative to atmosphere with about 1.3 ppbv background Cl<sub>x</sub> and with no CFC (S0A).

## MODEL PREDICTIONS

**Table 13-3.** Change in Ozone at 40 km for Steady State Scenarios Containing  $Cl_x$  Perturbations. Numbers in Parentheses Refer to Calculated Changes Including Temperature Feedback.

Scenario	Change in 40 km Ozone (%)					
	LLNL (Wuebbles)	Harvard (Prather)	AER (Sze)	DuPont (Owens)	IAS (Brasseur)	MPIC (Bruehl)
S1A CFC 1980 Flux only	-63 (-56)	-64	-62	-62 (-57)	(-81)	(-59)
S2A 8 ppbv $Cl_x$ only	-55 (-50)	-57	-56		(-67)	(-57)
S2B 8 ppbv $Cl_x$ + 2 × $CH_4$ + 1.2 × $N_2O$	-50 (-45)	-50	-49	-58	(-62)	(-50)
S2C 8 ppbv $Cl_x$ + 2 × $CH_4$ + 1.2 × $N_2O$ + 2 × $CO_2$	(-35)			(-49)	(-55)	(-45)
S3A 15 ppbv $Cl_x$ only	-74 (-68)	-78	-77		(-83)	(-76)
S3B 15 ppbv $Cl_x$ + 2 × $CH_4$ + 1.2 × $N_2O$	-69 (-64)	-73	-64	-74	(-81)	(-71)
S3C 15 ppbv $Cl_x$ + 2 × $CH_4$ + 1.2 × $N_2O$ + 2 × $CO_2$	(-58)				(-78)	(-67)

Relative to atmosphere with about 1.3 ppbv background  $Cl_x$  and with no CFC (S0A).

at Lawrence Livermore National Laboratory (D. Wuebbles), Harvard University (M. Prather), Atmospheric and Environmental Research, Inc. (D. Sze), E.I. DuPont de Nemours & Company (A. Owens), the Belgium Institute for Aeronomy (G. Brasseur), and the Max Planck Institute (MPIC) in Mainz, West Germany (Bruehl and Crutzen). Each of these models has updated model chemistry to correspond to the rates prescribed in this report (Appendix A). However, treatments of other physical and chemical processes are done differently in each of these models. In particular, as discussed in Chapter 12 many of the models make different assumptions about transport parameters, diurnal averaging procedures, and photodissociation cross sections.

MODEL PREDICTIONS

**Table 13-4.** Changes in Ozone for Steady State Scenarios. Results Are Relative to Present Atmosphere (SO), Except for AER and DuPont Calculations, Which Are Relative to Background Atmosphere Without CFCs (SOA). Numbers in Parentheses Refer to Calculated Changes When Including Temperature Feedback.

Scenario	Change in Total Ozone (%)					
	LLNL (Wuebbles)	Harvard (Prather)	AER (Sze)	DuPont (Owens)	IAS (Brasseur)	MPIC (Bruehl)
S4 2 × CH <sub>4</sub>	+2.0 (+2.9)	+0.3	+0.9	+1.7	(+1.6)	(+1.4)
S5 1.2 × N <sub>2</sub> O	-2.1 (-1.7)	-2.6	-1.8	-2.3	(-1.1)	(-1.2)
S6 2 × CO	+1.1 (+1.1)	+0.3	+0.6	+0.8		(+0.8)
S7 2 × CO <sub>2</sub>	(+3.5)		(+2.6)	(+2.8)	(+3.1)	(+1.2)
S8a NO <sub>x</sub> , injection 17 km, 1000 molec. cm <sup>-3</sup> s <sup>-1</sup>	-1.8 (-1.3)				(-1.4)	
S8b NO <sub>x</sub> , 17 km, 2000 molec. cm <sup>-3</sup> s <sup>-1</sup>	-5.7				(-3.4)	
S8c NO <sub>x</sub> 20 km, 1000 molec. cm <sup>-3</sup> s <sup>-1</sup>	-5.7 (-4.6)				(-3.9)	
S8d NO <sub>x</sub> , 20 km, 2000 molec. cm <sup>-3</sup> s <sup>-1</sup>	-12.2				(-8.8)	
S9 Br <sub>x</sub> 20 to 100 pptv	-3.0					

Tables 13-2 and 13-4 give the calculated changes in total ozone from each of the 1-D models relative to a calculated reference atmosphere (scenarios SO or SOA in Table 13-1) for the steady-state scenarios. Table 13-3 gives the change in ozone at 40 km from each model for those scenarios involving chlorine (Cl<sub>x</sub>) perturbations. In contrast to prior reports, most of the models now include radiative submodels that calculate atmospheric temperatures, and thereby include temperature feedback effects on atmospheric

## MODEL PREDICTIONS

chemistry and photochemistry. Results in Tables 13-2 through 13-4 including temperature feedback are represented in parentheses. Since the primary purpose of this section is to describe the mechanisms important to ozone change from the steady-state perturbations, and because of the complexity of discussing in depth the results from many different models, many of the figures in this section will be based on the results of a single model, primarily that at LLNL. Relevant differences in calculated results between models will be described in the text.

### Chlorocarbons only

A standard scenario for comparing model results for chlorine perturbations has historically been the calculation of CFC-11 and CFC-12 constant emissions to steady state. Results in Table 13-2 indicate a range in model-calculated change in total ozone of  $-5$  to  $-7\%$  for models without temperature feedback and  $-6$  to  $-9\%$  with temperature feedback; these results are for scenario S1A, which assumes a constant flux of CFC-11 and CFC-12 at 1980 levels to steady state. These values may be compared to the  $-5$  to  $-9\%$  ozone change in WMO (1981), and  $-2$  to  $-4\%$  determined in NRC (1984). Small changes in a number of chemical rate constants in the latest evaluation (see Appendix A) have tended to increase the calculated impact on ozone for this scenario since the 1984 NRC assessment. With and without temperature feedback, the calculated changes in total ozone range from  $-3$  to  $-9\%$  for 8 ppbv  $\text{Cl}_x$  (S2A relative to atmosphere without CFC's), and from  $-9$  to  $-22\%$  for 15 ppbv  $\text{Cl}_x$  (S3A). As will be discussed later, some of the differences between models, particularly for large  $\text{Cl}_x$  perturbations, is related to the ambient amounts of total odd-nitrogen calculated.

Percentage changes in ozone as a function of altitude for three scenarios are shown in Figures 13-1, 13-2 and 13-3 for the LLNL model. All of the models produce large percentage decreases in ozone in the upper stratosphere, near 40 km. As seen in Table 13-3, most models calculate similar ozone changes in this region. Figure 13-4 gives the change in calculated (AER) ozone concentration as a function of altitude for the same cases as Figures 13-2 and 13-3; the small percentage changes around 25 kilometers represent large changes in ozone concentration. Figure 13-5 shows the vertical distributions in the rates of reaction for the primary odd-oxygen loss mechanisms as calculated for the current atmosphere by LLNL. As indicated in this figure, the chlorine catalytic cycle peaks in the region near 40 km, where a large percentage decrease in ozone is calculated. Small increases in ozone are calculated for ozone in the lower stratosphere, primarily due to the ozone recovery mechanism (increased  $\text{O}_2$  photolysis and resultant ozone production at lower altitudes as ozone is destroyed above) and due to  $\text{Cl}_x$  interference with the dominating  $\text{NO}_x$  catalytic cycle (see Figure 13-5) from  $\text{ClONO}_2$  production.

Table 13-5 shows model calculated atmospheric lifetimes for CFC-11, CFC-12, and  $\text{N}_2\text{O}$ . Differences for the calculated lifetimes occur between models due to several factors: (1) use of different transport parameterizations, and (2) use of different assumptions for photolysis calculations.

Until recently, it was generally thought that the change in total ozone calculated in 1-D stratospheric models for chlorocarbon perturbations was approximately linear, that is, the percentage change in total ozone relative to the amount of stratospheric chlorine ( $\text{Cl}_x$ ) was nearly constant. In contrast to previous model results in WMO (1981), a study by Cicerone *et al.* (1983a) indicated that for small  $\text{Cl}$  perturbations ( $< 4$  ppbv), the response of total ozone in their updated model is highly nonlinear. They reported very little calculated change in total ozone for these amounts of  $\text{Cl}_x$  and found the extent of the nonlinearity to be sensitive to the detailed treatment of physical and chemical processes in the model. Herman and McQuillan (1985) did not find this nonlinear relation and suggest that the presence of a nonlinear response

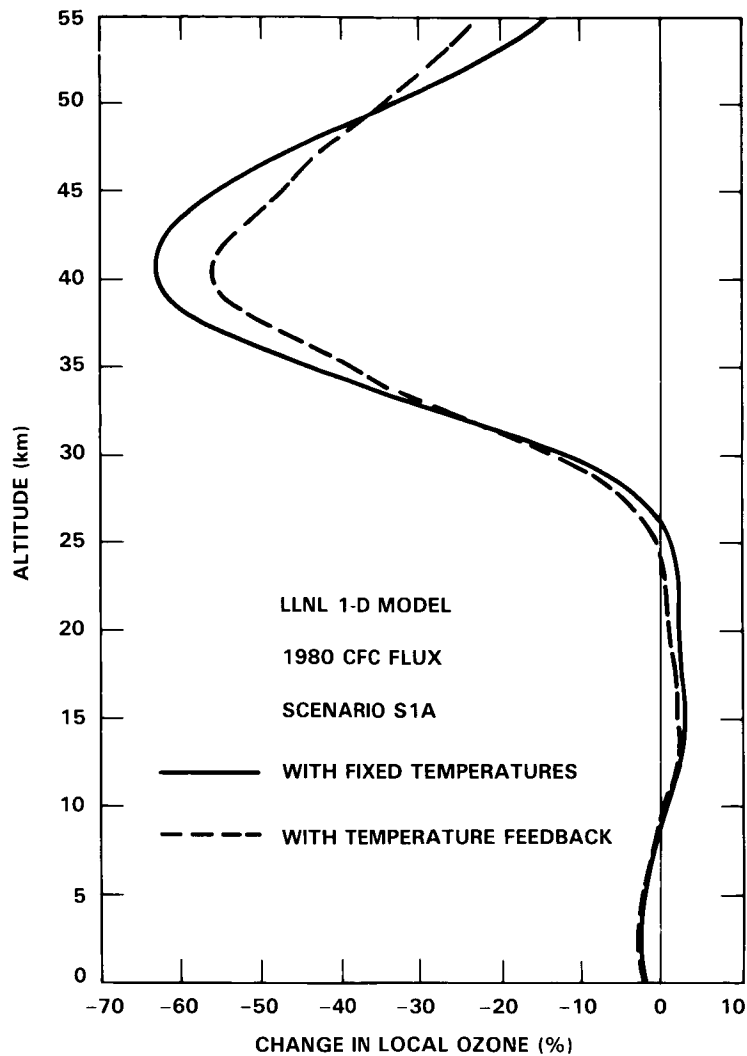


**Figure 13-1.** Calculated percentage change in local ozone at steady state for constant CFC-11 and CFC-12 fluxes at 1980 rates relative to the atmosphere with no CFC.

is dependent on model assumptions about diurnal averaging. All models used in this study appear to have an approximately linear response in total ozone response to small  $\text{Cl}_x$  changes.

For large  $\text{Cl}_x$  perturbations ( $> 12$  ppbv), Prather et al. (1984) found a significant nonlinearity in the ozone- $\text{Cl}_x$  relationship, with a rapid decrease in the total ozone column occurring for incremental additional  $\text{Cl}_x$  when the  $\text{Cl}_x$  level approximately exceeds that of stratospheric odd-nitrogen. The nonlinearity for large  $\text{Cl}_x$  perturbations may have significant implications for the interpretation of effects if chlorocarbon emissions increase substantially. Other models (e.g. Wuebbles and Connell, 1984; Stolarski, 1984) have found a similar behavior.

Figure 13-6 shows recent model results from Owens and Fisher of DuPont, which illustrates a number of interesting points. The independent variable is total  $\text{Cl}_x$  in the upper stratosphere, regardless of the scenario by which it was achieved. The calculated ozone change is presented as a function of stratospheric

## MODEL PREDICTIONS

Table 13-5. Calculated Lifetimes of CFC-11, CFC-12, and N<sub>2</sub>O in Representative 1-D Models.

	t (years)		N <sub>2</sub> O
	CFC-11	CFC-12	
LLNL	75	137	118
Harvard (Prather)	84	144	166
AER (Sze)	64	126	152
DuPont (Owens)	68	140	165
IAS (Brasseur)	87	154	166

Cl<sub>x</sub> for several different values of stratospheric NO<sub>y</sub>. For large NO<sub>y</sub> (about 30 ppbv) the decrease of ozone is small and very nearly linear with increasing Cl<sub>x</sub>, but for small background NO<sub>y</sub> (13 ppbv) ozone is strongly and nonlinearly reduced by Cl<sub>x</sub>. This effect of NO<sub>y</sub> is large: with 31 ppbv NO<sub>y</sub>, 18 ppbv Cl<sub>x</sub> is calculated to reduce ozone by 4.5%; but with 13 ppbv NO<sub>y</sub>, 18 ppbv Cl<sub>x</sub> is calculated to reduce the ozone column by 45%. There are several interactions between the NO<sub>x</sub> and Cl<sub>x</sub> systems, and a major one is indicated by Figure 13-5. In the 20 to 40 km range of the "1985" stratosphere, the NO<sub>x</sub> catalytic cycle is the most important mechanism of ozone destruction. An increase in Cl<sub>x</sub> causes an ozone reduction by way of the Cl<sub>x</sub> catalytic cycle, but ClO binds catalytically active NO<sub>2</sub> into the inactive form of chlorine nitrate, which reduces the dominant mid-stratospheric ozone-reducer (NO<sub>x</sub>) to give an ozone increase by virtue of a double negative. When Cl<sub>x</sub> approximately exceeds NO<sub>y</sub>, then chlorine becomes the dominant source of ozone reduction in the middle stratosphere, and further increases of Cl<sub>x</sub> have their full effect on ozone with relatively minor counter effect from reducing the NO<sub>x</sub> ozone-reducer.

### Methane

Model results for a doubling of methane, from approximately 1.6 to 3.2 ppmv, give an increase of ozone ranging from 0.3% to 2.9%, as shown in Table 13-4. Results from most of the models are relative to the 1980 reference atmosphere (SO, 2.5 ppbv Cl<sub>x</sub>) but results from AER and DuPont are relative to non-CFC reference case (SOA, 1.3 ppbv Cl<sub>x</sub>). Each of the models gives similar qualitative changes in ozone with altitude to that in the LLNL model, shown in Figure 13-7. Absolute differences between models appear to be explainable in terms of the sensitivity of changes in ozone from CH<sub>4</sub> increase due to differences in local amounts of Cl<sub>x</sub>, NO<sub>x</sub>, and HO<sub>x</sub> as a function of altitude. This sensitivity will be discussed in the following paragraphs.

In the LLNL model, a doubling of methane increases ozone from the surface to 45 km. In terms of total ozone change, the largest absolute increases in ozone occur around 15 km and around 35 km. In the troposphere and lower stratosphere methane oxidation produces ozone through the CH<sub>4</sub>-NO<sub>x</sub>-smog-reactions (Crutzen, 1973a; Johnston, 1984; Chapter 4). A doubling of surface CH<sub>4</sub> concentrations increases net photochemical production of ozone between the surface and 18 km by about 50%. This result will depend critically on the tropospheric and lower stratospheric abundance of NO. If NO concentrations are

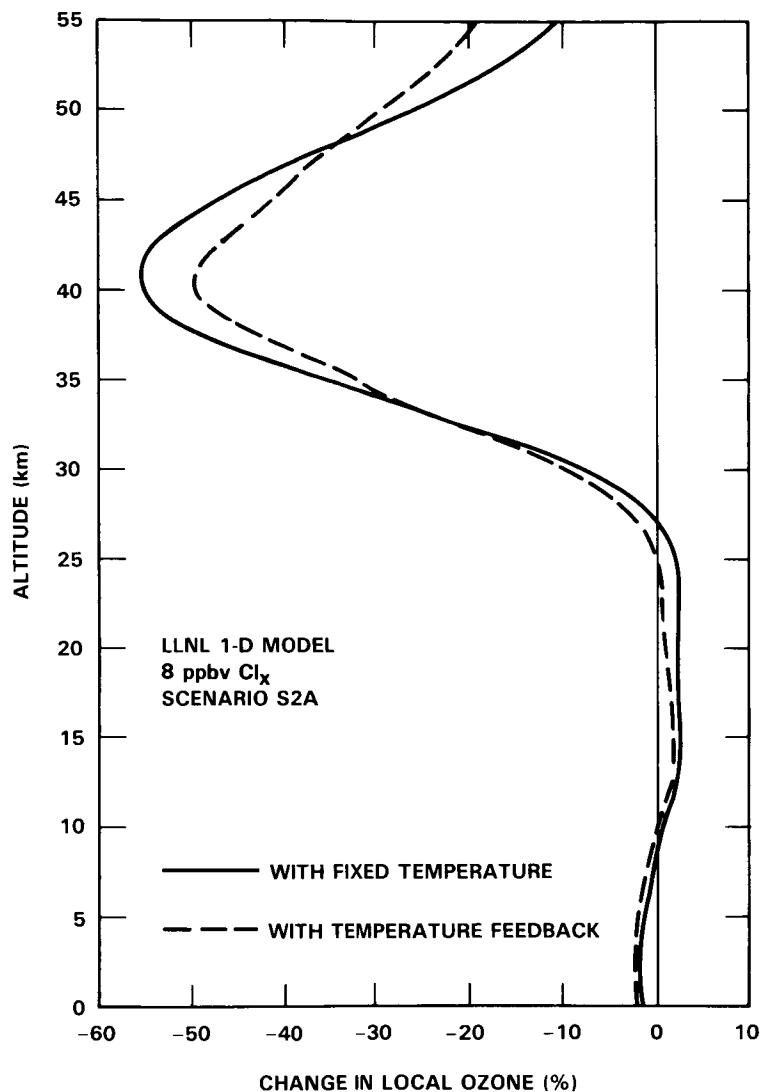


**Figure 13-2.** Calculated percentage change in local ozone at steady state for 8 ppbv stratospheric Cl<sub>x</sub> relative to background with 1.3 ppbv Cl<sub>x</sub>.

small enough, the added HO<sub>x</sub> from methane oxidation would decrease ozone. For the present simulation, the CO surface mole fraction was held fixed. Since CH<sub>4</sub> is a source of CO in the atmosphere, the impacts on tropospheric OH and O<sub>3</sub> would be somewhat larger if a constant surface flux boundary condition were assumed for CO.

The changes in ozone above the tropopause result from direct effects of the increased CH<sub>4</sub> and indirect effects due to the HO<sub>x</sub> produced by methane oxidation. For a doubling of methane, stratospheric OH concentrations are increased between 20 and 50% and stratospheric HO<sub>2</sub> is increased up to 100% in the LLNL model. The resulting increase in HNO<sub>3</sub> and HNO<sub>4</sub> production reduces NO<sub>2</sub> concentrations. There is a subsequent reduction of 5 to 15% in the NO<sub>x</sub> catalytic loss rate from NO<sub>2</sub> + O and an increase in O<sub>3</sub> due to this mechanism throughout much of the stratosphere.

## MODEL PREDICTIONS

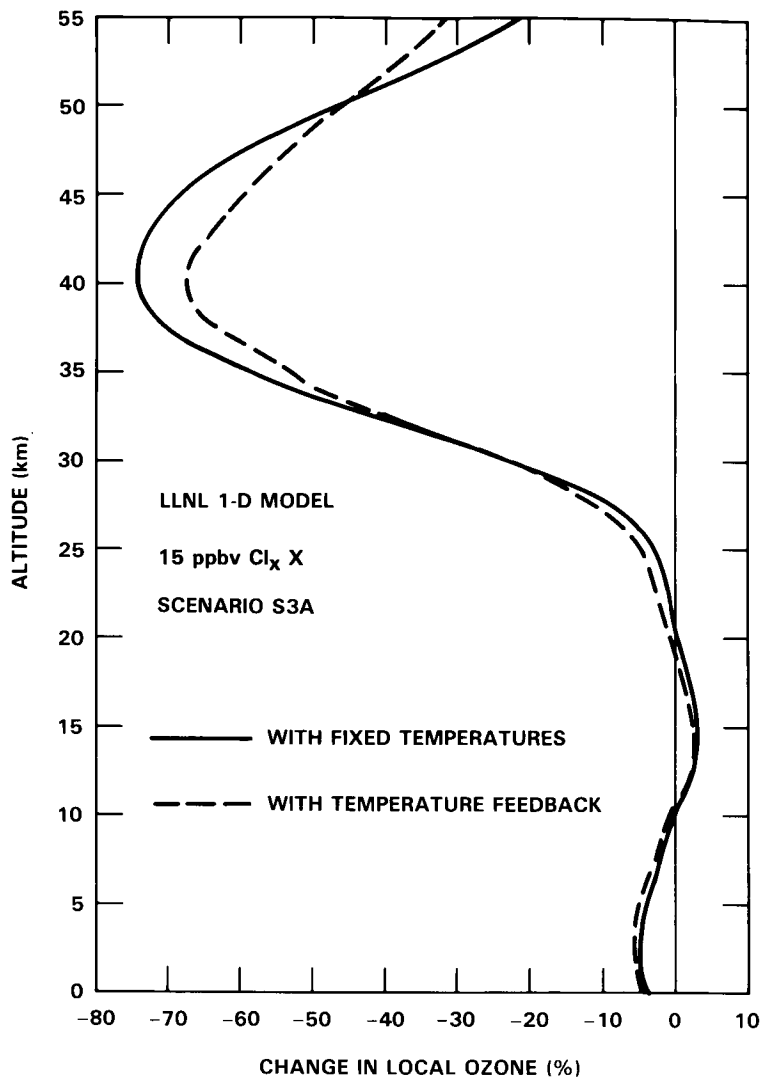


**Figure 13-3.** Calculated percentage change in local ozone at steady state for 15 ppbv stratospheric Cl<sub>x</sub> relative to background with 1.3 ppbv Cl<sub>x</sub>.

Methane is both a source and sink for Cl<sub>x</sub> in the stratosphere [ $\text{CH}_4 + \text{Cl} = \text{HCl} + \text{CH}_3$ ,  $\text{OH}$  (from methane) +  $\text{HCl} = \text{Cl} + \text{H}_2\text{O}$ ]. The pronounced ozone increase near 35-40 km in the LLNL model primarily results from an approximately 25% decrease in ClO, where the Cl<sub>x</sub> loss to methane exceeds the Cl<sub>x</sub> recovery from the methane produced OH. Production of HCl by the reaction of Cl with CH<sub>4</sub> is the primary loss process for active chlorine radicals, and this loss of Cl<sub>x</sub> is greater than the increase of Cl<sub>x</sub> from the methane-produced hydroxyl radicals. Above 45 km, the increased HO<sub>x</sub> from methane oxidation leads to direct ozone catalytic destruction and a resultant net decrease in ozone at these altitudes (compare Owens *et al.*, 1982a).

### Nitrous Oxide

The reaction  $\text{O}(1\text{D}) + \text{N}_2\text{O} = 2 \text{NO}$  provides the major source of odd nitrogen (NO<sub>x</sub>) in the stratosphere. Stratospheric formation of NO<sub>x</sub> from N<sub>2</sub>O occurs primarily in the middle stratosphere, from

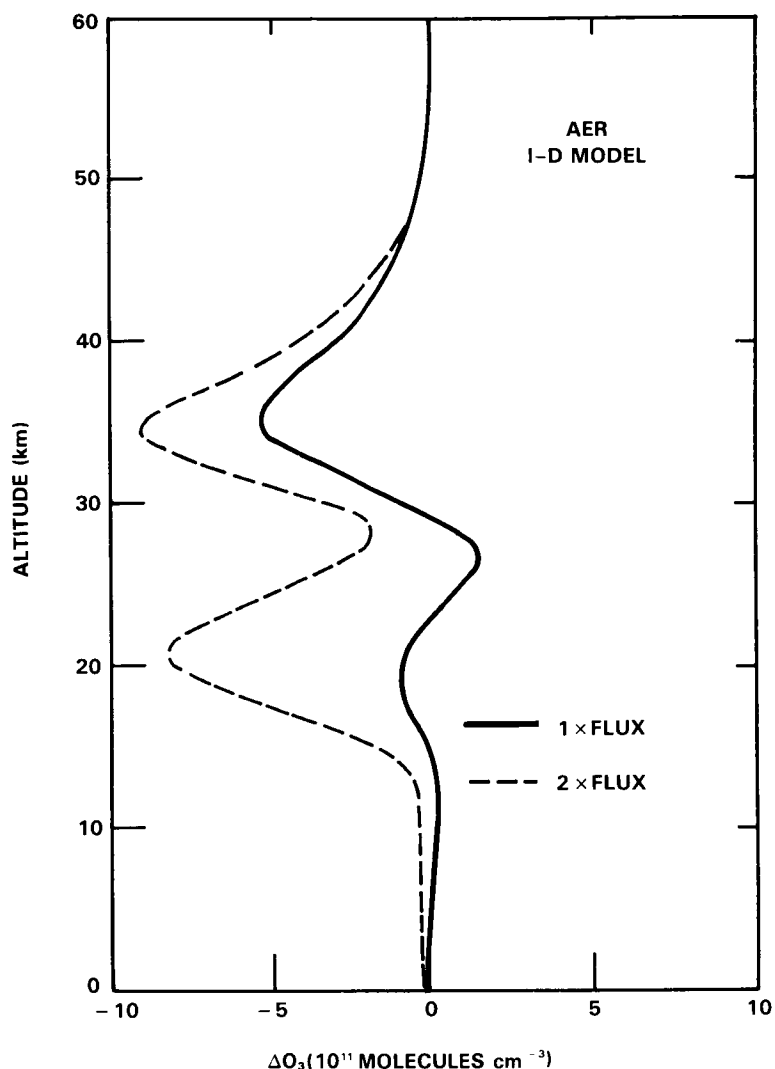


**Figure 13-4.** Calculated change in ozone concentration (molecules  $\text{cm}^{-3}$ ) by AER 1-D model as a function of altitude relative to a baseline with no CFC. A flux at the lower boundary equal to the 1980 CFC production rate is adopted for the 1x case (about 8 ppbv stratospheric  $\text{Cl}_x$ ) and the 2x case corresponds to twice the above flux (about 15 ppbv stratospheric  $\text{Cl}_x$ ).

about 20 to 40 km. As shown in Figure 13-5, catalytic destruction of ozone by  $\text{NO}_x$  is most efficient in this region, and increases in  $\text{N}_2\text{O}$  should lead to decreases in stratospheric ozone. From Table 13-4 model results indicate that an increase in the background concentrations of  $\text{N}_2\text{O}$  by 20% from about 300 to 360 ppbv, gives a decrease in total ozone ranging from 1.1 to 2.6%. As seen in Figure 13-8, peak ozone destruction occurs near 35-40 km in the LLNL model. Similar behavior is found in the results from other models. The small calculated increase in upper tropospheric and lower stratospheric ozone is due to increased efficiency of the  $\text{CH}_4\text{-NO}_x$ -smog reactions from the added  $\text{NO}_x$ . The small decrease in ozone in the lower troposphere results from a combination of increased  $\text{HO}_x$ , due to larger UV penetration (since  $\text{O}_3$  is decreased at higher altitudes) and consequent reaction of local  $\text{O}(^1\text{D})$  with  $\text{H}_2\text{O}$ , plus decreased  $\text{NO}_x$  due to increased conversion of  $\text{HNO}_3$  and  $\text{HNO}_4$  in the calculated downward flux of odd nitrogen from the stratosphere.

## MODEL PREDICTIONS

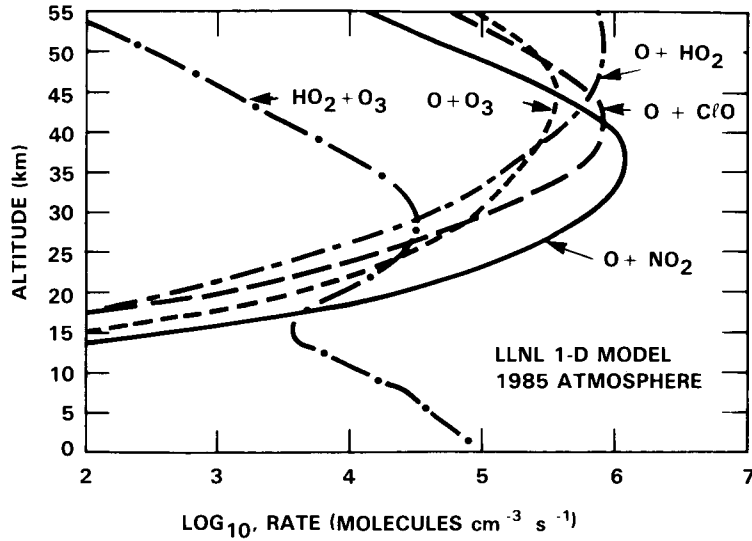


Figure 13-5. Calculated rates of key odd oxygen loss processes for 1985 atmosphere.

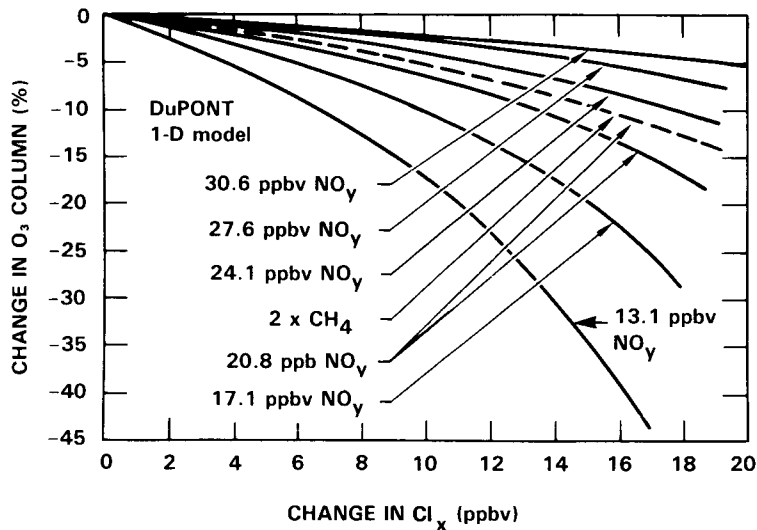


Figure 13-6. Calculated percentage change in ozone column as a function of stratospheric Cl<sub>x</sub> for various levels of stratospheric NO<sub>y</sub> and CH<sub>4</sub>.

## Carbon Monoxide

The perturbation scenario considered for CO is the doubling of present surface concentrations (from approximately 100 to 200 ppbv). For five 1-D models, the resultant changes in calculated total ozone vary from an increase of 0.3% to 1.1% (see Table 13-4). As seen in Figure 13-9 most of the change in ozone occurs in the troposphere. As discussed in Chapter 4, carbon monoxide participates in the chemistry of the free troposphere as a sink for OH by its oxidation to CO<sub>2</sub>, and as a source (or sink) for ozone by the "smog" reactions. For the LLNL model, doubling CO increases tropospheric ozone source terms by about 14% and the total atmospheric column by 1.1%.

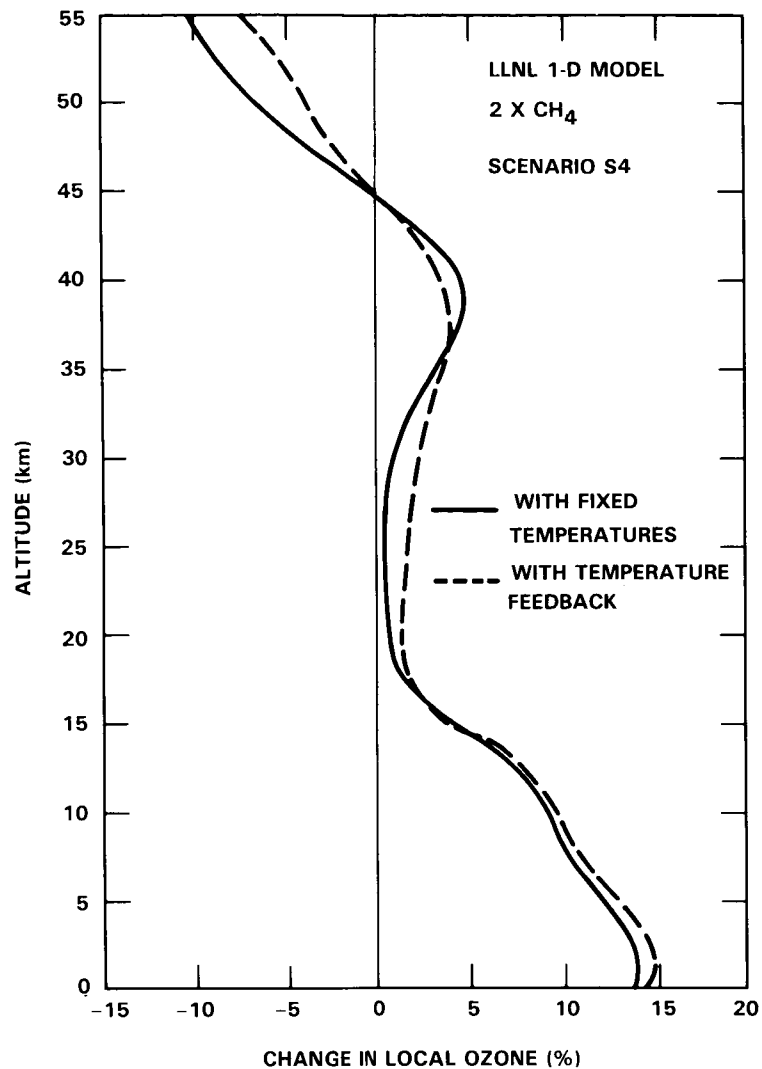


Figure 13-7. Calculated percentage change in local ozone as a result of doubled atmospheric methane.

There is a close relationship among OH, CH<sub>4</sub>, and CO concentrations; therefore, an increase of any one of these species has significant effects on the others and on other important trace gases (Levy, 1971, 1972; Wofsy *et al.*, 1972; Wofsy, 1976; Sze, 1977; Chameides *et al.*, 1977b). This calculation of doubled carbon monoxide with other surface concentrations held constant seems especially artificial, and it is to be emphasized that these single specie scenarios are artificial sensitivity studies (analogous to partial derivatives in the calculus of multiple variables).

### Carbon Dioxide

The calculated changes in ozone as a function of altitude as a result of doubling CO<sub>2</sub> are shown in Figure 13-10. The maximum percentage effect is near 40 km. Unlike the other trace gases that can perturb stratospheric ozone, carbon dioxide (CO<sub>2</sub>) does not affect ozone through direct chemical interactions. Absorption of solar radiation by stratospheric ozone and infrared emission to space by carbon dioxide are primarily responsible for balancing radiative energy in the stratosphere. Thus, an increase in CO<sub>2</sub> concentration

## MODEL PREDICTIONS

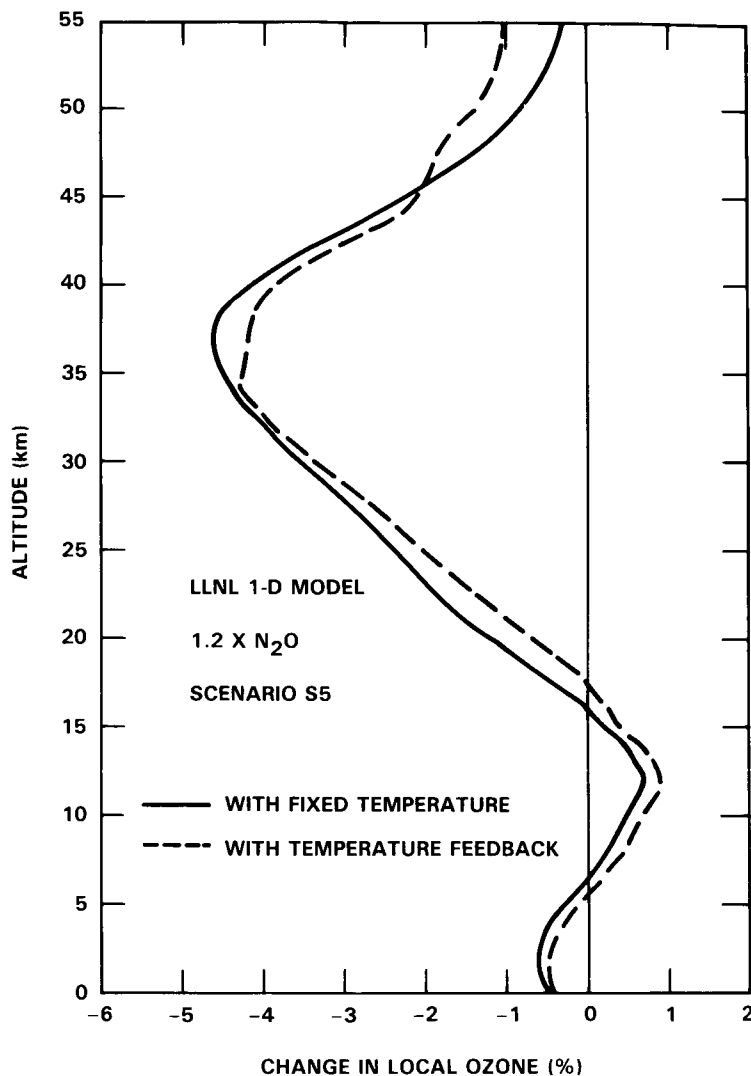


**Figure 13-8.** Calculated percentage change in local ozone for 20% increase in nitrous oxide.

alters the heat balance, reducing stratospheric temperatures, and leading to a slowing down of temperature-dependent ( $O + O_3$ ,  $NO + O_3$ ) ozone-destruction reactions. This results in a net increase in stratospheric ozone concentrations. (For very high chlorine perturbations, the opposite effect of  $CO_2$  may occur: lower temperature reduces the rate of  $Cl + CH_4$ , increasing the concentration of ozone destroying  $Cl$  and  $ClO$  relative to inert  $HCl$ ).

For a doubling of  $CO_2$  the various models calculate changes in temperature at 40 km between -7 and -9 K, calculate changes in local ozone at 40 km between +9 and +19%, and calculate changes in the ozone column between 1.2 and 3.5% (Table 13-6). All of the 1-D radiative convection models, except that of LLNL, calculate increases in surface temperature also; whereas the LLNL model has a fixed surface temperature. A sensitivity study by Wuebbles (1983a) indicates that this feature causes the LLNL model to overestimate the total ozone increases by about 0.4%.

**Table 13-6.** Percentage Changes in Ozone Column, Ozone at 40 km, and Temperature at 40 km for Scenario S7, a Doubling of CO<sub>2</sub> Relative To Present Atmosphere as Calculated by 1-D Models.

Model	Ozone Column %	Ozone at 40 km %	Temp. at 40 km K
LLNL (Wuebbles)	+3.5	+19.3	-8.0
AER (Sze)	+2.6	+9.4	-8.4
DuPont (Owens)	+2.8	+11.5	-7.4
IAS (Brasseur)	+3.1	+18.8	-9.0
MPIC (Bruehl)	+1.2	+13.0	-7.1

### Nitrogen Oxides

Historically, concern about the possible impact of anthropogenic trace gas emissions on ozone began in the early 1970's with studies of the effects from potential emissions of nitrogen oxides (NO<sub>x</sub>) from high-flying supersonic aircraft (e.g., see Johnston, 1971; CIAP, 1974; NRC, 1975). Although no such fleets are currently proposed, the scenarios assumed at that time for hypothetical fleets of stratospheric aircraft flying at altitudes of 17 and 20 km remain useful as an indication of the effects of nitrogen oxide emissions on atmospheric ozone. Results from the LLNL model for NO<sub>x</sub> emissions of 1000 molecules cm<sup>-3</sup>s<sup>-1</sup> and 2000 molecules cm<sup>-3</sup>s<sup>-1</sup> injected at altitudes of 17 and 20 km are given in Table 13-4 and Figure 13-11. Also shown in Table 13-4 are results from the model by Brasseur. Calculated changes in total ozone are comparable to model results in the mid-1970's (compare section 13.2.2.2). As seen in Figure 13-11, the primary effects of the emitted NO<sub>x</sub> occur near the altitude of injection, in the region where the NO<sub>x</sub> catalytic cycle is the dominant cause of ozone loss (Figure 13-5).

Of more immediate concern are impacts on ozone from surface emissions of odd nitrogen and from the emissions of NO<sub>x</sub> from subsonic aircraft in the troposphere and lower stratosphere. Several studies suggest that these emissions may be influencing tropospheric ozone concentrations, with a net increase in ozone generally expected from the methane-NO<sub>x</sub>-smog reactions (e.g. Logan *et al.*, 1981; Liu *et al.*, 1983; Callis *et al.*, 1983; Wuebbles *et al.*, 1983; Wuebbles, 1983a).

### Bromine

Sources of stratospheric bromine are discussed in Chapter 3. Although bromine chemistry is in many respects similar to that for chlorine, there are also significant differences. Dissociation and reactions of CH<sub>3</sub>Br and other important bromine sources occur at lower altitudes than for the major chlorine sources. While the reaction of Cl with CH<sub>4</sub> to produce HCl limits the abundance of active chlorine radical species in the stratosphere, the reaction of Br with CH<sub>4</sub> is endothermic and therefore negligibly slow. Also, the

## MODEL PREDICTIONS

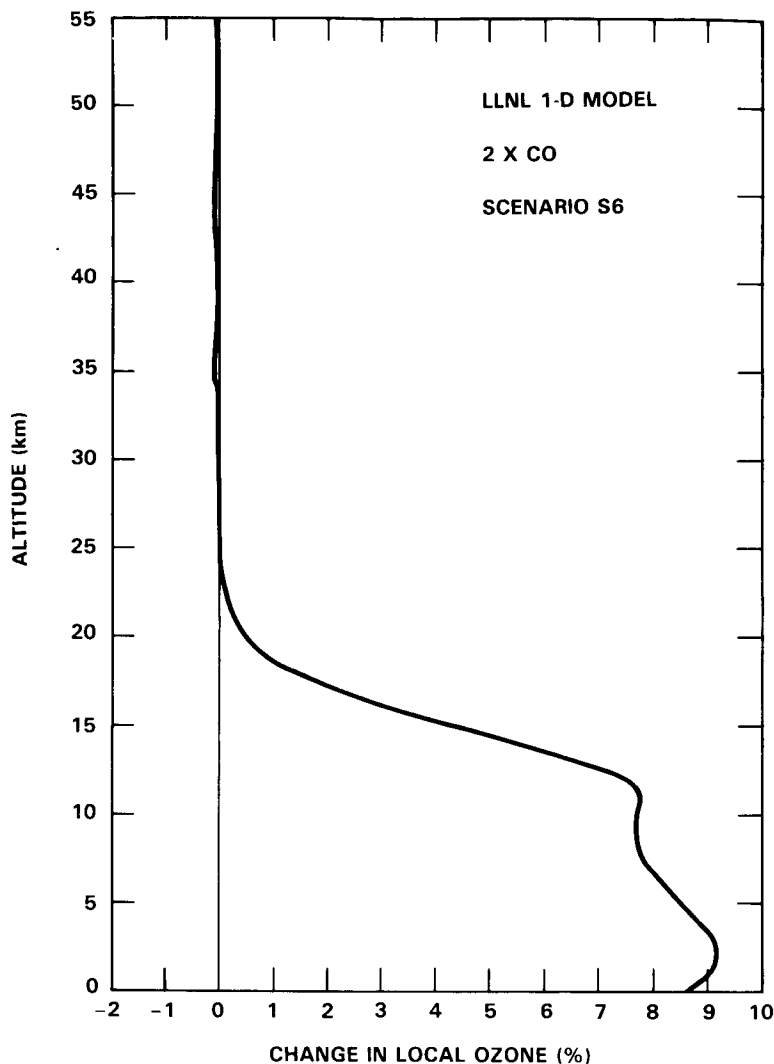


Figure 13-9. Calculated percentage change in local ozone for doubling of carbon monoxide.

photolysis of HBr is more rapid than that of HCl, and the reaction of OH with HBr is more rapid than its rate with HCl. Consequently, the majority of  $\text{Br}_x$  is present as the active species BrO. On a molecule for molecule basis, bromine is a much more efficient sink for stratospheric odd oxygen than chlorine. The details of  $\text{Br}_x$  chemistry are given in Chapter 2, Section 4.

The bromine perturbation scenario, posed as a sensitivity test only, considered is an increase in surface mole fraction of  $\text{CH}_3\text{Br}$  from 20 to 100 pptv. As seen in Table 13-4, the LLNL model was the only model used to calculate the perturbation. It gave a total ozone change of  $-3\%$  (without temperature feedback), in good agreement with the  $-4\%$  calculated change in total ozone for the same scenario by Prather *et al.* (1984). The relative change in ozone abundance as a function of altitude is shown in Figure 13-12. The major contribution to the change in the ozone column occurs around 20 km. The largest relative change in ozone (7% decrease) is at 15 km with a secondary peak at about 40 km.

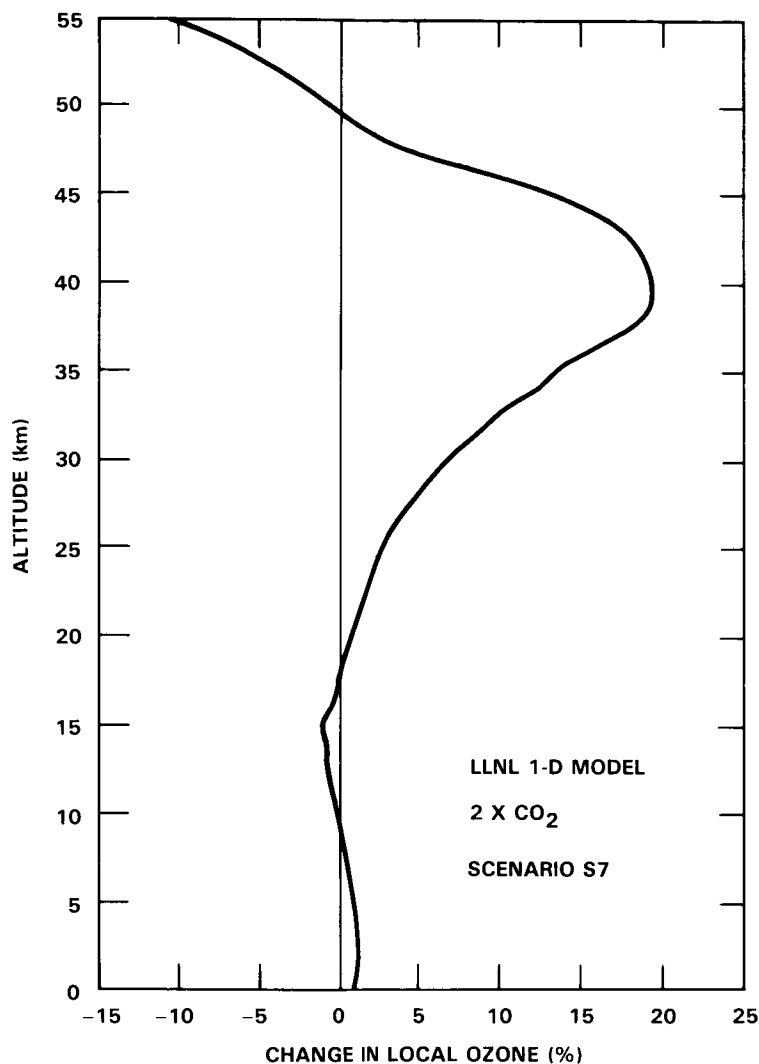


Figure 13-10. Calculated percentage change in local ozone for doubling of carbon dioxide.

Because the ozone depletion occurs mostly below the ozone concentration maximum, little increase in the penetration of UV, active in dissociating oxygen, is calculated. For this scenario the lower stratospheric ozone decrease results mostly from an increase of the rate of  $\text{BrO} + \text{BrO}$ . The reaction  $\text{BrO} + \text{ClO}$  contributes throughout the middle stratosphere. The small secondary peak at 40 km is caused largely by  $\text{BrO} + \text{O}$ .

### Combined Scenarios

The calculated steady-state changes in total ozone and ozone at 40 km are shown in Tables 13-2 and 13-3 respectively, for several combined scenarios (S2, b, c, and S3 b and c) involving chlorocarbon emissions to give about 8 ppbv or 15 ppbv of upper stratospheric  $\text{Cl}_x$ , doubled methane, nitrous oxide increased by 20%, and, in some cases, doubled carbon dioxide. Calculated changes in ozone versus altitude are shown in Figure 13-13. Each of the models used tend to show similar behavior, with large ozone decreases calculated in the upper stratosphere, and ozone increases in the troposphere and lower stratosphere. The addition of the  $\text{CO}_2$  perturbation reduces the ozone decrease in the upper stratosphere.

## MODEL PREDICTIONS

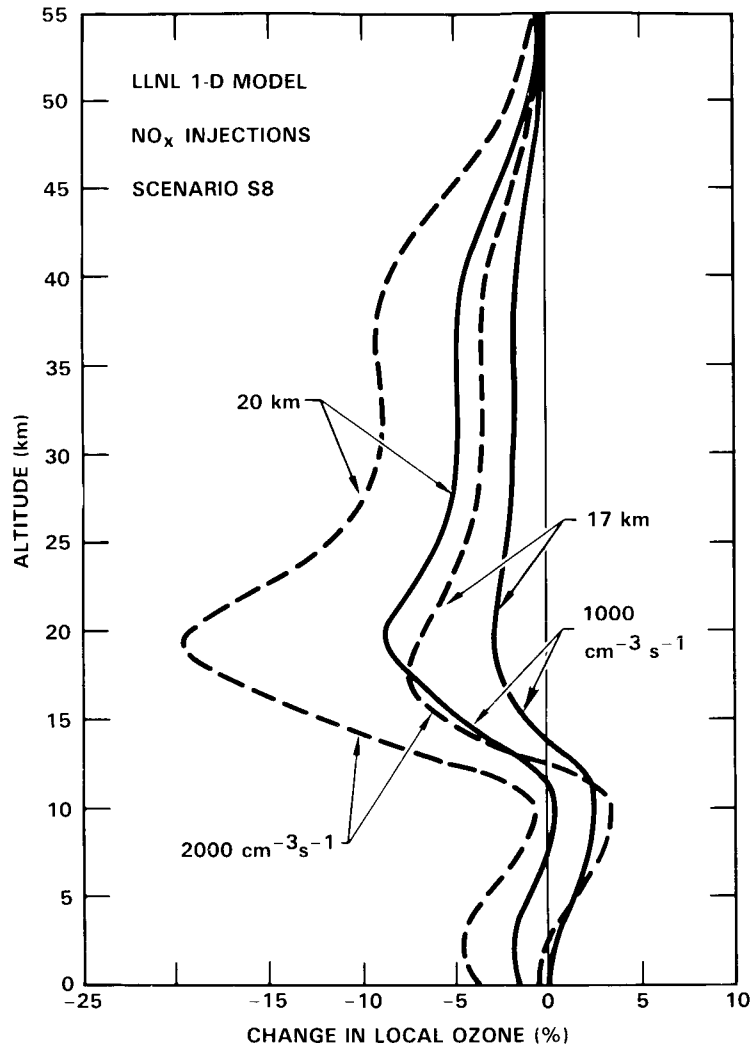


**Figure 13-11.** Calculated percentage changes in local ozone for 17 and 20 km NO<sub>x</sub> injections of 1000 and 2000 molecules cm<sup>-3</sup> s<sup>-1</sup>.

The single-specie scenarios discussed above give the qualitative explanations for the multi-specie scenario, but the calculated changes in total ozone are much less than the sum of the individual perturbations involved. The upper stratospheric ozone decrease primarily results from increased chlorine in the assumed scenarios, while the methane change dominates the effects on ozone in the troposphere and lower stratosphere. The ozone recovery mechanism and interaction between NO<sub>x</sub> and Cl<sub>x</sub> chemistry also plays a role in the lower to middle stratosphere.

### 13.1.2.2 Time-Dependent Perturbations

Time-dependent calculations including multiple-specie perturbations are regarded as the most nearly realistic of the one-dimensional model assessments. Several studies have considered such time-dependent multiple-species scenarios (e.g. Wuebbles *et al.*, 1983; Callis *et al.*, 1983a; Sze *et al.*, 1983; DeRudder and Brasseur, 1984; Owens *et al.*, 1985a,b; Brasseur *et al.*, preprint 1985).

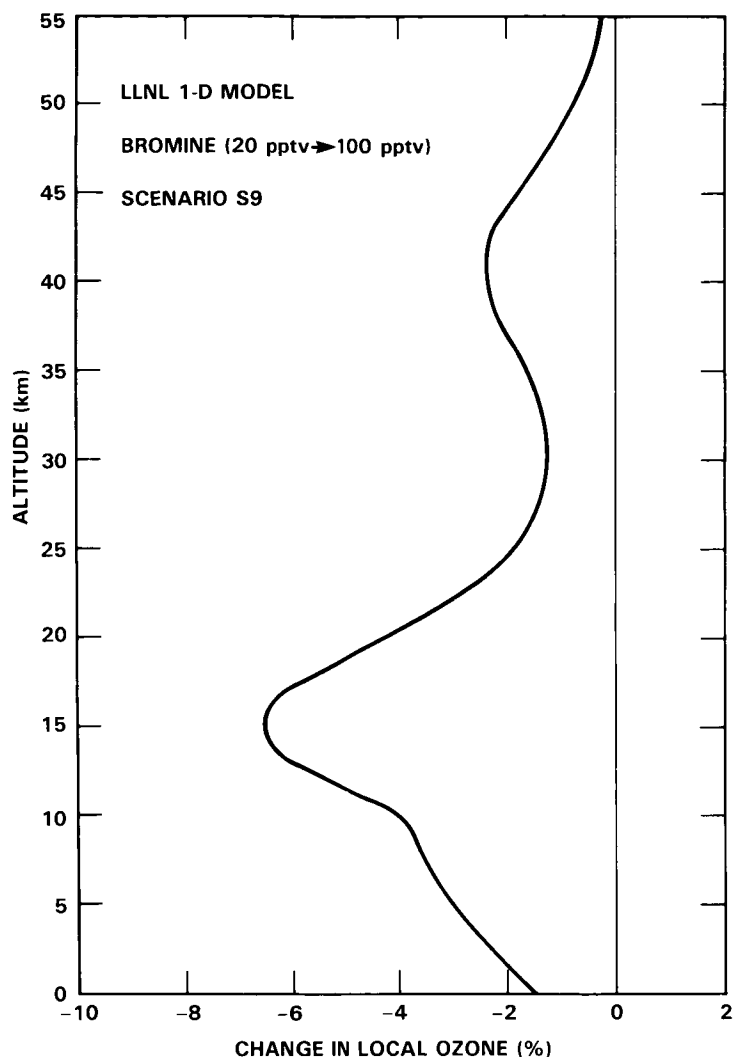


**Figure 13-12.** Calculated percentage change in local ozone when surface  $\text{CH}_3\text{Br}$  concentration is increased from 20 to 100 pptv.

Shown in Figure 13-14 are the calculated changes in total ozone from several models for scenario T2B, where CFC-11 and CFC-12 emissions are assumed to increase 1.5% per year,  $\text{CH}_4$  concentrations to increase 1% per year,  $\text{N}_2\text{O}$  concentrations to increase 0.25% per year, and  $\text{CO}_2$  to increase about 0.5% per year, corresponding to the analyses of Edmonds *et al.* (1984) as discussed in Wuebbles *et al.* (1984). Calculations with temperature feedback tend to give a smaller decrease in total ozone for this scenario than calculations with fixed temperatures, primarily due to the impact of temperature-ozone interaction from increasing  $\text{CO}_2$  concentrations.

Figure 13-15 shows the change in ozone at 40 km for this same scenario. With the exception of the Brasseur model, similar changes in ozone at this altitude are found in those models with similar temperature treatments. Figure 13-16 shows the change in ozone with altitude for this scenario at selected times and calculated with the LLNL model.

## MODEL PREDICTIONS

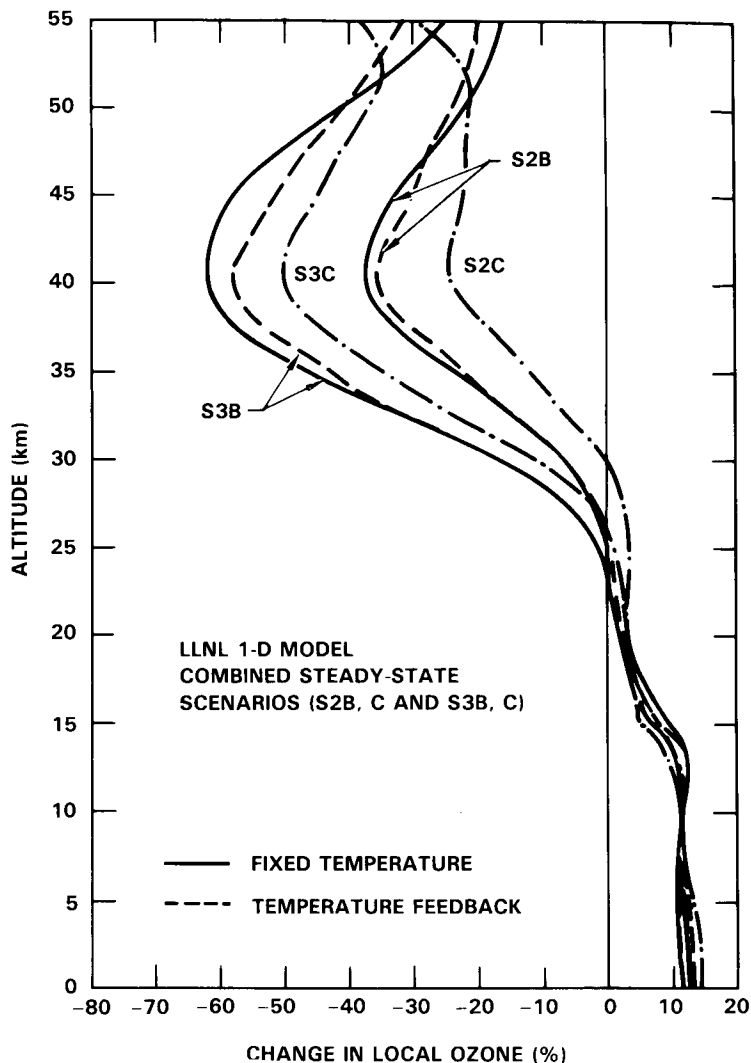


**Figure 13-13.** Calculated percentage change in local ozone for steady-state combined scenarios: S2B (8 ppbv  $\text{Cl}_x$ ,  $2 \times \text{CH}_4$ ,  $1.2 \times \text{N}_2\text{O}$ ); S2C (S2B and  $2 \times \text{CO}_2$ ); S3B (15 ppbv  $\text{Cl}_x$ ,  $2 \times \text{CH}_4$ ,  $1.2 \times \text{N}_2\text{O}$ ); S3C (S3B and  $2 \times \text{CO}_2$ ), all referred to background with 1.3 ppbv  $\text{Cl}_x$ .

Figure 13-17 shows the changes calculated with the LLNL model in total ozone for other scenarios (Table 13-1) as a function of time. Several conclusions can be reached from these results. Future ozone changes can be drastically affected by the choice of specific trace gas scenarios. With these 1-D models, even the sign of the change in total ozone depends on the specific changes in CFC's,  $\text{CH}_4$ ,  $\text{CO}_2$ , and  $\text{N}_2\text{O}$ . Also, little change in global-average ozone may be expected in the next few decades from the combined scenarios unless significant sustained growth in CFC emissions or drastic differences in present growth rates of other source gases were to occur (see Section 13.1.3 for another, latitude-dependent interpretation of this statement in terms of two-dimensional models). Over this time period, effects of projected  $\text{CO}_2$  and  $\text{CH}_4$  concentrations are expected at least partially to counterbalance the calculated decrease in ozone due to CFC's alone. As suggested by Figure 13-16, significant differences are calculated in the altitude distribution of ozone in even those model calculations showing little change in total ozone calculated for combined source gas scenarios. Large decreases occur in ozone above about 30 km and increases or small

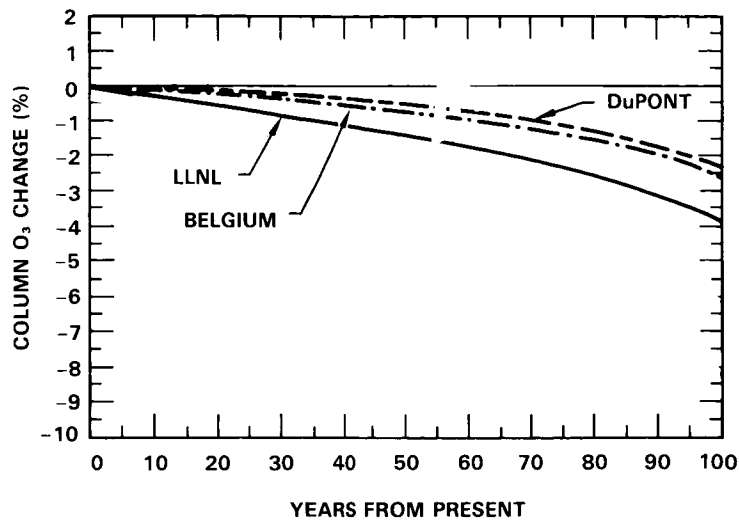


**Figure 13-14.** Calculated (by four different 1-D models) change in ozone column as a function of time for scenario T2B (CFC emissions begin at 1980 rates and grow 1.5% per yr compounded, CH<sub>4</sub> increases at 1% per yr, N<sub>2</sub>O increases at 0.25% per yr, and CO<sub>2</sub> increases according to the DOE scenario).

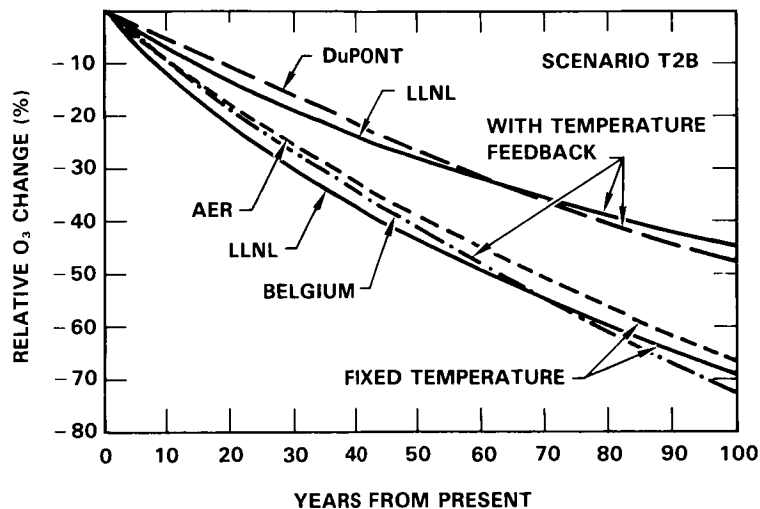


**Figure 13-15.** Calculated percentage change in local ozone at 40 km altitude with time for scenario T2B (compare Figure 13-14).

decreases below. Calculated increases in tropospheric ozone are extremely sensitive to the assumed CH<sub>4</sub>, CO, and hydrocarbon perturbations but not to the Cl<sub>x</sub> scenarios.

Results for scenario T3B (Figure 13-17), which assumes a 3% per year growth in CFC emissions along with the previously defined scenarios for CH<sub>4</sub>, N<sub>2</sub>O, and CO<sub>2</sub>, show large ozone decreases even with the concurrent increase of the trace gases. After 70 years the ozone decrease is 10% and still strongly increasing.

## MODEL PREDICTIONS

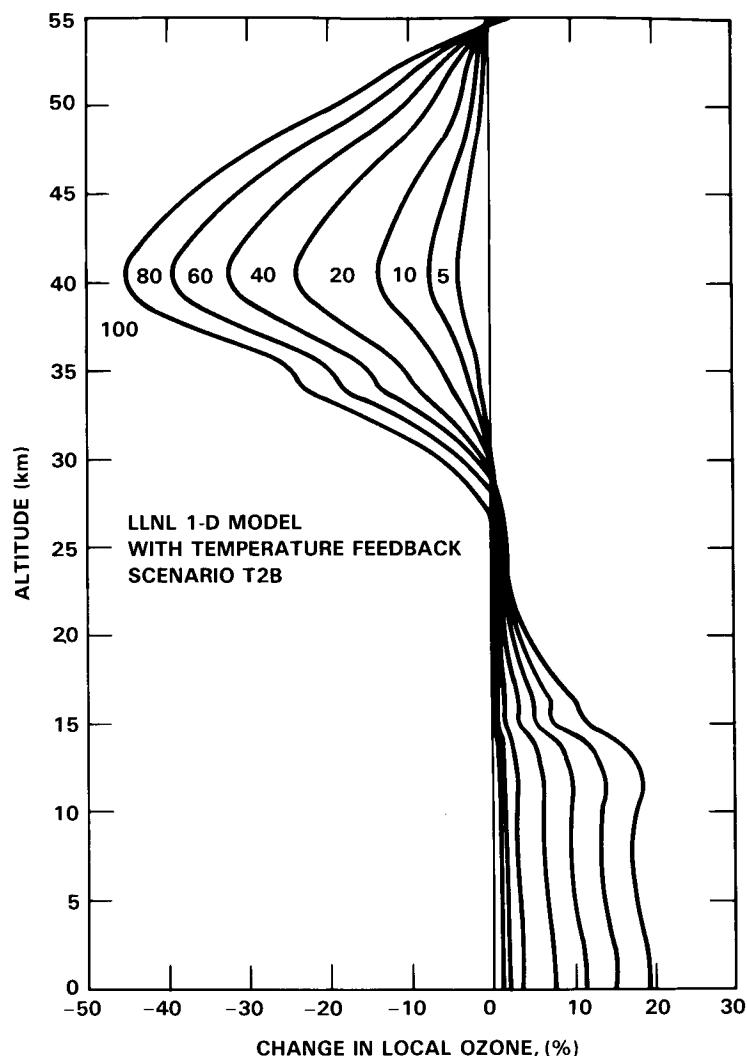
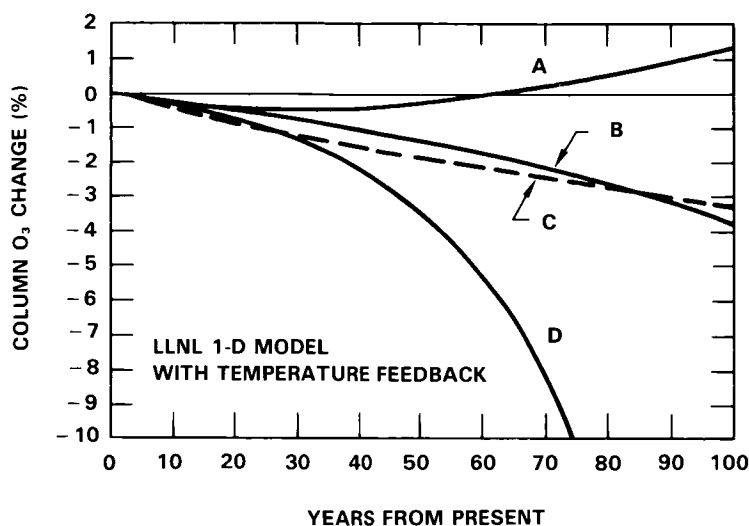


Figure 13-16. Calculated percentage change in local ozone at selected times (5 to 100 years) for scenario T2B (compare Figure 13-14).

### 13.1.3 Assessment Calculations with 2-D Models

In recent years, many detailed photochemical and dynamical two-dimensional models of the stratosphere have been developed (Chapter 12). These have achieved a measure of success in simulating the zonally and seasonally averaged distributions of constituents influenced both by photochemistry and transport in the stratosphere, such as methane and nitrous oxide (see Miller *et al.*, 1981; Gidel *et al.*, 1983; Garcia and Solomon, 1983; Jones and Pyle, 1984; Guthrie *et al.*, 1984; Ko *et al.*, 1984, 1985). Ozone densities below about 20-25 km are predominantly controlled by transport of ozone from the middle and upper stratosphere. Since most of the ozone column abundance at extra-tropical latitudes is located in this dynamically dominated region, it is important to examine ozone perturbations using multi-dimensional models that include at least a first order representation of transport in the meridional (height-latitude) plane. Such studies reveal latitudinal variations in ozone depletions, which are of importance for ozone monitoring programs, and they provide insight beyond that obtained with comparable one-dimensional model studies.



**Figure 13-17.** Calculated changes in ozone column with time for time-dependent scenarios: T1B (CFC flux continues at 1980 level, CH<sub>4</sub> increases 1% per yr, N<sub>2</sub>O increases 0.25% per yr, and CO<sub>2</sub> increases according to the DOE scenario); T1C (same as T1B, but without increases in CH<sub>4</sub> and N<sub>2</sub>O); T2B (CFC emissions begin at 1980 rates and increase at 1.5% per yr, other trace gases change as with T1B); T3B (same as T2B except CFC emissions increase at 3% per yr).

The work by Pyle (1980), Haigh and Pyle (1982), and Haigh (1984) using a two-dimensional chemical model suggests, for example, that substantial latitude gradients in ozone depletions should be expected, with much larger depletions occurring in the lower stratosphere at high latitude than at lower latitudes. Indeed, the total column changes predicted in high latitudes by Haigh (1984) using a two-dimensional model with detailed radiation and photochemistry were about two or even three times larger than those calculated with comparable one-dimensional models. (Of course, 1-D models do not calculate latitudinal features, but the point of this comparison is that the nominally global average result given by 1-D models systematically underestimates the ozone reductions that are predicted by 2-D models to occur in high temperate and polar regions. This two-dimensional consideration needs to be added to all one-dimensional results in order not to overlook the worst-case ozone reduction). Haigh (1984) also predicted a similarly large ozone column depletion at high latitudes even when simultaneous carbon dioxide increases were considered in the calculations. This result is also quite different from that obtained in one-dimensional models, wherein the effect of simultaneous carbon dioxide and chlorocarbon perturbations leads to a decrease in the anticipated total column change (see for example, Wuebbles *et al.*, 1983).

Some two-dimensional model perturbation studies (for example, Brasseur and Bertin, 1978/79; Gidel *et al.*, 1983; Steed *et al.*, 1982) suggest less latitude gradient in ozone depletion than that found in the studies by Pyle (1980) and Haigh (1984). It is of interest to understand the origin of these differences between these two-dimensional models.

In this subsection, perturbation studies with three two-dimensional models will be presented. The model referred to here as MPIC is that of Gidel *et al.* (1983); the calculations were done by Schmailzl and Crutzen. The model (GS) is that of Garcia and Solomon (1983) and Solomon and Garcia (1984b). The model (AER) is that described by Ko *et al.* (1985). The photochemical reaction rates used were those of NASA-JPL (1985) or Appendix 1, and the solar flux, oxygen and ozone cross sections were taken from Chapter 7,

## MODEL PREDICTIONS

but the authors used different methods in the treatment of the Schumann-Runge bands and used different boundary conditions. Table 13-7 shows the scenarios used in each model.

For each of these scenarios, the global, seasonal average reduction of ozone is given in Table 13-8. These results are analyzed and discussed in a later section, but first the two-dimensional structure of the ozone reductions is presented by various graphical means.

### Perturbation by $Cl_x$ Only

Figure 13-18 presents latitude-altitude cross sections of the percentage ozone depletion obtained for winter and spring from the MPIC model for scenario SMA ( $Cl_x$  increase, 6.8 ppbv; reference  $Cl_x$ , 2.7 ppbv). Similar plots are shown for all four seasons according to the AER model for scenario S2A ( $Cl_x$  increase, 6.8 ppbv; reference  $Cl_x$ , 1.3 ppbv) in Figure 13-19 and for scenario S3A ( $Cl_x$  increase, 14.2 ppbv; reference  $Cl_x$ , 1.3 ppbv) in Figure 13-20. Results of the GS model for winter and spring are given as a latitude-altitude plot of percentage ozone reduction in Figure 13-21 for scenario S2A.

For these three models, essentially the same  $Cl_x$  perturbation is represented by Figure 13-18a (winter, MPIC), Figure 13-19a (January, AER), and Figure 13-20a (December, GS). Certain similarities and differences can be noted. In all three models, the maximum percentage ozone reduction at 40 km is 50 to 60%, which is in agreement with 1-D results (Table 13-3 and Figures 13-1 to 13-3). At this altitude, the AER and GS models show similar latitude profiles with ozone-reduction maxima near the poles. Both show a saddlepoint minimum of ozone reduction of about 35% near the equator. The MPIC maximum percentage

Table 13-7. Two-dimensional Model Scenarios.

Code	$Cl_x$ /ppbv			$2 \times CH_4$ $1.2 \times N_2O$	Model	Symbol
	Total	Ref.	Incr.			
S2A	8.	1.3	6.7	no	Garcia and Solomon (1983)	GS
S2A	8.2	1.3	6.9	no	Ko <i>et al.</i> (1985)	AER
S3A	15.5	1.3	14.2	no		AER
S2C	8.	1.3	6.7	yes	Garcia and Solomon (1983)	GS
SMA	9.5	2.7	6.8	no	Gidel <i>et al.</i> (1983)	MPIC
—	2.7	1.3	1.4	no		MPIC
—	9.5	1.3	8.2	no		MPIC
SMB	9.5	2.7	6.8	yes		MPIC
SMC	18.	2.7	15.3	yes		MPIC

MODEL PREDICTIONS

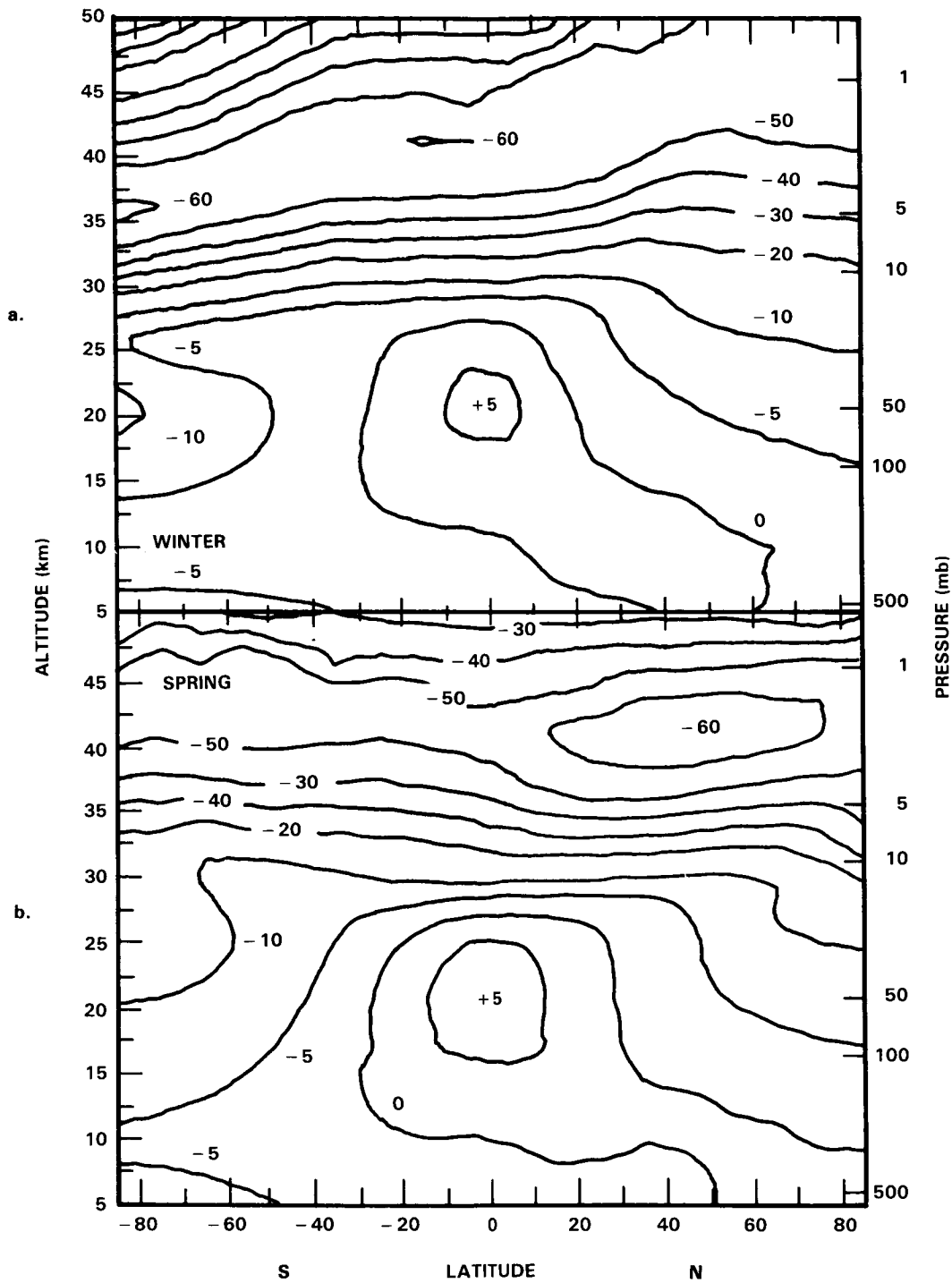


**Figure 13-18.** Calculated steady-state local percentage ozone change as a function of latitude and altitude—for 1980 fluorocarbon emission given 9.5 ppbv  $Cl_x$  relative to reference atmosphere with 2.7 ppbv  $Cl_x$ , or an increase of 6.8 ppbv (Table 13-7, Scenario SMA, MPIC 2-D Model). a. Southern Hemisphere winter, b. Southern Hemisphere spring.

## MODEL PREDICTIONS

**Table 13-8.** Percentage Change in Global, Seasonal Average Ozone According to Two-dimensional Models for Steady-state Scenarios Containing  $\text{Cl}_x$  Perturbations, and Model "Sensitivity" of Ozone to  $\text{Cl}_x$ . Sensitivity, S, Is Percent Ozone Decrease Divided by ppbv  $\text{Cl}_x$  Increase.

Initial	$\text{Cl}_x/\text{ppbv}$		$2 \times \text{CH}_4$ $1.2 \times \text{N}_2\text{O}$	% Ozone Decrease	S -%/ppbv	Model
	Final	Increase				
1.3	2.7	1.4	no	1.9	1.36	MPIC
2.7	9.5	6.8	no	7.2	1.06	
1.3	9.5	8.2	no	9.1	1.11	
2.7	9.5	6.8	yes	4.5	0.66	MPIC
2.7	18.	15.3	yes	11.1	0.73	
1.3	8.2	6.9	no	8.5	1.23	AER
1.3	15.5	14.2	no	18.	1.27	

ozone reduction is an almost uniform ridge from  $85^\circ \text{N}$  at 45 km to  $85^\circ \text{S}$  at 35 km. In all three models the  $-20\%$  contour is flat almost from pole to pole at an altitude of about 30 km. At 20 km altitude the three models show qualitatively similar features, an ozone increase in the tropics and ozone reduction at extra-tropical latitudes; but the quantitative values differ: GS varies as  $-5\%$  at  $90^\circ \text{S}$ ,  $+15\%$  at the equator,  $-5\%$  at  $90^\circ \text{N}$ ; AER values are  $-10\%$  at the South Pole,  $+20\%$  at the equator,  $-30\%$  at the North Pole; and MPIC varies as  $-10\%$  at  $80^\circ \text{S}$ ,  $+5\%$  at the equator,  $-5\%$  at  $80^\circ \text{N}$ .

The model results for this scenario during the spring season can be compared among Figure 13-18b (MPIC) and Figures 13-19b and 13-20 (AER). For the AER and MPIC models, the results for the Northern Hemisphere are qualitatively similar with a maximum ozone-reduction closed counter near 40 km, but this feature is absent for the MPIC model in the Southern Hemisphere. Along the high altitude maximum ozone-reduction ridge, the AER model shows somewhat greater latitude variation than the MPIC model. In the middle stratosphere the two models show similar flat contours of ozone reduction. In the lower stratosphere the AER model shows larger ozone increases in the tropical region and larger ozone reductions in temperate and polar regions than the MPIC model.

The percentage changes in the ozone vertical column are shown as a function of latitude and season in Dobson contour maps. The result of the MPIC model for  $\text{Cl}_x$  perturbation SMA is given in Figure 13-22a; and the results of the AER model are shown for scenarios S2A and S3A in Figure 13-23. The scenario for Figure 13-22a (MPIC) is essentially the same as that for Figure 13-23a (AER), which provides a direct comparison between the models. For the MPIC model, larger ozone reductions are obtained at high latitudes than at low latitudes by almost a factor of two in the winter (Figure 13-22a). However, for the AER model there are much greater differences with latitude, more than a factor of four in February, for example (Figure 13-23a). The contour intervals of ozone change are the same (every 2%) for Figures 13.22a and 13.23a, and it is obvious by inspection that the AER model shows more variation with latitude and season than the MPIC model. A direct comparison is given by Figure 13-24, which gives the latitude dependence of ozone column reduction for these two models (spring).

MODEL PREDICTIONS

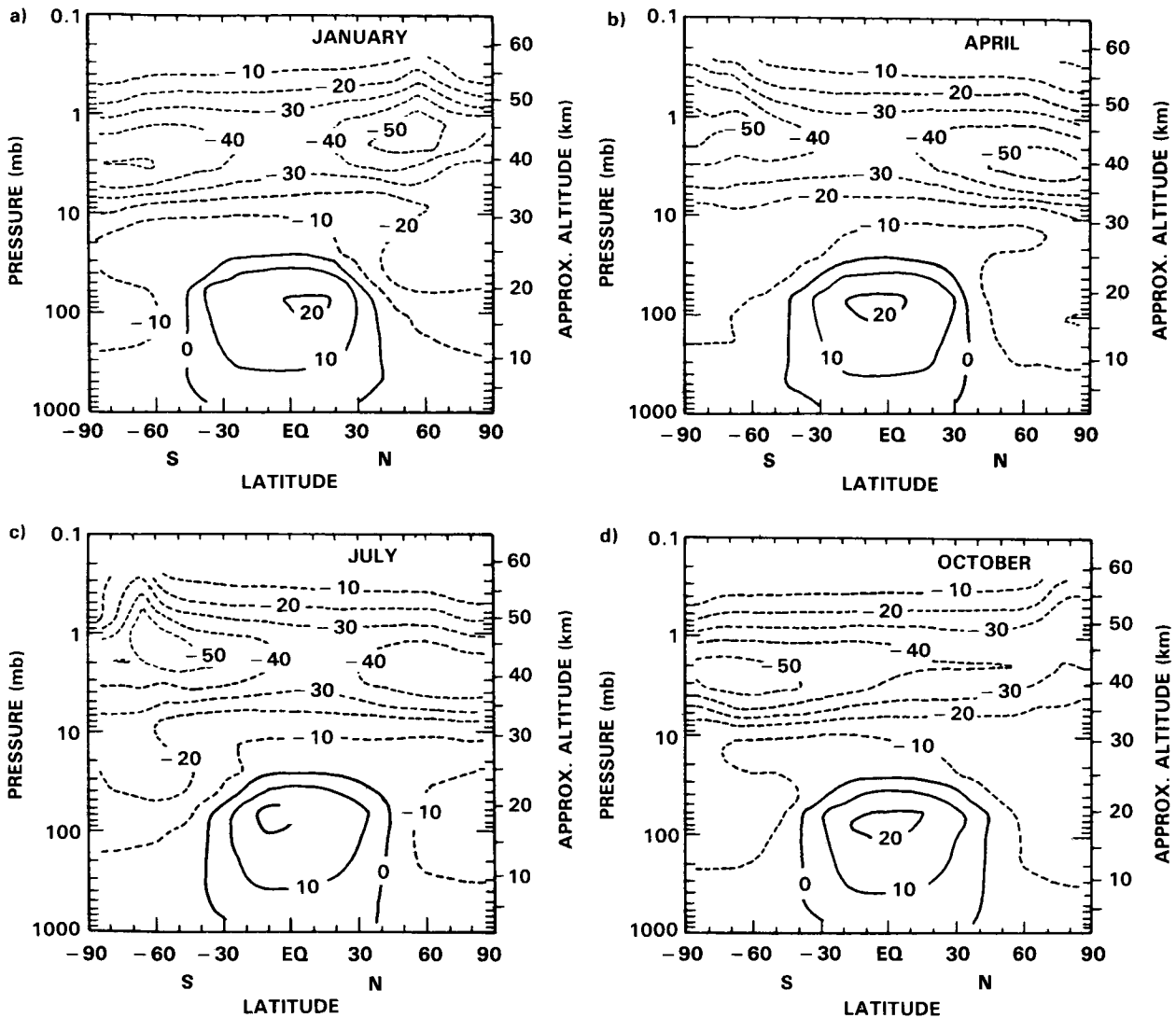


Figure 13-19. Calculated steady-state local percentage ozone change as a function of latitude, season, and altitude—for fluorocarbon emission giving 8.2 ppbv  $Cl_x$  relative to reference atmosphere with 1.3 ppbv  $Cl_x$ , or an increase of 6.9 ppbv (Table 13-7, Scenario S2A, AER 2-D Model). a. January, b. April, c. July, d. October.

Some of the reasons for these latitudinal gradients in ozone depletion were examined using the model by Garcia and Solomon. Figure 13-25 presents the calculated distribution of ozone mixing ratio obtained in that model (see Solomon *et al.*, 1985b) along with the calculated odd oxygen replacement time (the local concentration of ozone divided by twice the molecular oxygen photolysis rate by solar radiation at wavelengths below 242 nm) for the present day atmosphere. Assuming a typical time scale for meridional transport of ozone of the order of 100 days in the stratosphere, the shaded area shows the region that is substantially controlled by dynamics (i.e. below about 25-30 km, poleward of about 40-50° in both summer and winter). Near 40 km ozone is photochemically controlled, and its lifetime reveals little gradient with latitude except in the polar night region. The latitude gradients in ozone depletion obtained near 40 km in the AER and GS models are the direct result of calculated gradients in methane. Large gradients in methane have indeed been observed near 40 km by the SAMS satellite and are reasonably well reproduced

## MODEL PREDICTIONS

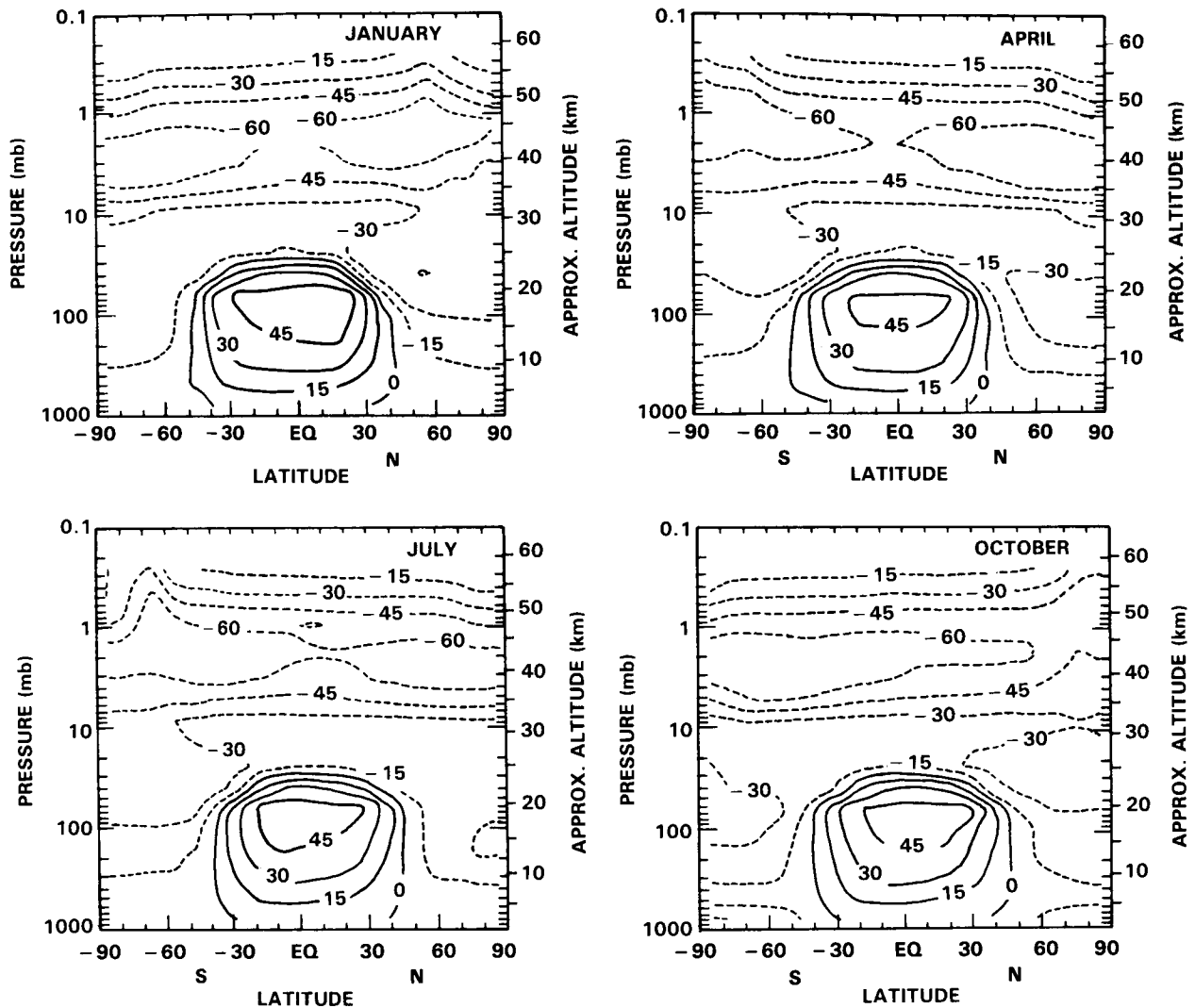
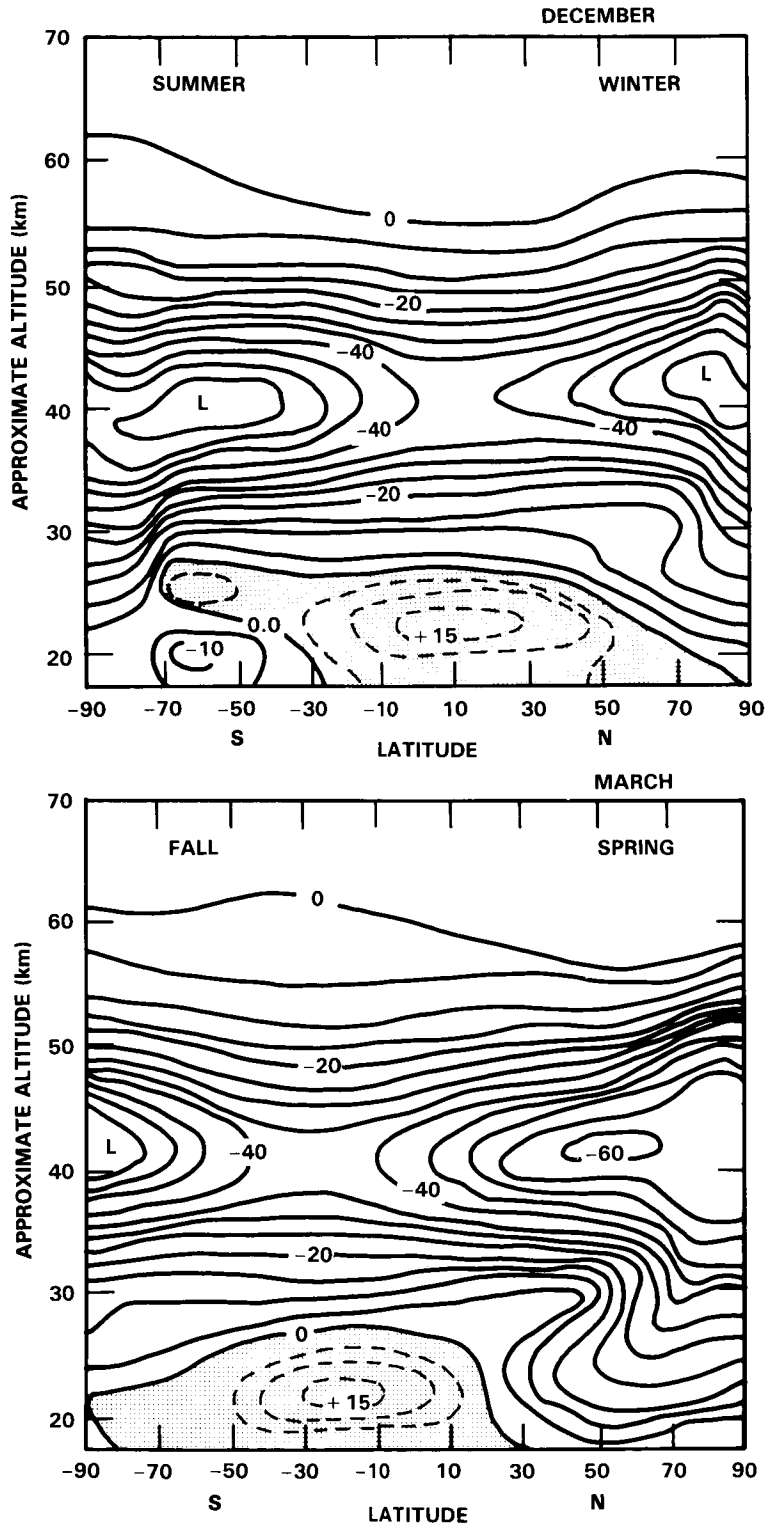


Figure 13-20. Same as Figure 13-19, but with 15.5 ppbv  $\text{Cl}_x$  or a change of 14.2 ppbv (Scenario S3A).

in some two-dimensional models (see Jones and Pyle, 1984; Solomon and Garcia, 1984b; Ko *et al.*, 1984). The satellite data suggest a gradient in methane at 40 km of about a factor of three from the tropics to about  $70^\circ$  latitude. Methane, in turn, controls the partitioning of active chlorine between the inert reservoir, HCl, and the ozone-destroying species, Cl and ClO, near 40 km. The methane gradient therefore results in a greater abundance of catalytic chlorine free radicals at high latitudes, where methane abundances are substantially lower than they are in the tropics at 40 km (Solomon and Garcia, 1984b). As the chlorine content in the atmosphere increases, its perturbing influence is therefore predicted to be much greater at high latitude. This effect is not observed in the winter MPIC model because the calculated methane gradient is much smaller (see Chapter 12). The reason for this difference between models is discussed further below.

The ozone changes obtained at lower altitudes largely control the behavior of the total column. As already mentioned, below about 25 km at middle and high latitudes, ozone is principally controlled by dynamics because the ozone photochemical replacement times are long. Photochemical self-healing therefore



**Figure 13-21.** Calculated steady-state local percentage ozone change as a function of latitude and altitude—for 1980 fluorocarbon emission giving 8.0 ppbv  $Cl_x$  relative to reference atmosphere with 1.3 ppbv  $Cl_x$ , or an increase of 6.7 ppbv (Table 13-7, Scenario S2A, GS 2-D model).

MODEL PREDICTIONS

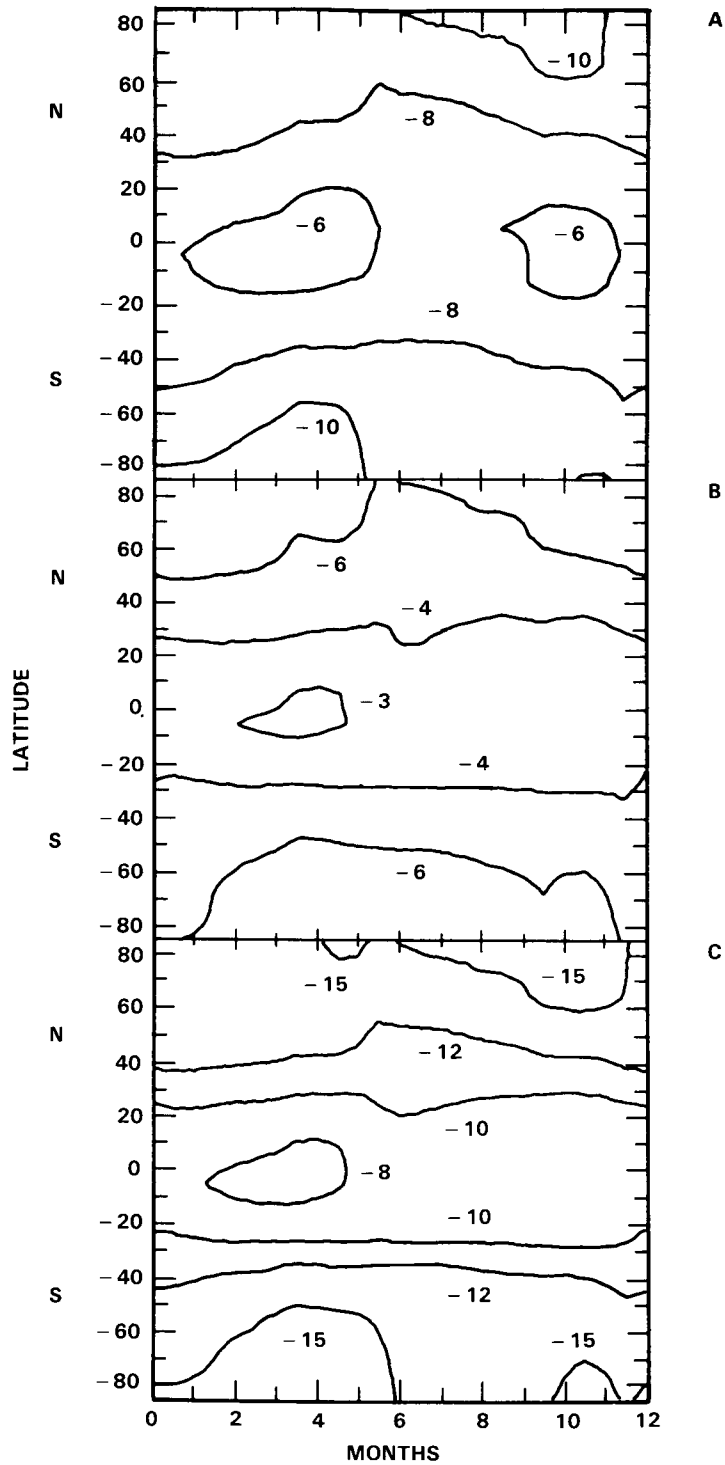


**Figure 13-22.** Calculated steady-state percentage change of the ozone column relative to a reference atmosphere with 2.7 ppbv  $Cl_x$  as a function of latitude and season for three scenarios in Table 13-7: (A) SMA, 1980 fluorocarbon emission giving 9.5 ppbv  $Cl_x$  or an increase of 6.8 ppbv  $Cl_x$ ; (B) SMB, which is same as SMA, but also  $2 \times CH_4$  and  $1.2 \times N_2O$ ; (C) SMC, twice the 1980 fluorocarbon flux giving 18 ppbv  $Cl_x$  or 15.3 ppbv change and increase of methane and nitrous oxide (MPIC 2-D model).

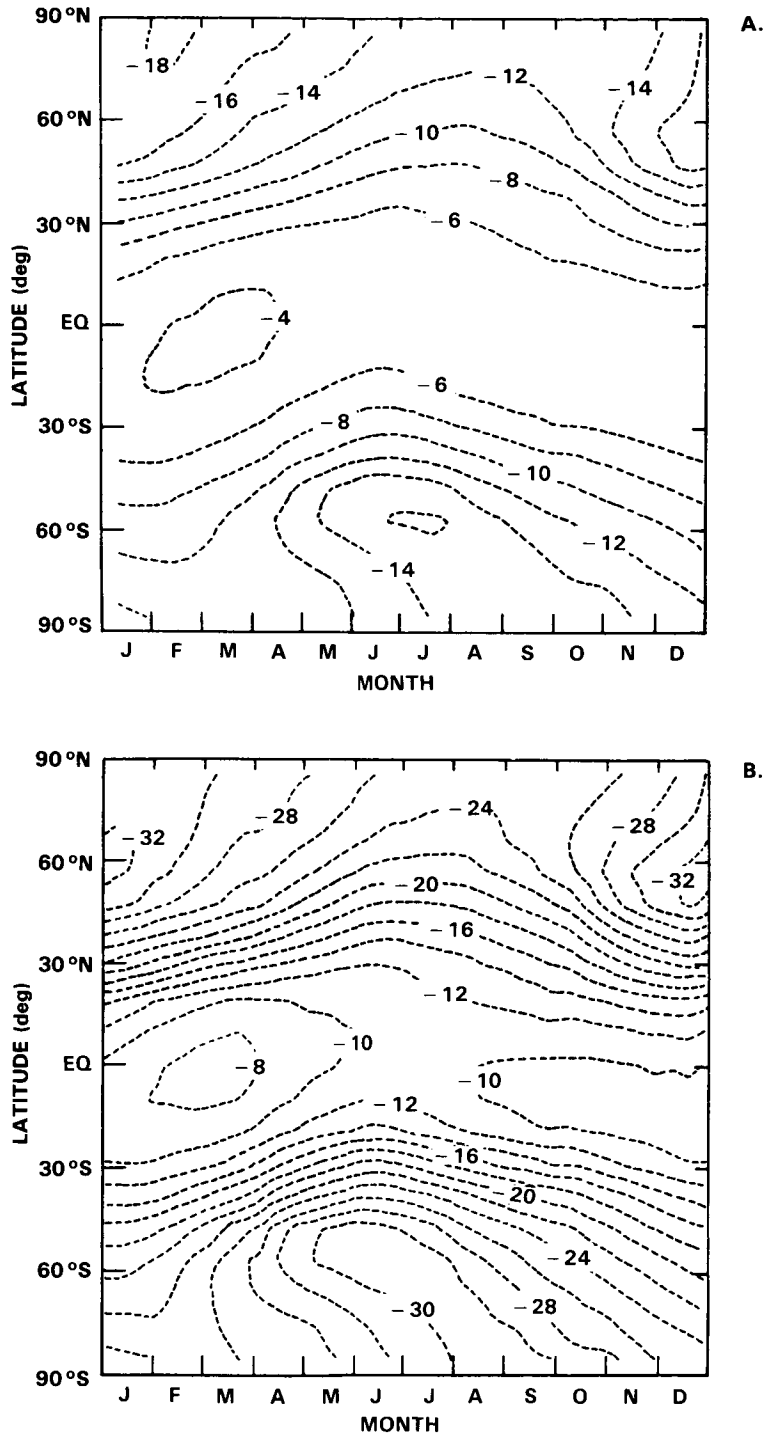


**Figure 13-23.** Calculated steady-state percentage change of the ozone column relative to a reference atmosphere with 1.3 ppbv  $Cl_x$  as a function of latitude and season for two scenarios in Table 13-7: (a) S2A, 1980 fluorocarbon emission giving 8.2 ppbv  $Cl_x$  or an increase of 6.9 ppbv  $Cl_x$ ; (b) S3A, twice the 1980 flux of CFC giving 15.5 ppbv  $Cl_x$  or an increase of 14.2 ppbv  $Cl_x$ . The global average ozone changes are -8.5% and -18%, respectively. (AER 2-D model).

## MODEL PREDICTIONS

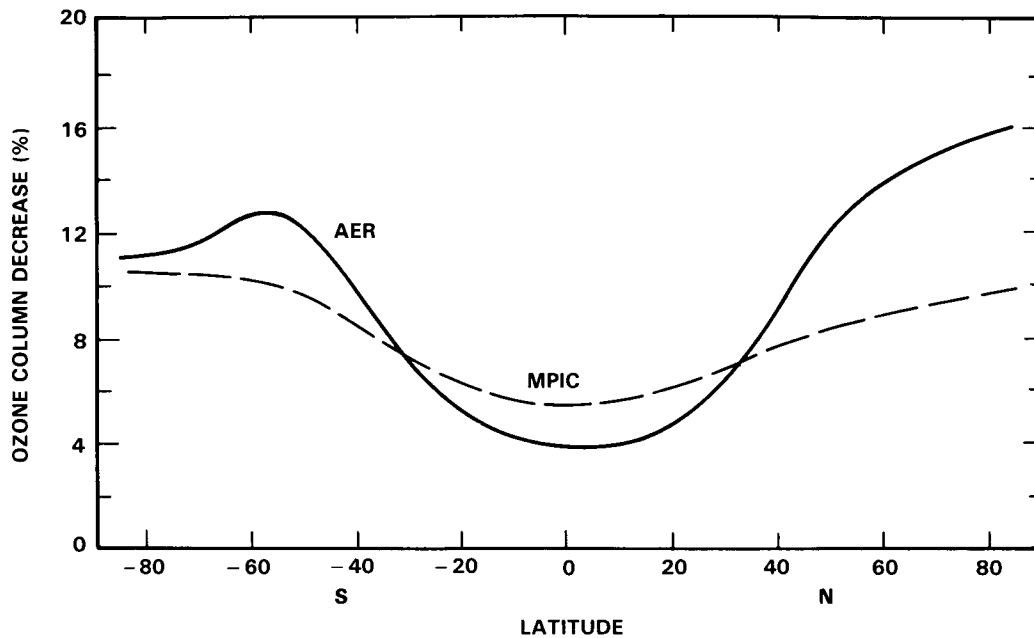


**Figure 13-24.** The effect of type of atmospheric dynamics used in two-dimensional models on the latitudinal variation of calculated ozone-column reduction (April). The increase of  $\text{Cl}_x$  is about 7 ppbv in each case: AER model, scenario S2A; MPIC model, scenario SMA.

occurs too slowly compared to dynamics to significantly increase the ozone densities at the lower altitudes. Particularly in the winter, it is likely that transport will be largely downward and poleward, at least in the zonal and seasonal average. This brings down air parcels that are severely depleted in ozone, having come from the photochemically controlled region above 35 km where ozone changes are expected to be large in all the models. The ozone change characteristic of the upper stratosphere may be thought of as “frozen” as air descends into the winter lower stratosphere, where photochemistry is too slow to change it locally. On the other hand, oxygen photolysis occurs on a time scale that is substantially shorter than the dynamical time scale at altitudes as low as about 20 km in the tropics. Therefore, photochemical self-healing can be very effective at tropical latitudes, yielding important increases in local ozone density that offset the depletions occurring at higher altitudes, similar to but larger than that seen in the one-dimensional models.

An important element in the evaluation of latitudinal gradients in the ozone changes to be expected, however, is the strength of horizontal mixing. If horizontal mixing rather than vertical motion dominates the transport of ozone into high latitudes in the lower stratosphere, the large changes in ozone due to descending motion will be reduced by mixing with air in which self-healing may occur. It therefore is important to understand the temporal and spatial structure of downward flow (particularly in the winter and spring) and the competition between mixing and advection. As discussed in more detail in Chapter 12, the primary differences between the models presented here are due to their differences in the formulation of dynamics. The MPIC model is a classical Eulerian model in which large eddy diffusion coefficients are employed. The AER and GS models are isentropic and residual Eulerian models, respectively, and employ much smaller horizontal mixing coefficients relative to the MPIC model. This implies that the latitudinal gradients in methane and in ozone depletion should be expected to be greater in the AER and GS models than in the MPIC model. More detailed comparisons and discussions of these two types of models are presented in Chapter 12.

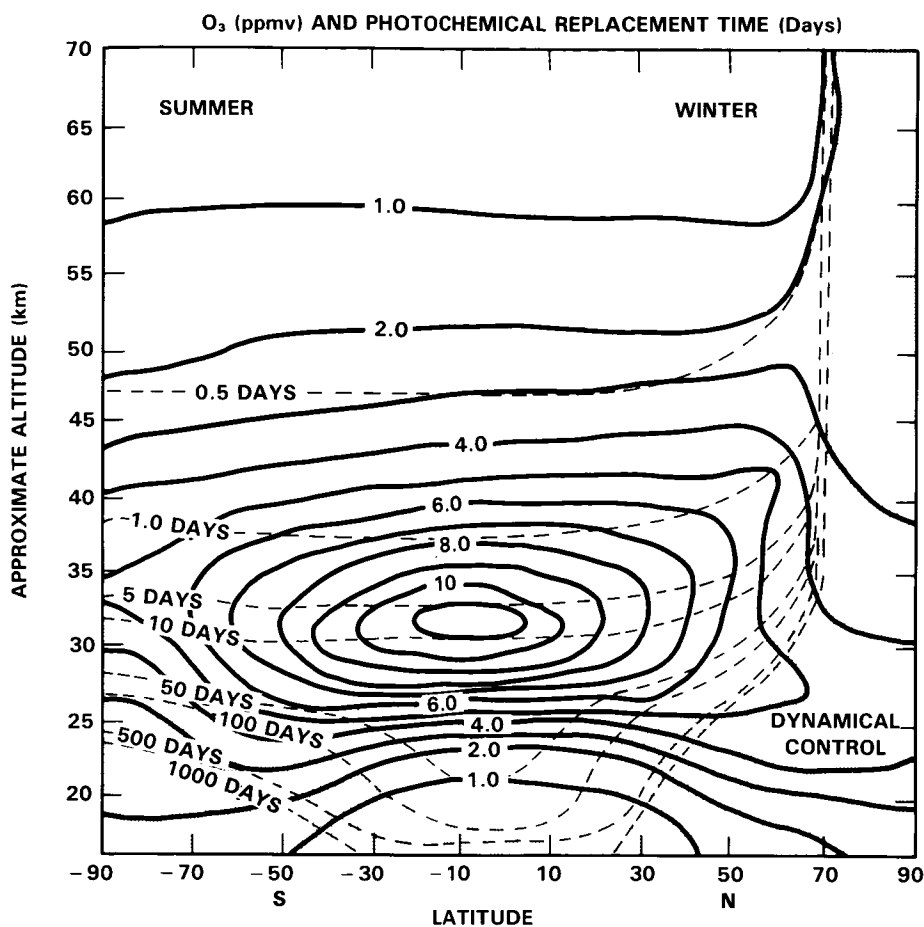


**Figure 13-25.** Computed local photochemical ozone replacement time ( $t = \text{local ozone concentration} / \text{twice the rate of molecular oxygen photolysis}$ ) in days (dashed lines) and ozone mixing ratio in ppmv (solid lines) for the end of December from the GS model. Note the long ozone photochemical replacement times ( $> 100$  days) in the lower stratosphere, particularly at high latitudes in the winter hemisphere. The shaded area indicates the region where ozone is likely to be dynamically controlled.

### Mixed Scenarios

Two-dimensional steady-state model studies were carried out in which it was assumed that methane increased by a factor of two and nitrous oxide increased by a factor of 1.2 while  $\text{Cl}_x$  increased by 6.7 ppbv (GS), 6.8 ppbv (MPIC), and 15.3 ppbv (MPIC), compare Table 13-7. Latitude-altitude contour maps of percentage ozone change are presented for the GS calculation for (NH) winter and spring (Figure 13-26a,b), for the MPIC model with 6.8 ppbv increase of  $\text{Cl}_x$  for (NH) winter (Figure 13-27a) and for spring (Figure 13-27b), and for 15.3 ppbv  $\text{Cl}_x$  for winter (Figure 13-28). Several interesting comparisons can be made among these figures.

The general effect of increasing the methane abundance is to reduce the magnitude of the calculated ozone changes. For the GS model, the qualitative features of the altitude-latitude contours are unchanged, Figure 13-21 vs Figure 13-26, but there are interesting quantitative differences. The high altitude polar maxima of ozone reduction are 55% without increasing  $\text{CH}_4$  and  $\text{N}_2\text{O}$  and 45% with the combined scenario.

MODEL PREDICTIONS

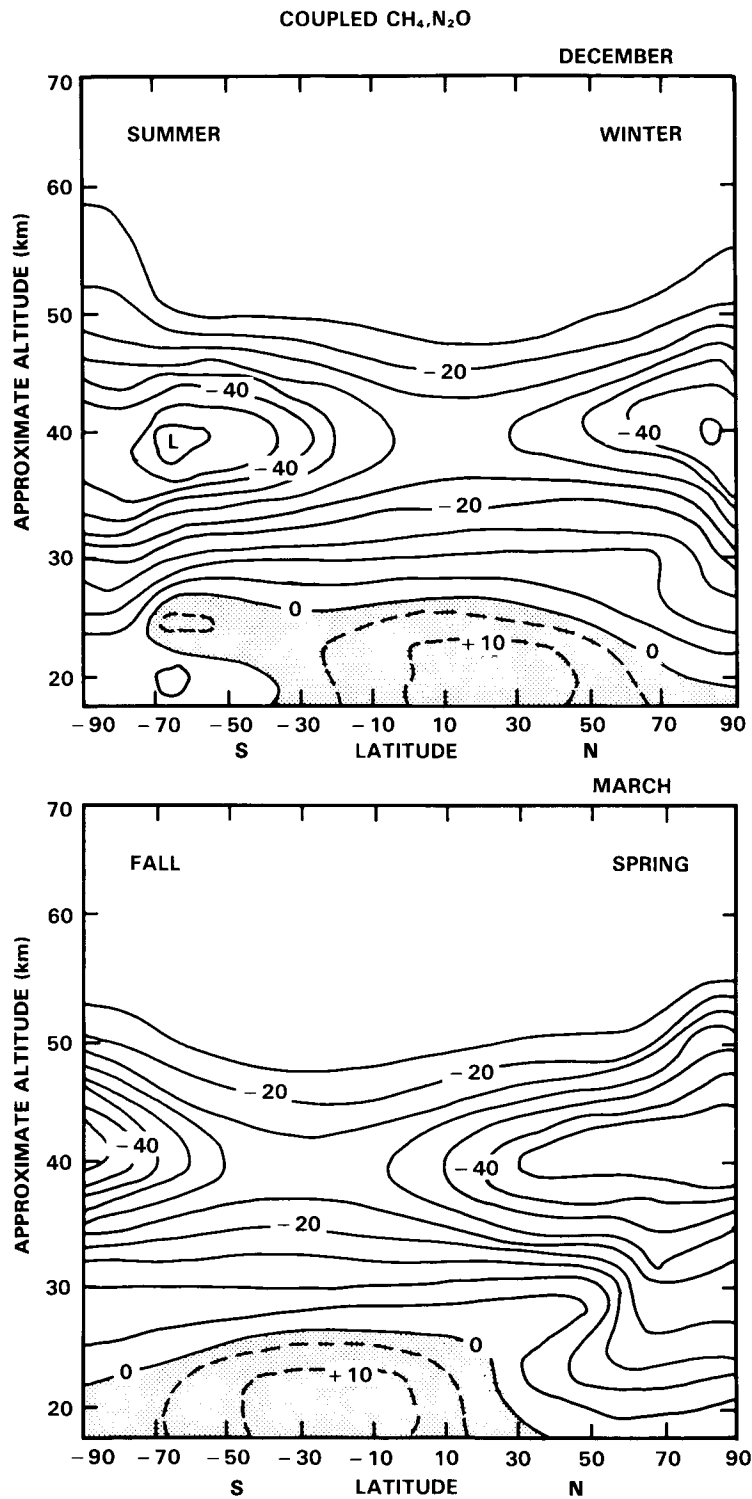


**Figure 13-26.** Effect of coupled perturbations—compare with Figure 13-21 Calculated steady-state local percentage ozone change as a function of latitude and altitude—for 1980 fluorocarbon emission giving 8.0 ppbv Cl<sub>x</sub> relative to reference atmosphere with 1.3 ppbv Cl<sub>x</sub>, or an increase of 6.7 ppbv and 2 × CH<sub>4</sub>, 1.2 × N<sub>2</sub>O (Table 13-7, Scenario S2C, GS 2-D model).

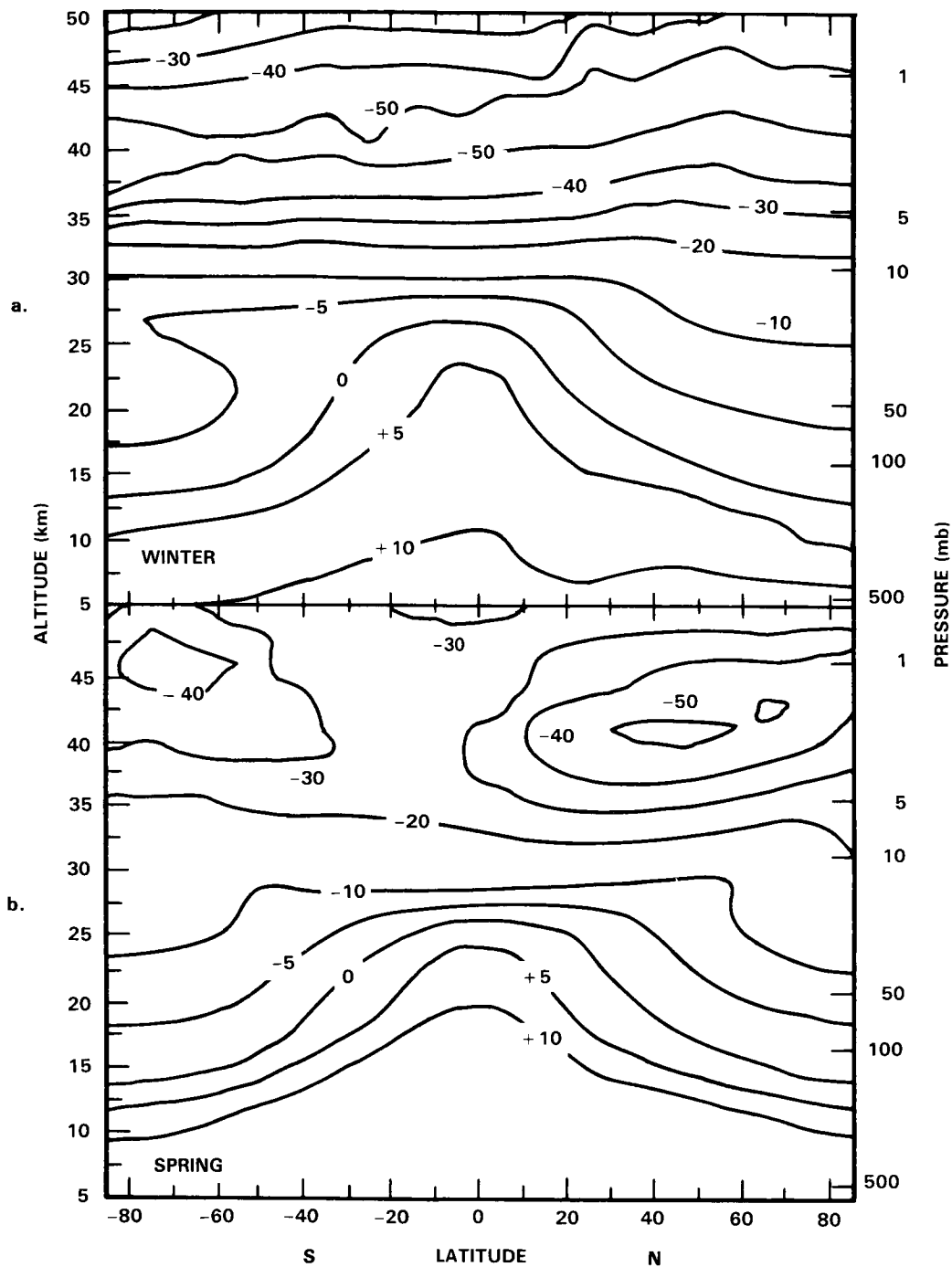


**Figure 13-27.** Effect of coupled perturbations—compare Figure 13-18. Calculated steady-state local percentage ozone change as a function of latitude and altitude—for 1980 fluorocarbon emission given 9.5 ppbv  $Cl_x$  relative to reference atmosphere with 2.7 ppbv  $Cl_x$ , or an increase of 6.8 ppbv and doubled methane,  $1.2 \times N_2O$  (Table 13-7, Scenario SMB, MPIC 2-3 Model).

## MODEL PREDICTIONS

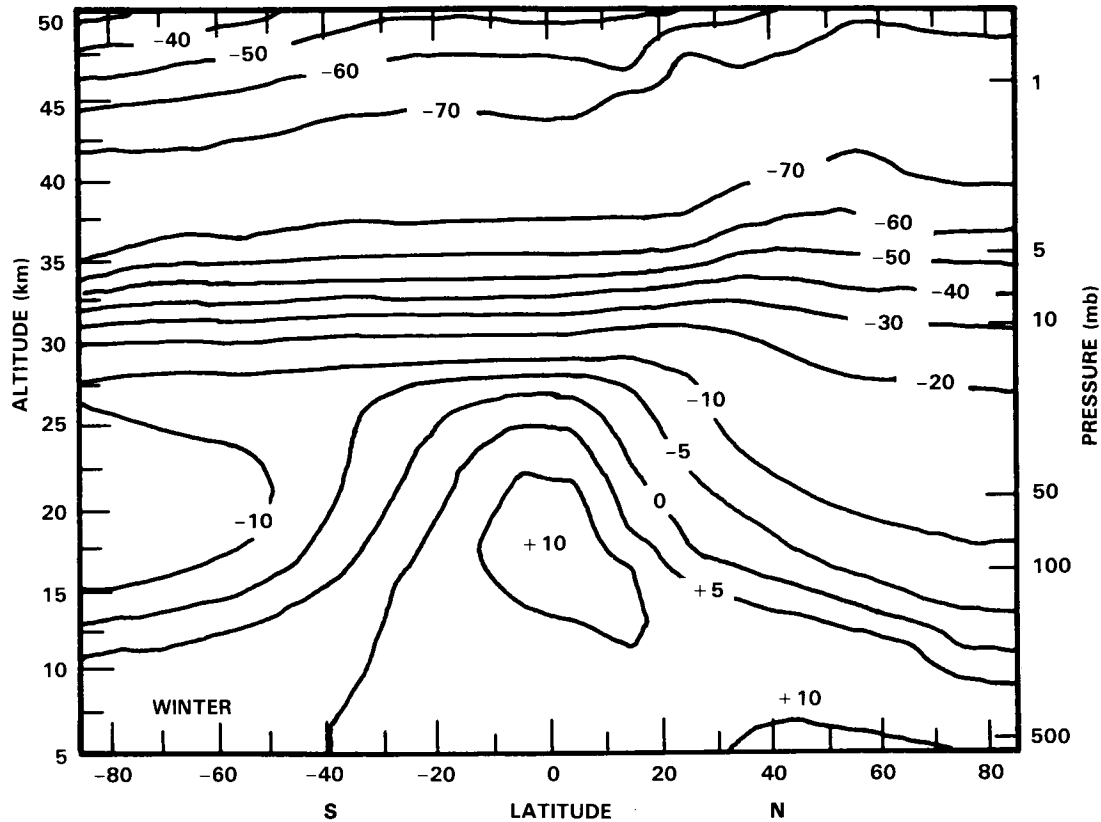


**Figure 13-28.** Same as Figure 13-27a but for twice the 1980 fluorocarbon flux, giving an increase of 15.3 ppbv  $\text{Cl}_x$  (Scenario SMC, MPIC model).

The saddlepoint near the equator is reduced from 35-40% (S2A) to 25-30% (S2C, combined scenario). The calculated latitudinal gradient in ozone depletion at 40 km is slightly greater than in the chlorine only case. In both cases the ozone depletion near 30 km is almost independent of latitude. The region of increased ozone in the lower stratosphere (at 18 km) is very nearly the same in both cases, but it covers a slightly greater range of latitude at low altitude for the case of the combined perturbation. In the region of ozone increase, the maximum value of the increase is 15% for S2A and 10% for S2C. These maximum values near the equator are consistent with the interpretation as ozone self healing (greater penetration of oxygen-dissociating radiation to lower altitudes as ozone is reduced), since larger ozone reduction in the upper stratosphere shows larger ozone increase at 20 km at the equator. The GS model results in Figures 13-21 and 13-26 extend down only to 18 km, and thus do not show effects in the lowest stratosphere.

The MPIC cases in winter of 6.8 ppbv added  $\text{Cl}_x$  (Figure 13-18a) and  $\text{Cl}_x$  plus change of methane and nitrous oxide (Figure 13-27a) are given down to 5 km altitude, and these figures allow for comparisons throughout the stratosphere. Ozone reductions are somewhat smaller in the combined scenario in the upper and middle stratosphere, but the structure of the contours is similar. In the lower stratosphere and upper troposphere, there is a larger region of ozone formation in the case of added methane and nitrous oxide than for the case of  $\text{Cl}_x$  only. Ozone decreases in Figure 13-18a are turned into ozone increases in Figure 13-27a in the lower Southern Hemisphere (summer) stratosphere above about  $40^\circ$ , and in this region there is insufficient solar radiation at wavelengths below 242 nm for this ozone increase to be "ozone self healing" in the same sense that it was discussed in connection with the GS model (additional ozone

formation from oxygen photolysis). The explanation might be called "ozone self-healing of the second kind". As ozone is reduced by  $\text{Cl}_x$  in the upper stratosphere, there is increased penetration of solar radiation at wave lengths below the ozone cross-section maximum (250 nm) which produces significant oxygen dissociation at wavelengths around 210 nm down to about 20 km in the tropics. Also, there is increased penetration of solar radiation above 250 nm, which produces significant singlet atomic oxygen (from ozone photolysis) at wavelengths below 310 nm, down to the surface of the earth. This singlet atomic oxygen, in part, reacts with water vapor or with methane to produce hydroxyl radicals. The hydroxyl radicals undergo a series of reactions that both destroy and produce ozone (Chapter 4). In particular, there are the methane- $\text{NO}_x$ -smog reactions, which give a net formation of ozone in the lower stratosphere and upper troposphere (Chapter 4). In the lower stratosphere the  $\text{NO}_x$  species slowly but non-negligibly destroy ozone, and hydroxyl radicals convert the catalytically active  $\text{NO}_2$  into the inert reservoir species  $\text{HNO}_3$ . In this way hydroxyl radicals destroy an ozone destroyer, and this increases ozone by way of a double negative. Even though the time scale for meridional transport of ozone is about 100 days, the residence time of carbon-14 and presumably ozone at about 20 km is the order of one year (Telegadas, 1971; Johnston *et al.*, 1976), and the relatively slow  $\text{HO}_x$  and  $\text{NO}_x$  photochemistry, which is largely driven by the penetrating solar radiation near 300 nm, significantly modifies ozone even at high latitudes at this longer time scale. Nitrous oxide is photochemically inactive at these low altitudes, and the increase of ozone as methane is increased (Figure 13-18 vs 26) identifies the methane- $\text{NO}_x$ -smog reactions as an important component in the model at these low altitudes. The "ozone self-healing of the second kind" and related photochemical reactions that slowly destroy ozone make important contributions to the model-calculated ozone column. This discussion is supplementary to that for "ozone self-healing" in connection with solar radiation near 200 nm, which dissociates molecular oxygen.

The MPIC model for spring with 6.8 ppbv added  $\text{Cl}_x$  and with increased methane and nitrous oxide (Figure 13-27b) shows in the upper stratosphere the two polar maxima and the equatorial saddlepoint minimum that are characteristic of the GS and AER models at almost all seasons, with or without the combined scenario (Figures 13-19, 20, 21, 26). The MPIC model without added methane for spring (Figure 13-18b) also shows this structure to some extent.

An interesting feedback between chlorine and nitrogen oxides in the stratosphere is illustrated by the two-dimensional MPIC model. Table 13-9 shows that as  $\text{Cl}_x$  increases the maximum mixing ratio of  $\text{NO}_y$  ( $\text{NO} + \text{NO}_2 + \text{NO}_3 + 2\text{N}_2\text{O}_5 + \text{HNO}_3 + \text{HNO}_4 + \text{ClNO}_3$ ) increases. Upon photolysis, nitrous oxide ( $\text{N}_2\text{O}$ ) is converted to nitrogen and oxygen; and when nitrous oxide reacts with singlet atomic oxygen, the principal product is nitric oxide ( $\text{NO}$ ), which is the dominant source of stratospheric nitrogen oxides ( $\text{NO}_y$ ). Nitrous oxide is photolyzed by solar radiation with wavelengths below about 210 nm, but singlet atomic oxygen is mostly formed from ozone photolysis at wavelengths near 300 nm. The absolute amount of solar radiation around 300 nm is greater than that around 200 nm, so that reduction of ozone by  $\text{Cl}_x$  in the upper stratosphere more strongly increases nitric oxide formation (radiation near 300 nm) than it increases nitrous oxide photolysis (radiation near 200nm) in the middle stratosphere. The net effect is to increase the column of nitrogen oxides as stratospheric chlorine increases, which is demonstrated in Table 13-9.

Model calculations indicate that ozone changes may have already occurred in the present day atmosphere (2.7 ppbv total chlorine) compared to the atmosphere of 1965 (about 1.3 ppbv total chlorine), and these calculations have implications for ozone monitoring. Figure 13-29 presents a contour plot of the calculated percentage ozone changes for this period from the GS model for a  $\text{Cl}_x$  only scenario and neglecting temperature feedback, and Figure 13-30 shows the same calculation from the MPIC model. These changes should be considered upper limits because the mitigating effects of simultaneous methane and carbon dioxide

## MODEL PREDICTIONS

**Table 13-9.** Effect of Increasing  $Cl_x$  on Maximum Value of Stratospheric  $NO_y$  Mixing Ratio and on Nitrous Oxide and Chlorofluorocarbon Lifetimes. MPIC 2-D Model.

Scenario	ppbv $Cl_x$ at 40 km	ppbv $NO_y$ Maximum	Lifetime/Centuries		
			$N_2O$	CFC-11	CFC-12
1964	1.3	18	1.85	—	—
1985	2.7	18	1.8	0.5	1.5
1980 CFC Emission	9.5	22	1.65	0.5	1.4
1980 CFC Emission, $2 \times CH_4$ , $1.2 \times N_2O$	9.5	24	1.65	0.5	1.4
Twice 1980 CFC Flux, $2 \times CH_4$ , $1.2 \times N_2O$	18.	28	1.5	0.5	1.3

increases have not been considered (see one-dimensional model calculations). At 40 km, both models indicate large local ozone reductions in the north polar region (GS, 30%; MPIC, 20%) and in the south polar region (GS, 30%; MPIC, 10%), and both models give at least a 10% ozone reduction from pole to pole. The GS model shows significant local ozone reductions even at 25 km in the summer and winter polar regions, due to downward transport. This suggests that a monitoring strategy aimed at detecting an ozone response at the earliest possible time should provide measurements at high latitudes, both in the lower and upper stratosphere. Further, detailed measurements of the latitudinal distributions of methane and HCl would be of value in evaluating how realistic these predicted gradients in ozone depletion at high latitude might be. Most of the ozone at high latitudes is located at low altitudes (below 25 km) where it is not readily accessible to satellite observations. This poses a severe challenge to attempts to detect changes in the ozone column and vertical profiles at high latitudes, where large changes in total ozone may occur at the earliest times as the atmospheric chlorine content increases. However, a carefully designed program would be needed to detect a clear trend against the extreme zonal and temporal variability at high latitudes in late winter and spring, particularly in the Northern Hemisphere.

### Comparisons

The AER and GS models represent one method of treating atmospheric motions in two dimensional models, and the MPIC model represents a different method (Chapter 12). In comparison with atmospheric observations, one method is more successful than the other in some cases, and the reverse applies in other cases. As pointed out in Chapter 12, for example, the AER and GS models severely underestimate nitrogen oxides in the lower stratosphere, at 30 degrees north for example, as compared with the observations by the LIMS satellite. For 30° north during March,  $NO_y$  vertical profiles are given in Figure 13-31 as calculated by AER and by MPIC, and these are compared with the observed LIMS profile of  $NO_2$  and  $HNO_3$  at night, which is a lower limit to  $NO_y$ . For this example, the AER model underestimates nitrogen oxides by a factor between 3 and 8 over the range of 25 to 20 km, whereas the MPIC model is more

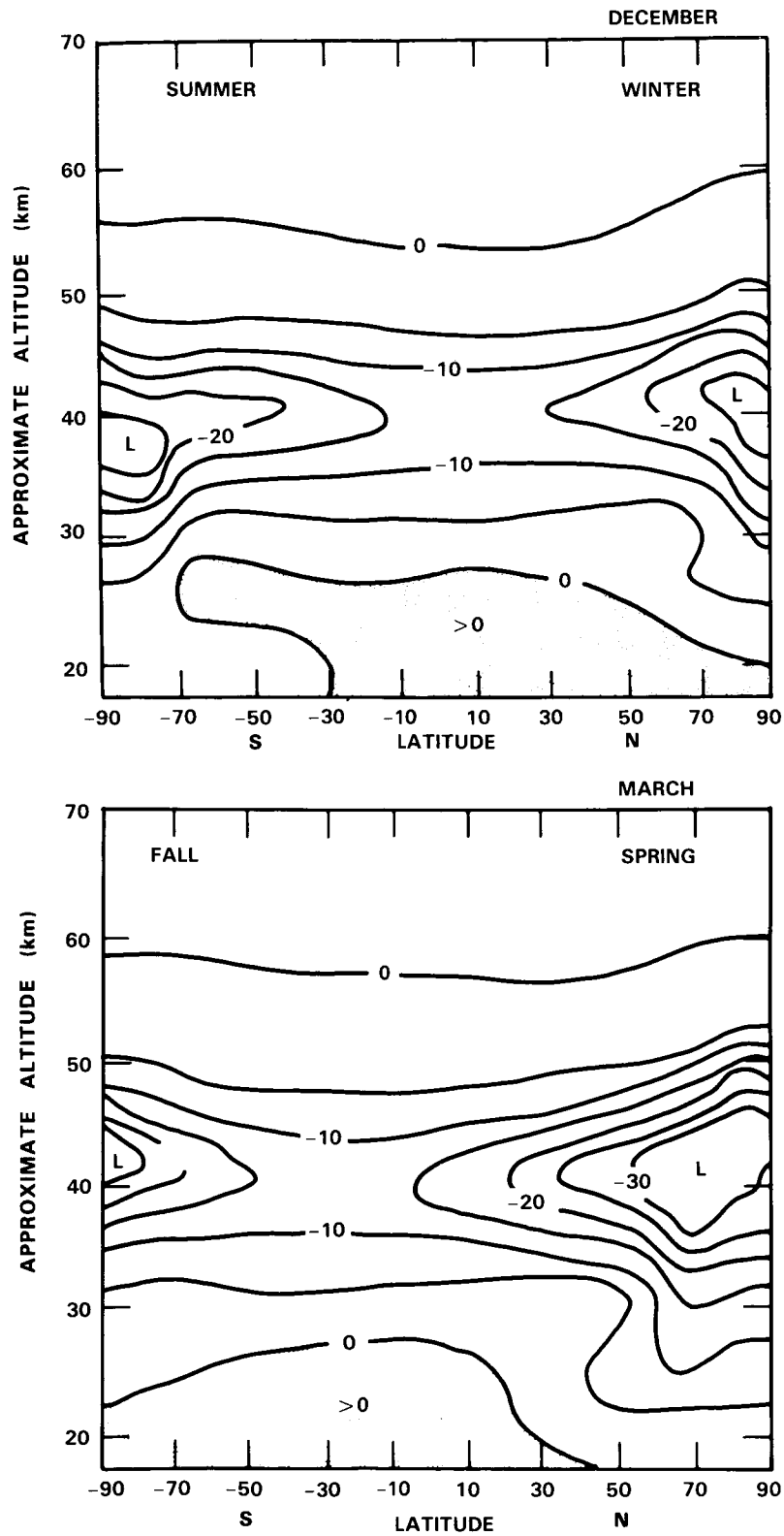


Figure 13-29. Calculated local percentage ozone changes from 1965 (1.3 ppbv Cl<sub>x</sub>) to 1985 (2.7 ppbv Cl<sub>x</sub>) using GS model and Cl<sub>x</sub> only perturbation.

## MODEL PREDICTIONS

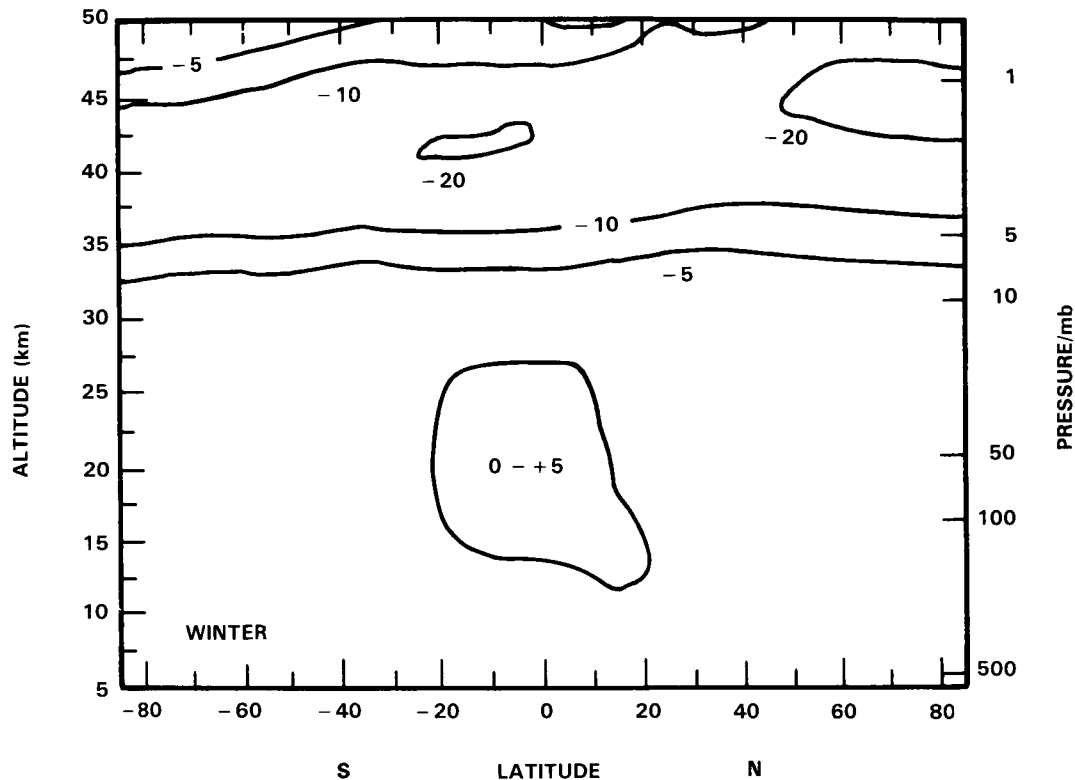


Figure 13-30. Similar to Figure 13-29 (MPIC 2-D model).

successful in this range. In the middle and upper stratosphere, both models give satisfactory agreement with observations. In the upper stratosphere the AER and GS models more nearly reproduce the methane latitudinal variations. In spite of the differences in treatment of atmospheric motions and in spite of the various agreements and disagreements between model calculations and observations, these two types of model give the same general practical results so far as ozone changes by chlorine is concerned, for example, Figure 13-24. Both types of model show ozone depletion by added chlorofluorocarbons at all latitudes, both show a strong latitudinal gradient with minimum ozone reduction in the equatorial region.

It is interesting to compare two-dimensional global average calculations against local properties in the same model. The global average vertical profile of ozone reduction for scenario S2A (6.7 ppbv increase of  $\text{Cl}_x$ ) according to the Garcia-Solomon model is shown by Figure 13-32, and the local profiles are shown for  $4^\circ \text{N}$  and  $61^\circ \text{N}$ . The ozone decrease at high latitude is substantially larger than the global average at all altitudes. For the AER model with S2A perturbation, the ozone-column decrease is plotted as a function of latitude for all four seasons with the global average value indicated by a dashed line (Figure 13-33), and a similar graph is given as a function of months of the year for 0, 28, 47, and 66 degrees north latitude (Figure 13-34).

### 13.1.4 Comparison of 1-D and 2-D Results

Percentage changes of total ozone as calculated by one-dimensional models for various scenarios including chlorofluorocarbons are summarized in Tables 13-2 and 13-3. Many of these cases are illustrated by figures in Section 13.1.2, giving the vertical profile of calculated ozone change as a function of altitude.

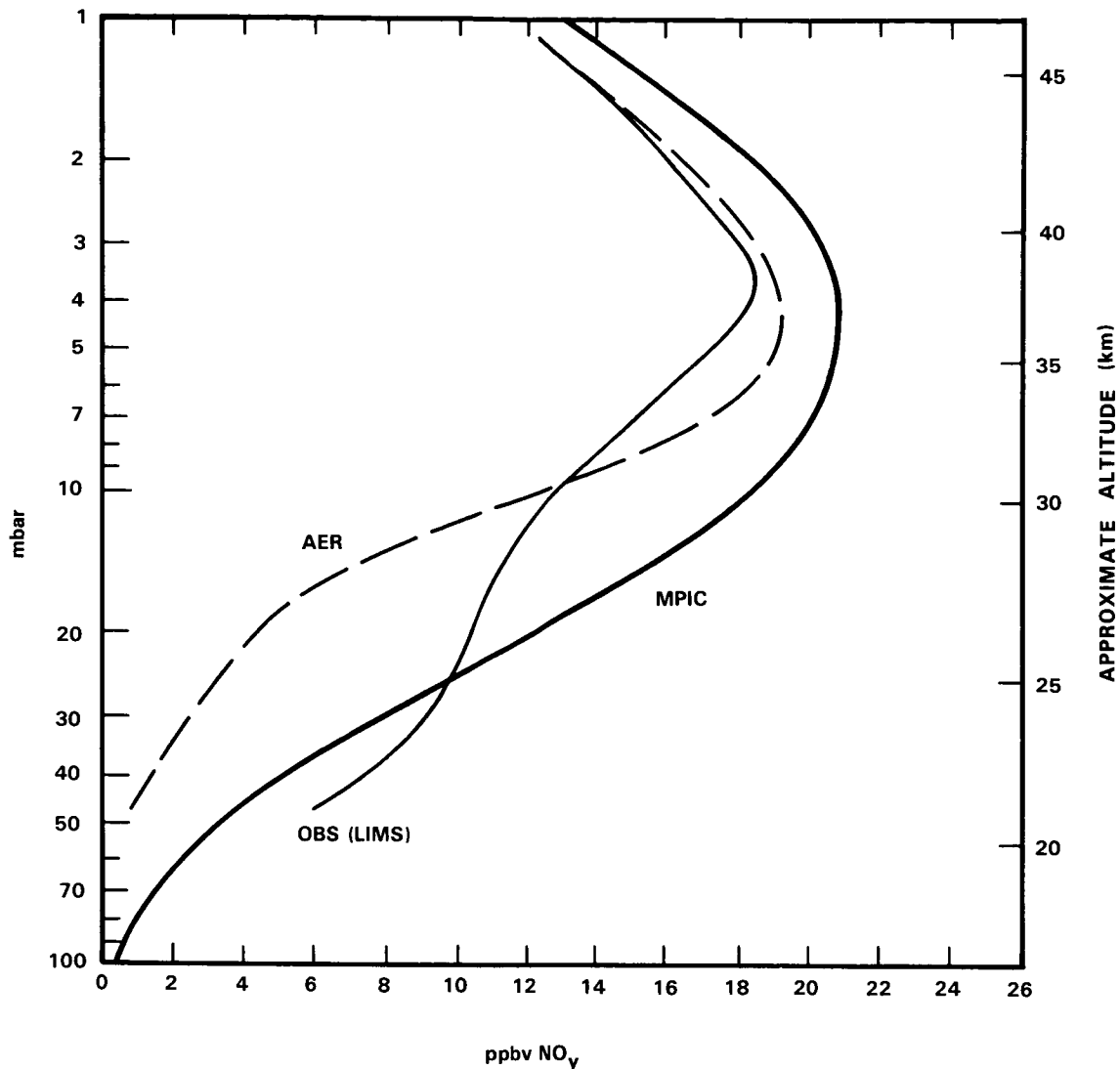


**Figure 13-31.** Comparison of calculated  $\text{NO}_y$  according to AER and MPIC 2-D models with LIMS satellite observed  $\text{NO}_2 + \text{HNO}_3$  at night at  $30^\circ \text{N}$  during March.

Global-average percentage ozone changes according to two-dimensional models are given by Table 13-8. The seasonal and latitudinal dependence of the change of the ozone vertical column as calculated by 2-D models are shown by figures in Section 13.1.3. This section compares the results of these 1-D and 2-D models with respect to calculated ozone changes.

Three profiles of percentage change in local ozone from the AER 2-D model at  $0^\circ$ ,  $30^\circ \text{N}$ , and  $60^\circ \text{N}$  in April are compared with the AER 1-D model profile in Figure 13-35 for 8 ppbv  $\text{Cl}_x$  relative to 1.2 ppbv  $\text{Cl}_x$  as reference. The 1-D profile does not correspond closely to any local 2-D profile. For instance, the calculated self-healing effect occurs at a higher altitude (23 to 30 km) in the 1-D model than those of the  $0^\circ$  and  $30^\circ \text{N}$  profiles calculated by the 2-D model, which calculates no significant self-healing for the  $60^\circ \text{N}$  profile. The 1-D model calculates larger ozone reductions above 40 km than the 2-D model, due in part to differences between the 1-D and 2-D model atmospheres (that is, temperature and air density)

## MODEL PREDICTIONS

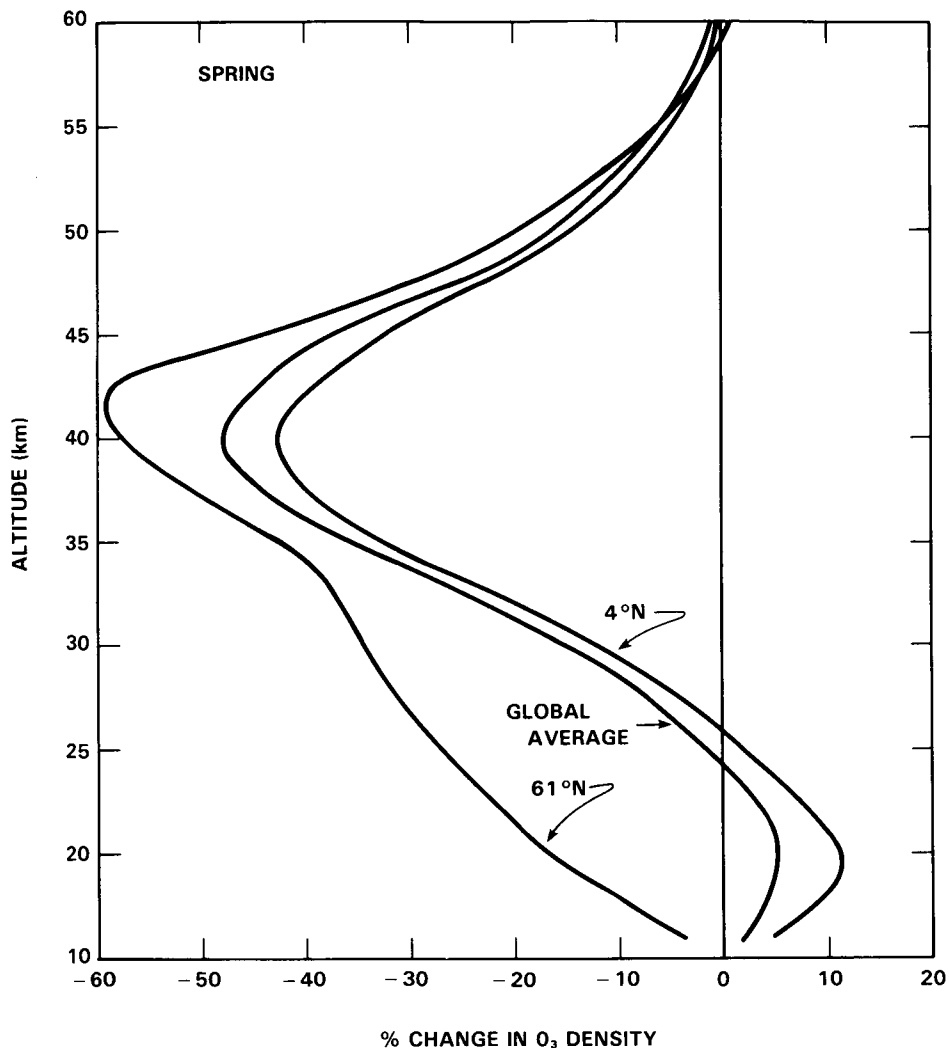


**Figure 13-32.** Vertical profiles of the calculated ozone changes shown in Figure 13-21 for 4° N, 61° N, and for the global average. (GS 2-D model, 6.7 ppbv increase of Cl<sub>x</sub>).

and in part to the differences in the concentrations of transport dominated species such as water and methane between the two models.

For the AER models, the calculated ozone reduction at the spring equinox is plotted against latitude in Figure 13-36, together with the 1-D model result for the same perturbation. An important feature of this comparison is that the 2-D model gives much larger ozone reductions over the temperate and polar zones than that given by the 1-D model.

The global average 2-D results from Table 13-8 are compared with the 1-D results from Tables 13-2 and 13-3, and these comparisons are given in Tables 13-10 and 13-11. These tables are organized in terms of a quantity called "sensitivity", *S*, which is defined as the percentage ozone reduction divided by the ppbv of increased Cl<sub>x</sub>. For about a 7 ppbv increase of Cl<sub>x</sub>, the sensitivity of the 2-D models is 1.06 and 1.32 % per ppbv, and the 1-D models give values between 0.41 and 1.06. In general the global average

MODEL PREDICTIONS

**Table 13-10.** Comparison of 1-D and 2-D Model (Global Average) Results with Respect to Sensitivity S and Linearity L, Where  $Cl_x$  Is the Only Perturbation. Sensitivity Is Percentage Ozone Reduction Divided by ppbv  $Cl_x$  Increase. Linearity Is  $S(2)/S(1)$ , Which Is 1.00 if the Ozone Reduction Is Directly Proportional to  $Cl_x$  Increase.

Initial	$Cl_x$ /ppbv		% Ozone Decrease	S -%/ppbv	L	Model
	Final	Increase				
1.3	8.2	6.9	8.5	1.23		2-D
1.3	15.5	14.2	18.	1.27	1.03	AER
1.	8.	7.	4.6	0.66		1-D
1.	15.	14.	15.	1.07	1.63	AER
		7.	5.1	0.73		1-D
		14.	12.2	0.87	1.20	LLNL
		7.	2.9	0.41		1-D
		14.	17.8	1.27	3.10	Harvard
1.1	8.1	7.	9.1	1.30		1-D
2.5	8.1	5.6	7.4	1.32		
2.5	14.8	12.3	20.6	1.67	1.27	MPIC
1.0	7.5	6.5	4.1	0.63		1-D
1.0	14.0	13.0	8.8	0.68	1.08	IAS
2.7	9.5	6.8	7.2	1.06		2-D MPIC

2-D ozone reduction is greater than that of the 1-D models. For about a 14 ppbv increase of  $Cl_x$ , the sensitivity of the AER 2-D model is 1.27 % per ppbv, and the range of 1-D results is 0.87 to 1.67, which averages to a value almost as large as that of the AER 2-D model (compare Figure 13-36).

For ozone reductions with doubled methane and with a 20% increase in nitrous oxide in addition to increases in  $Cl_x$ , 1-D and 2-D model results (MPIC) are compared in terms of "sensitivity" in Table 13-11. Added methane reduces the sensitivity of both 2-D and 1-D models. For about 7 ppbv  $Cl_x$  increase, the global average MPIC model gives 35% greater ozone reduction than the average of the five 1-D models in Table 13-11. For about 14 ppbv  $Cl_x$  increase, the 2-D model is 16% more "sensitive" than the average of these 1-D models. The number of 2-D model calculations in this study is small, but within this small sample it is found that the global average ozone reduction calculated by the 2-D models is greater than that calculated by 1-D models for the same scenario.

For 1-D models, the reduction of ozone by increased  $Cl_x$  is not a linear function, as illustrated by Figure 13-6. A plot of "change of ozone column" against "change of  $Cl_x$ " shows downward curvature. The term "sensitivity" defined above increases with "change of  $Cl_x$ ". An interesting question is whether 2-D models are linear or nonlinear in this sense of the word. In this study there are not enough 2-D model

## MODEL PREDICTIONS

**Table 13-11.** Comparison of 1-D and 2-D (Global Average) Model Results with Respect to Sensitivity S and Linearity L (for Definitions See Table 13-10). Increasing  $Cl_x$  and  $2 \times CH_4$  and  $1.2 \times N_2O$ .

Initial	$Cl_x$ /ppbv		% Ozone Decrease	S -%/ppbv	L	Model
	Final	Increase				
2.7	9.5	6.8	4.5	0.66		2-D
2.7	18.	15.3	11.1	0.73	1.10	MPIC
1.1	8.1	7.0	6.0	0.86		1-D
2.5	8.1	5.6	4.3	0.77		
2.5	14.8	12.3	12.0	0.98	1.27	MPIC
		7.	3.4	0.49		1-D
		14.	7.8	0.56	1.15	LLNL
		7.	3.0	0.43		1-D
		14.	8.2	0.59	1.37	Harvard
		7.	3.3	0.47		1-D
		14.	8.8	0.63	1.47	AER
		7.	3.1	0.44		1-D
		14.	7.2	0.51	1.16	DuPont
1.0	7.5	6.5	2.3	0.35		1-D
1.0	14.0	13.0	5.6	0.43	1.23	IAS

results to test for linearity by means of a plot such as that of Figure 13-6. For any 2-D model used here, there are only three values of  $Cl_x$ : a reference value, a value near 8 ppbv, and a value near 15 ppbv. These three points can be used to estimate linearity in terms of change of sensitivity with increase of  $Cl_x$ . In Tables 13-10 and 13-11, a quantity "linearity" L is defined as the ratio of two sensitivities. If this ratio is 1.00 the change of ozone is linear over the range of  $Cl_x$  included in the test. For nonlinearity in the sense of that shown by 1-D models (Figure 13-6), the value of L is greater than 1.00. With opposite curvature L is less than one.

For added  $Cl_x$  as the only perturbation, the AER 2-D model is compared with the 1-D models of this study for linearity in Table 13-10 as ratio of sensitivities, S. The values of L are given as the sixth column of the table. For the AER 2-D model the global average value of L is 1.03, whereas the value for the AER 1-D model for the same range of  $Cl_x$  is 1.63. The AER 1-D model result is strikingly more nonlinear than global average results from the AER 2-D model. The other 1-D models give values of L between 1.20 and 3.1. As discussed in Chapter 12, these differences in linearity among the models is related to the amount of  $NO_y$  predicted by the models. Over the range of 1 to 15 ppbv  $Cl_x$ , the global average results of the AER 2-D model are much more nearly linear than the results of the 1-D models.

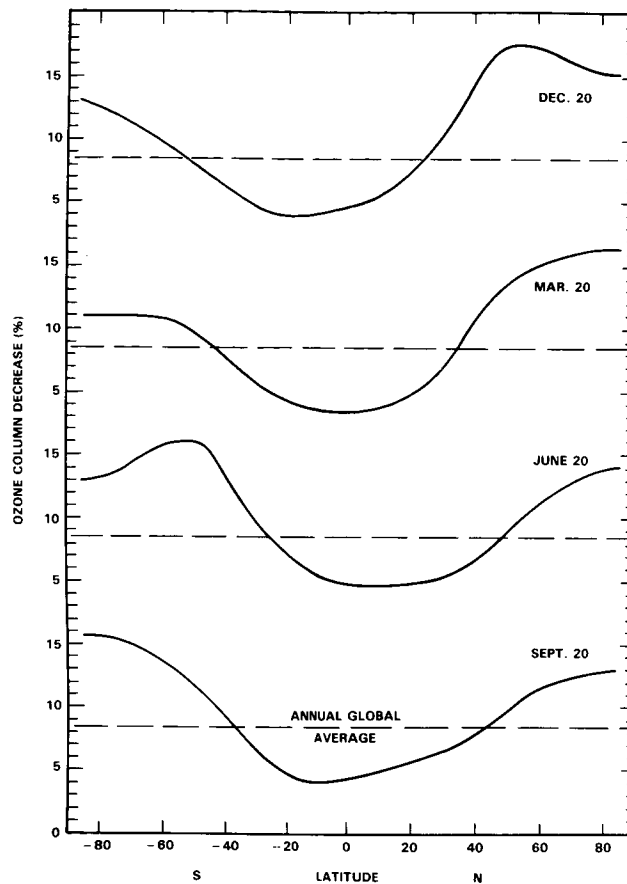


**Figure 13-33.** Calculated ozone-column decrease as a function of latitude for each of four seasons for conditions of Figure 13-23a with the annual, global-average value included as horizontal line (AER 2-D model).

A similar result is obtained in Table 13-11, where increases of methane and nitrous oxide are included. The MPIC 2-D model gives 1.10 as its value of  $L$ , where 1.00 represents linearity, and the MPIC 1-D model has the value 1.27. The ozone-reduction results of the MPIC 2-D model are much more nearly linear than those of the MPIC 1-D model. The 1-D models of Table 13-11 cover the range 1.15 to 1.41 in the ratio  $L$ . With added methane and nitrous oxide, the 1-D models are less nonlinear than they are in the cases of added  $Cl_x$  only.

By use of the sensitivity function  $S$  for specific values of latitude and season for two different increases in  $Cl_x$ , one can calculate a two dimensional map of the function  $L$ , which gives the local and seasonal degree of nonlinearity of the 2-D models. For the AER 2-D model, values of  $S$  for both 6.9 and 14.2 ppbv are listed for seven latitudes and for four seasons in Table 13-12. Also included in the table are the values of  $L$  for the same range of seasons and latitudes. At all seasons and latitudes, local changes of ozone according to the 2-D model are much more nearly linear than any of the 1-D models (compare Table 13-10). The range of values of  $L$  is 0.82 to 1.08, while the global average value is 1.03. The values of  $L$  between  $28^\circ S$  and  $28^\circ N$  are all greater than that for the global average, that is more nonlinear; and values in the polar region are somewhat less than 1.00, which corresponds to slight nonlinearity in the opposite sense.

**MODEL PREDICTIONS**

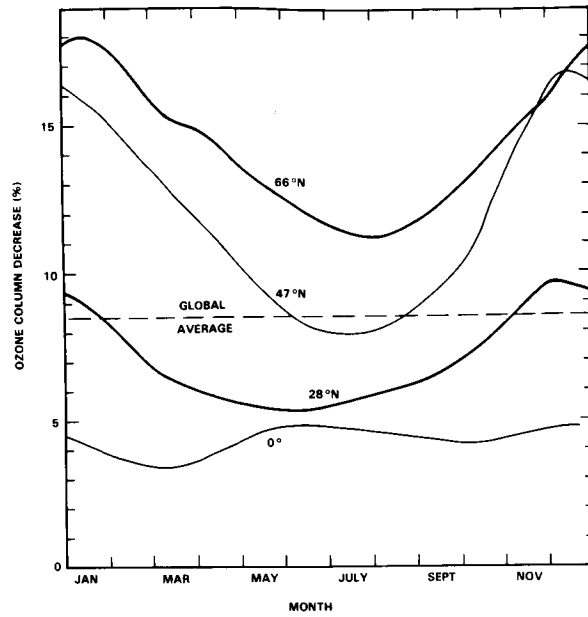


**Figure 13-34.** Same as Figure 13-33, except displayed as a function of the months of the year at 4 selected latitudes.

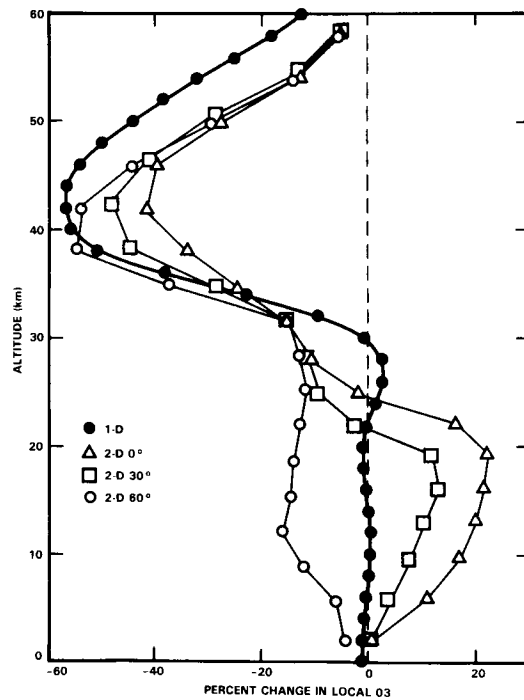


**Figure 13-35.** Comparison of percentage change of local ozone as a function of altitude as calculated by the AER 1-D model with three such profiles at 0, 30 and 60 degrees N calculated by the AER 2-D model for April.

MODEL PREDICTIONS

**Table 13-12.** Local and Seasonal Ozone Sensitivity S (Percent Ozone Decrease Divided by ppbv Cl<sub>x</sub> Increase) and Test for Local and Seasonal Linearity L (S for 14.2 ppbv Cl<sub>x</sub>/S for 6.9 ppbv Cl<sub>x</sub>) in Terms of AER Two-dimensional Model.

Case	Season	Latitude						
		85°S	56°S	28°S	0	28°N	56°N	85°N
S(14.2)	W	1.70	1.37	0.71	0.63	1.37	2.23	2.15
	Sp	1.71	1.93	1.05	0.59	0.93	1.78	1.91
	Su	2.05	2.13	1.37	0.71	0.87	1.48	1.78
	F	2.02	1.65	0.90	0.68	1.19	1.89	1.80
S(6.9)	W	1.79	1.30	0.64	0.61	1.29	2.47	2.48
	Sp	1.64	1.84	0.97	0.56	0.86	1.80	2.33
	Su	2.07	2.28	1.20	0.67	0.81	1.47	2.00
	F	2.18	1.71	0.81	0.63	1.08	1.91	1.92
L	W	0.95	1.06	1.11	1.04	1.06	0.90	0.87
	Sp	1.04	1.05	1.08	1.05	1.08	0.99	0.82
	Su	0.99	0.93	1.06	1.07	1.07	1.01	0.89
	F	0.93	0.96	1.11	1.08	1.10	0.99	0.94

Global Average: S(14.2) = 1.27; S(6.9) = 1.23; L = 1.03.

AER 1-D: S(14. ) = 1.07; S(7. ) = 0.66; L = 1.63

For Cl<sub>x</sub> perturbations including increase of methane and nitrous oxide, values of the sensitivity function S and the linearity test function L are given for the MPIC 2-D model as a function of latitude and season in Table 13-13. The global average value of L is 1.10, and the range of values in Table 13-13 is 0.96 to 1.22. The difference between the maximum value and minimum value of L is 0.26, which happens to be exactly the same as that for the AER model (Table 13-12). This result indicates that the latitudinal and seasonal variation of linearity of the MPIC model and the AER model are about the same. On the average, however, the MPIC model with L of 1.10 is more nonlinear than the AER model with average L equal to 1.03.

In 1-D models the nonlinear phenomenon is thought to be driven by the strong chemical interactions between the chlorine (Cl<sub>x</sub>) and nitrogen (NO<sub>y</sub>) species. Prather *et al.* (1984) argued that as stratospheric concentration of Cl<sub>x</sub> approaches that of NO<sub>y</sub> a significant portion of NO<sub>y</sub> in the lower stratosphere will be tied up in the form of ClNO<sub>3</sub>, a chlorine reservoir species formed by recombination of NO<sub>2</sub> and ClO. Formation of ClNO<sub>3</sub> reduces the concentrations of other forms of NO<sub>y</sub> species, including NO, NO<sub>2</sub>, HNO<sub>3</sub>, and HNO<sub>4</sub>, resulting in higher OH in the lower stratosphere (since OH is removed mainly by reaction

## MODEL PREDICTIONS

**Table 13-13.** Local and Seasonal Ozone Sensitivity S (Percent Ozone Decrease Divided by ppbv Cl<sub>x</sub> Increase) and Test for Local and Seasonal Linearity L (S for 15.3 ppbv Cl<sub>x</sub>/S for 6.8 ppbv Cl<sub>x</sub> in Terms of MPIC Two-Dimensional Model, Including Double Methane and 20% Increase of Nitrous Oxide.

Case	Season	Latitude						
		85°S	55°S	25°S	0	25°N	55°N	85°N
S(15.3)	W	1.02	0.86	0.67	0.59	0.66	0.93	0.96
	Sp	1.05	0.98	0.64	0.50	0.64	0.90	0.98
	Su	0.97	0.95	0.64	0.62	0.68	0.80	1.00
	F	0.97	0.89	0.63	0.60	0.64	0.85	0.98
S(6.8)	W	0.91	0.80	0.59	0.55	0.57	0.94	0.98
	Sp	0.92	0.90	0.55	0.45	0.58	0.92	1.02
	Su	0.93	0.91	0.53	0.56	0.60	0.72	0.91
	F	0.97	0.87	0.54	0.55	0.55	0.72	0.96
L	W	1.12	1.08	1.12	1.08	1.15	0.99	0.98
	Sp	1.14	1.10	1.16	1.12	1.11	0.98	0.96
	Su	1.05	1.04	1.22	1.10	1.13	1.11	1.11
	F	1.00	1.02	1.19	1.10	1.16	1.18	1.14

Global Average: S(15.3) = 0.73; S(6.8) = 0.66; L = 1.10.

MPIC 1-D: S(12.3) = 0.98; S(5.6) = 0.77; L = 1.27

with HNO<sub>3</sub> and HNO<sub>4</sub> in the lower stratosphere). These factors, higher OH and lower NO, contribute to the greater efficiency of the chlorine catalyzed ozone removal cycles at the high chlorine concentrations. However, the region of the chemically induced nonlinearity occurs in the lower stratosphere of the model (below 30 km), where ClNO<sub>3</sub> formation is appreciable. This is also the region where transport is known to play an important role in regulating the distribution of O<sub>3</sub>. Since the description of transport is quite different in 1-D and 2-D models, the effect of nonlinear chemistry on lower stratospheric ozone is different in these models.

The linear response of column ozone to stratospheric chlorine perturbations (Table 13-12, Figure 13-23) calculated by the AER 2-D model at high latitudes during winter and spring may be explained in a qualitative manner by the poleward-downward ozone transport argument put forward by Solomon *et al.* (1985b). The effect of nonlinear local chemistry on lower stratospheric ozone at high latitudes is small relative to the meridional ozone transport effect.

Isaksen and Stordal (1985) tested their two-dimensional model for linearity out to Cl<sub>x</sub> increases of 21 ppbv and for three levels of NO<sub>y</sub>. For the standard NO<sub>y</sub> level, they found the global average ozone reduction to be nearly linear with increasing Cl<sub>x</sub> out to 12 ppbv and then to become significantly nonlinear

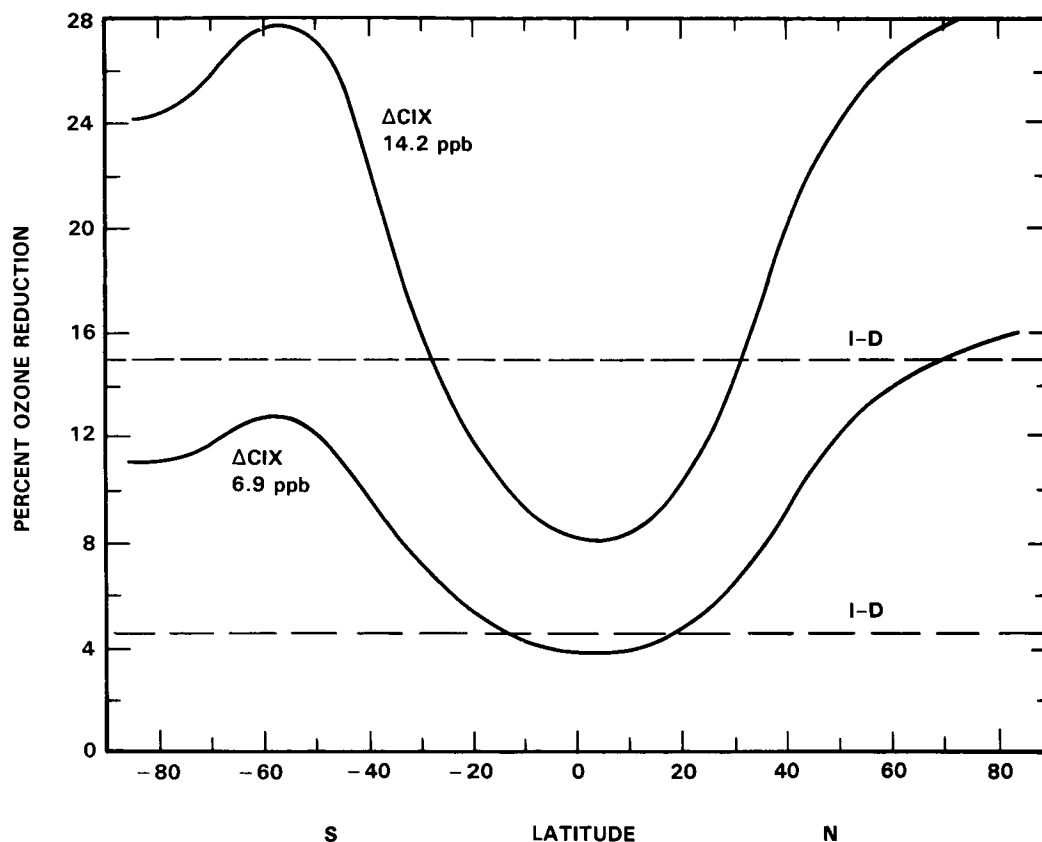


**Figure 13-36.** Comparison of percentage ozone-column reduction as a function of latitude as calculated by AER 2-D model with the values calculated by AER 1-D model for the same perturbation. For one case total  $Cl_x$  is 8.2 ppbv and the other it is 15.5 ppbv, and the reference case is 1.3 ppbv  $Cl_x$ .

by 20 ppbv. Their case of low  $NO_y$  was distinctly more nonlinear than the standard case, and the case of high  $NO_y$  was more nearly linear than the standard case.

In summary, for a given  $Cl_x$  perturbation the global average ozone reduction calculated by these 2-D models is greater than the value calculated by 1-D models, the 2-D models show strong latitude gradients of ozone reduction so that temperate and polar zones show larger ozone reductions than that found by 1-D models, and between 0 and 12 ppbv  $Cl_x$  the calculated ozone reductions as a function of increasing  $Cl_x$  is nearly linear for 2-D models and highly nonlinear for the 1-D models.

## 13.2 DISCUSSION OF CURRENT MODEL PREDICTIONS AND ASSESSMENT OF RECOGNIZED UNCERTAINTIES

### 13.2.1 Uncertainties in Model Predictions

The predictive value of the model results presented above cannot be judged without consideration of their sensitivity to uncertainties in model input data and assumptions. Recognized uncertainties include several factors: a) halocarbon release rate scenarios; b) long term trends in other photochemically active trace gases; c) long term trends in species that affect the climate ; d) the rate coefficients of photochemical

## MODEL PREDICTIONS

processes; e) atmospheric dynamics; and f) trends in solar radiation. It is possible to assess separately and quantitatively some of these uncertainties, while others can only be qualitatively noted and flagged for future concern.

### 13.2.2 History of Model Predictions for Assumed Perturbations

The history of model calculations gives a graphic hindsight picture of uncertainty in photochemical modeling. The calculated effects on ozone by two standard assumed perturbations have been evaluated approximately every year since 1974 by the group at Lawrence Livermore National Laboratory using the then current photochemistry (WMO, 1981, pages 3-26). The one-dimensional model, including vertical eddy diffusion, is calculated to steady-state for these perturbations. The assumed perturbations are: (1) A large fleet of stratospheric aircraft emitting 2000 molecules of nitric oxide per second per cubic centimeter over a one kilometer band centered at 20 kilometers; (2) chlorofluorocarbons 11 and 12 emitted steadily at the 1974 production rates. These perturbations were considered separately; and the photochemical rate coefficients, boundary values, and eddy diffusion function were those recognized at the time of the calculation. Between 1974 and 1981, the steady-state change of the ozone vertical column calculated for each perturbation underwent large excursions as new atmospheric species were found to be important and as values of rate coefficients were remeasured, or in some cases measured for the first time. For example, the calculated effect on the ozone column by the stratospheric aircraft went from  $-10\%$  in 1974 to  $+4\%$  in 1978 to  $-7\%$  in 1981; and the calculated steady-state effect on the ozone column by the CFCs went from  $-14\%$  in 1975 to  $-7\%$  in 1977 to  $-19\%$  in 1979 and to  $-5\%$  in 1981. These excursions were recognized as growing pains in the science of stratospheric modeling.

This study is brought up to date by Figure 13-37. There have been no large changes in these calculations during the last four years. The calculated change in the ozone vertical column by the standard CFC perturbation has changed from  $-5\%$  in 1981 to  $-4\%$  in 1984 to  $-7\%$  in 1985, and that for the standard  $\text{NO}_x$  perturbation has changed from  $-7\%$  in 1981 to  $-12\%$  in 1984 to  $-11\%$  in 1985. However, as can be seen from Section 13.2.3.1 (below), there is still room for future large changes in these perturbation calculations on the basis of recognized uncertainties in photochemical rate coefficients.

Since 1977, the changes in the  $\text{NO}_x$  effect have been strongly negatively correlated with changes in the CFC effect. The varying predictions of Figure 13-37 are not due to changes in rate coefficients in the  $\text{Cl}_x$  or  $\text{NO}_x$  systems, but instead are largely caused by revisions in the rate coefficients in the  $\text{HO}_x$  system (WMO, 1981; Johnston, 1984). Increases in the calculated hydroxyl radical concentration at 25 km are strongly correlated with greater ozone reductions by CFCs and with lesser ozone reductions by  $\text{NO}_x$ . The cause of this effect is that hydroxyl radicals bind catalytically active  $\text{NO}_2$  into the inactive form of nitric acid, but they also release catalytically active chlorine atoms from inactive hydrochloric acid. The sensitivity of these calculations to the calculated concentration of hydroxyl radicals at altitudes between 20 and 30 km emphasizes the need for these radicals to be measured in this range of the atmosphere.

### 13.2.3 Sensitivity to Chemistry and Photochemistry

Two types of uncertainty can arise in connection with photochemical processes. The first type is due to experimental uncertainties in measured photochemical rate coefficients included in the model. The second type concerns chemical species or photochemical reactions that are omitted from the model, either from lack of quantitative data or because no one has thought of them yet. The first class of sensitivity of model calculations to photochemical uncertainties is subject to quantitative analysis using evaluated rate data with assessed uncertainties (DeMore *et al.*, 1983, 1985; Appendix A) and previously developed methods.

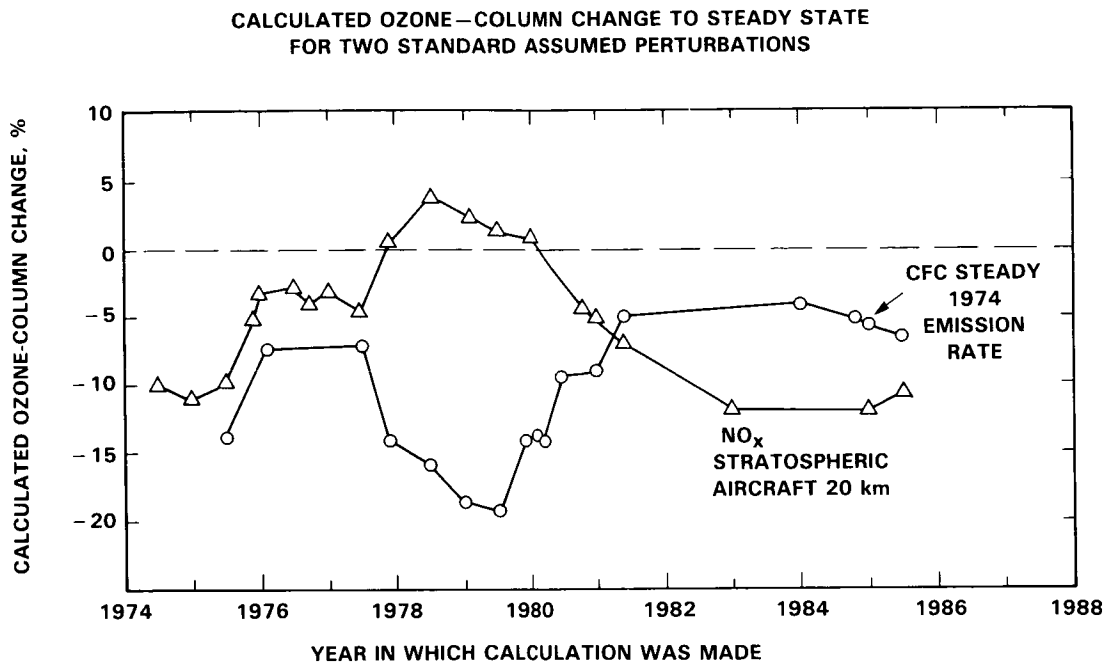


**Figure 13-37.** Calculated ozone-column change to steady state for two standard assumed perturbations: (a) 2000 molecules  $\text{cm}^{-3} \text{s}^{-1}$  of nitric oxide emitted over one kilometer interval centered at 20 km (originally based on a hypothetical, large fleet of stratospheric aircraft); (b) CFC-11 and CFC-12 emitted continuously at 1974 rate. These calculations were made at LLNL over this 11 year period using then current photochemical parameters, eddy diffusion functions, and boundary conditions.

### 13.2.3.1 Ensemble Sensitivity to Uncertainty in Rate Parameters

A method of evaluating the effects of uncertainties in rate parameters was introduced by Stolarski *et al.* (1978) and was used in the NRC 1979 evaluation (NRC, 1979, Appendices A and D). It uses a Monte Carlo simulation where individual rate parameter values for each reaction are chosen at random within an assumed probability distribution, which is based on the assessed uncertainties of the rate coefficients (DeMore *et al.*, 1983, 1985). With enough calculations of this type (typically several hundred to several thousand), the ozone-change probability distribution implied by the joint uncertainty in all the modeled reaction rates can be obtained.

Two separate Monte Carlo uncertainty analyses were performed for this assessment with currently recommended values and evaluated uncertainties for chemical and photochemical rate coefficients (Appendix A).

The first of these studies (Grant *et al.*, 1985) utilized the LLNL 1-D model with fixed concentration boundary conditions and without temperature feedback for the steady-state scenario S3B (15 ppbv  $\text{Cl}_x$  vs a background of 1.3 ppbv  $\text{Cl}_x$ ,  $2 \times \text{CH}_4$ ,  $1.2 \times \text{N}_2\text{O}$ ) as presented in Table 13-2. In performing this study, the maximization of information gained per model run was a major concern. Since the standard error is proportional to the square root of the sample size, it was impractical to reduce the error sufficiently simply by increasing the number of model runs. In order to significantly decrease the number of samples required to achieve the needed level of estimation accuracy, a variance reducing technique known as Latin Hypercube

## MODEL PREDICTIONS

Sampling (LHS), (McKay *et al.*, 1979; Iman *et al.*, 1981; Iman and Shortencarier, 1984) was chosen. A detailed account of the sampling procedure used will be published (Grant *et al.*, 1985).

In the LLNL study, two sets of 50 Monte Carlo runs plus a base line calculation were performed for each of the ambient (no CFC) and perturbed (S3B,  $Cl_x = 15$  ppbv,  $2 \times CH_4$ ,  $1.2 \times N_2O$ ) scenarios. Two pair of runs, each predicting extremely large ozone perturbations (beyond 3.5 standard deviations) were eliminated to avoid unduly influencing the analysis. These two sets of runs also gave  $NO_y$  levels much smaller than indicated by available measurements. The calculated ozone change, its single standard deviation, and the moments of skewness and kurtosis are shown in Table 13-14 for the remaining 98 paired runs. Distribution histograms for the total ozone column perturbations and for ozone perturbations at 20, 30, and 40 km are displayed in Figure 13-38.

As indicated by Figure 13-38 and Table 13-14 the uncertainty for the column total is less than that for individual altitudes, indicative of a tendency for the variations applied to alter the  $O_3$  profile in addition to changing total ozone. The column total and the perturbations for the altitudes of 20 and 30 km display the negative skewness previously observed by Stolarski *et al.* (1978). These estimates also show a more peaked distribution than a normal distribution with the same standard deviation.

For the total ozone column, the calculated single standard deviation range was  $-1.9\%$  to  $-13.5\%$  for the full Monte Carlo calculation with the S3B scenario, and this result compares fairly well with range of  $-4.2\%$  to  $-14.4\%$  calculated for the nine single reaction variation treatment presented in the next section for the same perturbation scenario.

The second Monte Carlo treatment using current reaction rate evaluation inputs was performed by Stolarski and Douglass using the Goddard Space Flight Center one-dimensional model (Rundel *et al.*, 1978) as an update of their previous Monte Carlo studies (NRC, 1979; Stolarski, *et al.*, 1978). These studies have been performed as a function of CFC flux into the model atmosphere and carried to steady-state; the CFC flux is imposed on a 1 ppbv background of  $Cl_x$  from  $CH_3Cl$  and  $CCl_4$  but no  $Cl_x$  from CFC's. The calculation is parameterized in terms of 1985 CFC input flux which was taken to be  $9.2 \times 10^6$   $cm^{-2}$  for CFC-11 and  $1.28 \times 10^7$   $cm^{-2} s^{-1}$  for CFC-12. Boundary conditions for species like  $N_2O$  and  $CH_4$  were set at today's measured values with small uncertainties due to measurement uncertainties.

**Table 13-14.** Statistical Moments for Percent Change in Ozone (Perturbed Chemistry Relative to Ambient) Relative to That for the Unvaried Baseline Case Obtained for 98 Paired Runs (Grant, *et al.*, 1985).

Altitude km	Baseline % Change	Standard Deviation	Moment of Skewness	Moment of Kurtosis
Total Column	-7.7	5.80	-1.58	1.76
20	+3.9	6.28	-1.88	3.24
30	-11.2	9.96	-1.18	0.22
40	-69.1	8.96	0.90	-0.34

MODEL PREDICTIONS

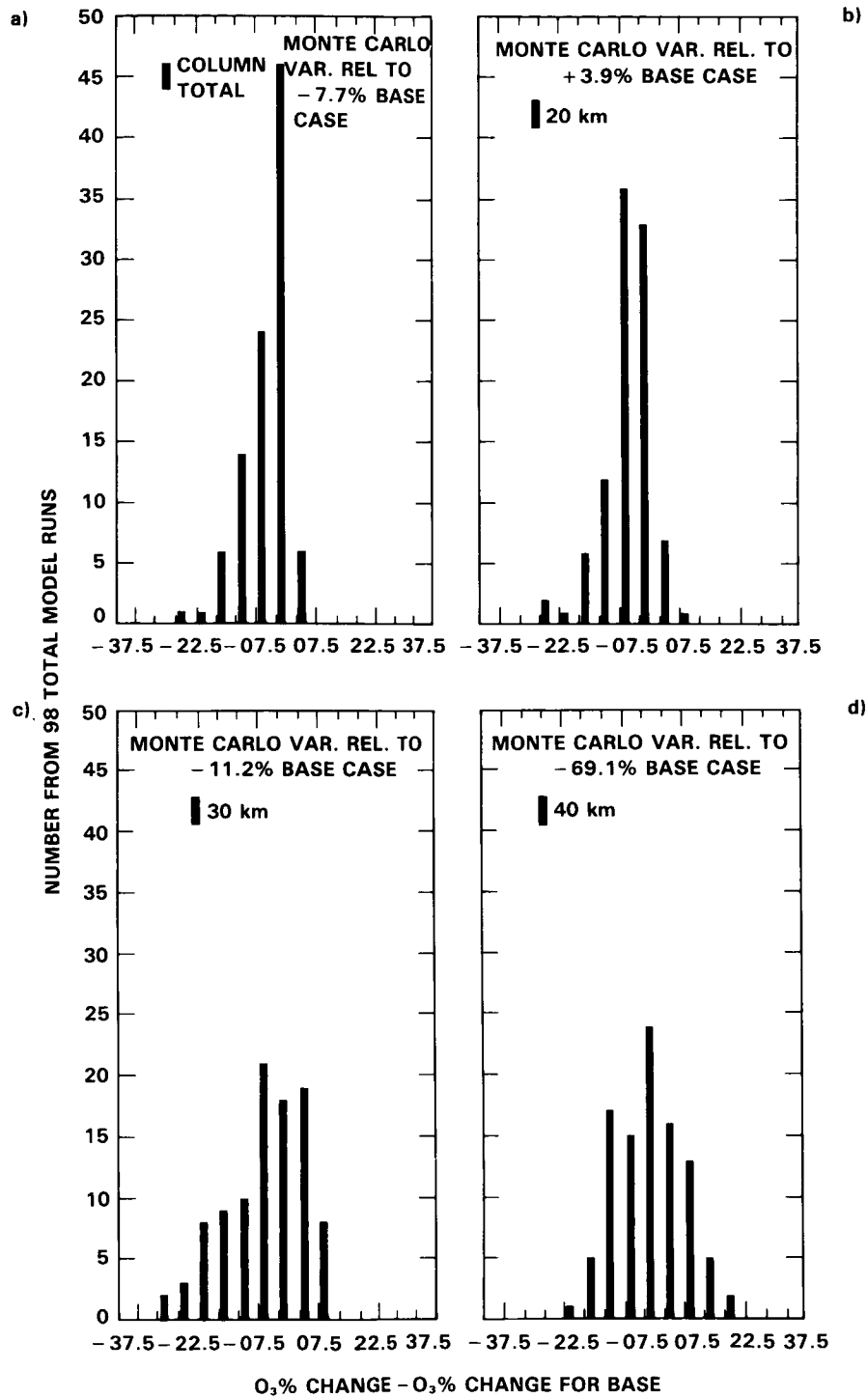


**Figure 13-38.** Monte Carlo calculated ozone changes in LLNL 1-D model. Distribution obtained for percentage change in ozone column (perturbed chemistry relative to ambient) relative to percentage change obtained for unvaried baseline case. (a) Ozone column with baseline case change of  $-7.7\%$ . (b) Ozone at 20 km with baseline case change of  $+3.9\%$ . (c) Ozone at 30 km relative to baseline case change of  $-11.2\%$ . (d) Ozone at 40 km relative to baseline case change of  $-69\%$ . (LLNL model).

## MODEL PREDICTIONS

species necessary to maintain these mixing ratios were then determined, and these fluxes are held constant when a CFC perturbation is imposed on the model. This means that when significant ozone depletions occur in the model, the concentrations of these species will decrease, contrary to the present observed trend.

The results of the Goddard Monte Carlo calculations are displayed in Figure 13-39, the solid line shows the calculated depletion in the ozone column as a function of CFC flux when the recommended values for all input parameters are used in the model. The dashed curve is the mean depletion in the ozone column for 329 cases in which probability distributions were included for all input parameters. These two curves do not coincide, and the differences are statistically significant. Use of recommended values for the cases of steady-state CFC release at the present-day fluxes gives a column ozone change of  $-5.0\%$ , while including the uncertainties, shifts this mean to  $-6.2\%$  with a standard error of the mean of less than  $0.3\%$ . The curves cross for larger CFC fluxes and diverge until at 3.5 times the present CFC flux, the recommended values give  $-40\%$ , and the mean is  $-31\%$  with a standard error of the mean of approximately  $1\%$ . Also shown in Figure 13-39 are the one standard deviation uncertainties about the mean derived from the data for the 329 cases. They are seen to increase as the size of the perturbation increases. For the present-day CFC fluxes, the standard deviation is  $5.5\%$  thus nearly encompassing zero on one side and reaching almost  $-12\%$  on the other. As larger perturbations are considered, the 1 sigma limits do move clearly away from zero but increase significantly in magnitude until at 3.5 times the present-day fluxes  $-31\% \pm 17\%$  is obtained.

All of these statistical parameters must be considered an approximate guide inasmuch as the output probability distributions are asymmetrical. Figure 13-40 shows a series of calculated probability histograms of the depletion of the ozone column for perturbations of 1, 1.5, 2, and 3 times the present-day CFC fluxes as compared to an atmosphere with no CFC's. The distribution for the current CFC fluxes is clearly asymmetrical with a mean of  $-6.2\%$  and a most probable value of between  $-2$  and  $-3\%$ . The median for this distribution increases as the fluorocarbon flux increases, and the distribution spreads toward higher values and becomes more symmetrical.

In a study initiated too late for complete inclusion in this report, Stolarski and Douglass (1985) have found that the uncertainty range of the Monte Carlo calculations can be narrowed from considerations of atmospheric observations. The Monte Carlo calculation seeks out all possible combinations of cases within the range of the assessed uncertainties of the photochemical coefficients, but certain combinations yield calculated species concentrations or distributions that are outside the range of extensive atmospheric measurements. These cases are then excluded from the study. This screening procedure was applied to the concentrations of NO, NO<sub>2</sub>, and ClO at 25 km. Keeping only those cases that fell within the range of measurements of these three species at 25 km resulted in 125 cases, which had a mean ozone depletion calculated for steady-state fluorocarbon emissions at the 1980 rate of  $-3.0\%$  and a standard deviation of  $2.2\%$ . This type of treatment of the ozone-CFC problem has the potential of bringing together and using simultaneously the full body of critically evaluated photochemical data and a large body of atmospheric observations, including satellite data. The method will, however, require careful development, including how to handle observational errors. A serious limitation is that of one-dimensional modeling and the uncertainty concerning what latitude and season of the real world observations are to be compared with the calculations of the model.

### 13.2.3.2 Sensitivity to Uncertainty in Individual Rate Parameters

The Monte Carlo calculations show large changes in model predictions arising from the joint uncertainties of all the rate coefficients. A special study was carried out to try to identify some individual reactions that are especially important sources of these large changes in model predictions. The effect on calculated

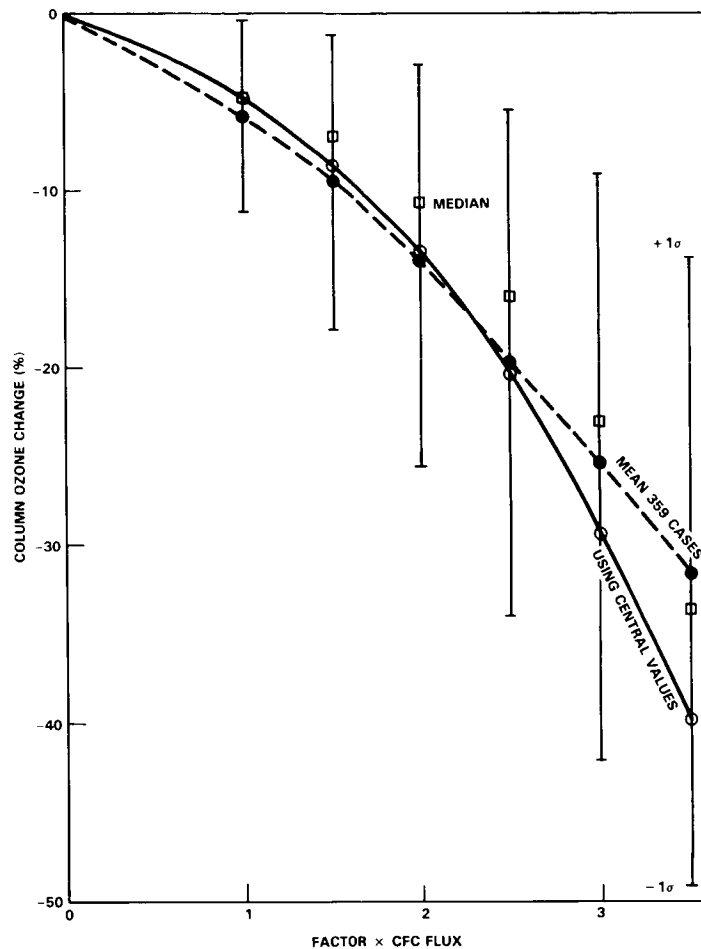


**Figure 13-39.** Monte Carlo calculated ozone-column changes (mean values, dashed line; medians, squares; standard deviation, range bar) for CFC flux factors normalized to 1985 values. The calculated changes based on the recommended rate parameters are shown as the solid line (Stolarski and Douglass model).

ozone depletion induced by varying nine selected photochemical rate coefficients within their ranges of evaluated uncertainties has been assessed.

This assessment of the impact of uncertainty in selected individual rate parameters has been performed for steady-state scenario S3B using the LLNL one-dimensional model without temperature feedback. This baseline scenario, as shown in Table 13-2 predicts a  $-7.8\%$  change in column  $O_3$  relative to a CFC-free atmosphere upon addition of 15 ppbv  $Cl_x$ , a doubling of current  $CH_4$  and a 1.2 factor rise in current  $N_2O$ .

The effect of uncertainties in selected individual rate constants was evaluated by changing individual rate parameter expressions by their one-sigma evaluated levels (DeMore *et al.*, 1985) and recalculating the steady-state ozone change for the transition from a CFC-free atmosphere with current  $CH_4$  and  $N_2O$  levels to a S3B scenario atmosphere.

In analogy with previous studies of this type, sensitivity parameters,  $r_i(\max)$ ,  $r_i(\min)$ , and  $r_i(\text{ave})$  can be defined such that:

## MODEL PREDICTIONS

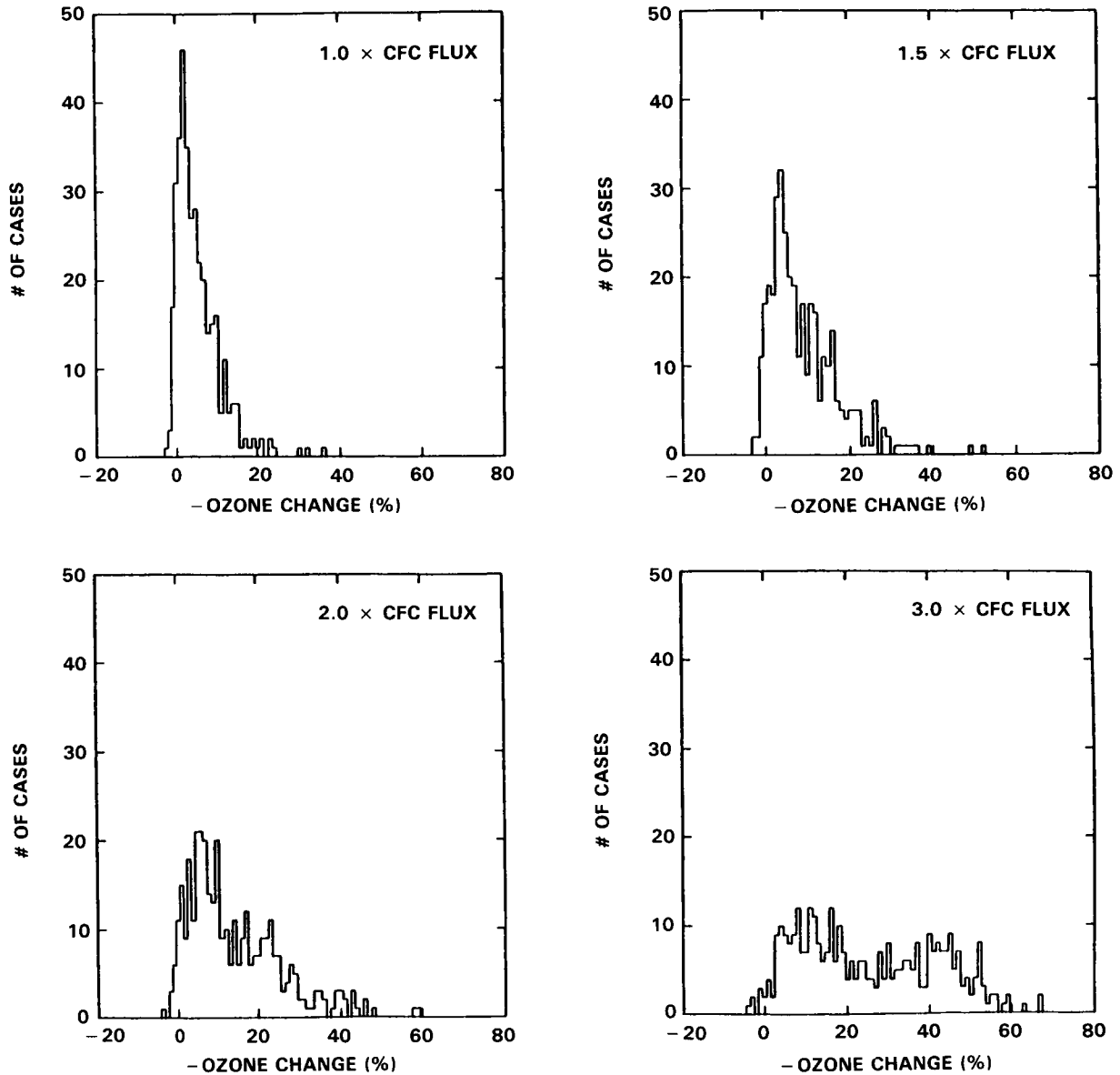


**Figure 13-40.** Monte Carlo calculated ozone-column-change distribution functions for four different CFC fluxes, at 1.0, 1.5, 2.0, and 3.0 times the 1985 CFC flux (Stolarski and Douglass model).

$$r_i(\text{max}) = \frac{R(\text{max}) - R(\text{rec})}{R(\text{rec})} / \frac{k(\text{max}) - k(\text{rec})}{k(\text{rec})}$$

$$r_i(\text{min}) = \frac{R(\text{min}) - R(\text{rec})}{R(\text{rec})} / \frac{k(\text{min}) - k(\text{rec})}{k(\text{rec})}$$

$$r_i(\text{ave}) = [r_i(\text{max}) + r_i(\text{min})]/2$$

where  $k(\text{rec})$  is the evaluation panel's recommended rate parameter,  $k(\text{max})$  is  $[k(\text{rec}) + \text{one sigma}]$  and  $k(\text{min})$  is  $[k(\text{rec}) - \text{one sigma}]$ ,  $R(\text{rec})$  is the calculated ozone change using the recommended rate constant

(-7.8%), R(max) is the ozone change using k(max), and R(min) is the ozone change using k(min). For many reactions, the NASA Evaluation Panel defines a one sigma uncertainty parameter, f, such that k(max) = f k(rec) and k(min) = k(rec)/f. For these cases:

$$\frac{k(\text{max}) - k(\text{rec})}{k(\text{rec})} = (f - 1)$$

$$\frac{k(\text{min}) - k(\text{rec})}{k(\text{rec})} = (1 - f)/f$$

DeMore *et al.* (1983) define:

$$f(T) = f(298) \exp \{(\Delta E/R)[1/T - 1/298]\}$$

where f(298) is the one-sigma correction for the room temperature rate constant and  $\Delta E/R$  is the uncertainty in the temperature dependent part of a bimolecular rate parameter as supplied by the evaluators. The values of f are, therefore, often temperature dependent but were evaluated only at 230 K for this assessment.

A single standard deviation error contribution factor,  $u_i$ , was calculated from

$$u_i = r_i(\text{ave}) \ln(f_i)$$

for each reaction. Nine reactions identified as important in  $\text{Cl}_x$  perturbation studies were selected for assessment. The reactions along with their calculated  $r_i$ ,  $f_i$ , and  $u_i$  factors are displayed in Table 13-15. The sign of the sensitivity factor and the error contribution factor indicates whether increasing the reaction rate parameter causes a larger (+) or smaller (-) decrease in column ozone for the S3B scenario.

The square root of the sum of the squares of the error contribution factors,  $u_i$ , for the nine reactions is written as  $\langle u \rangle$ ; and the one standard deviation cumulative uncertainty is calculated as:

$$U = \exp \langle u \rangle$$

and it has the value of 1.84. Thus, at the one sigma (68%) confidence level, the variation in the calculated -7.8% ozone change for the S3B scenario due to evaluated uncertainties in these nine reactions are within the range  $-7.8\%/1.84$  to  $-7.8\% \times 1.84$ , which is -4.2% to -14.4%.

The NRC 1979 study presented a similar analysis based on a 1978 constant CFC emission scenario for 20 reactions, including several shown in Table 13-15. In general, the  $r_i$  values reported there are similar to or smaller in magnitude than the cases in this table, while the evaluated  $f_i$  factors for overlapping reactions are nearly the same. However, all the  $f_i$  values in the 1979 analysis ignored the uncertainty in the temperature dependence of the assessed rate coefficients, so that the stated  $f_i$  values and the resulting calculated uncertainties were underestimated. As a result, the overall two-sigma uncertainty factor for the NRC (1979) twenty-reaction case was 1.72, slightly smaller than the one-sigma uncertainty value found for the nine-reaction case presented here.

This result should be discussed in context with the Monte Carlo calculation that uses atmospheric observations to screen the distribution of cases. It appears that within the range of uncertainty of the photochemical parameters, the models would predict unrealistic values for the concentrations or profiles of some measured species in the contemporary atmosphere. At present there is no systematic way to use

## MODEL PREDICTIONS

atmospheric observations to screen this method of sensitivity to uncertainty in individual rate parameters, unlike the situation with the Monte Carlo method. Unless an appropriate screening method can be developed for this method, future research on uncertainty analysis should probably be concentrated on the Monte Carlo method.

### 13.2.3.3 Uncertainties Due to Chemistry Omitted From the Models

As discussed in Chapter 2, several classes of reactions have been proposed which have the potential to significantly affect the impact of  $\text{Cl}_x$  and  $\text{NO}_x$  on stratospheric chemistry. However, current deficiencies

Table 13-15. Single Rate Constant Variation Studies.

No.	Reaction	Sensitivity Factors			Experimental Uncertainty Factor	Error Contribution Factor
		$r_i(\text{max})$	$r_i(\text{min})$	$r_i(\text{ave})$	$f_i$	$u_i$
1.	$\text{ClO} + \text{O} = \text{Cl} + \text{O}_2$	+0.60	+0.68	+0.64	1.43	+0.23
2.	$\text{Cl} + \text{CH}_4 = \text{HCl} + \text{CH}_3$	-0.48	-0.46	-0.47	1.16	-0.07
3.	$\text{OH} + \text{HCl} = \text{Cl} + \text{H}_2\text{O}$	+0.56	+0.79	+0.68	1.32	+0.19
4.	$\text{OH} + \text{HNO}_3 = \text{H}_2\text{O} + \text{NO}_3$	-0.51	-0.56	-0.53	1.30	-0.14
5.	$\text{OH} + \text{HNO}_4 = \text{H}_2\text{O} + \text{O}_2 + \text{NO}_2$	-0.16	-0.33	-0.25	2.20(a)	-0.20
6.	$\text{O}(^1\text{D}) + \text{M} = \text{O}(^3\text{P}) + \text{M}$	+0.60	+0.63	+0.62	1.32	+0.17
7.	$\text{O}(^1\text{D}) + \text{N}_2\text{O} = 2 \text{NO}$ $= \text{N}_2 + \text{O}_2$	-0.51	-2.00	-1.26	1.30(b)	-0.33
8.	$\text{ClO} + \text{NO}_2 + \text{M} = \text{ClONO}_2 + \text{M}$	-0.31	-0.37	-0.34	1.56(c)	-0.15
9.	$\text{O}_2 + h\nu (\text{S-R}) = 2.0$	-0.58	-0.85	-0.72	1.40(d)	-0.24

(a) Since the quoted uncertainty in the activation energy for this reaction is unsymmetrical ( $\Delta E/R = +270$  and  $-500$ ) the  $r_i$  was calculated for a  $k(\text{max})$  of  $1.96k(\text{rec})$  and a  $k(\text{min})$  of  $k(\text{rec})/2.46$ ; the  $f_i$  value used in the calculation of  $u_i$  is the square root of  $1.96 \times 2.46$ .

(b) The stated uncertainty of 1.30 is taken to be uncertainty in the branching ratio to 2 NO, not in the overall rate, which was held unchanged.

(c) The one-sigma variation on the rate was calculated for  $M = 3.69 \times 10^{17} \text{ cm}^{-3}$  and  $T = 230\text{K}$ , taken to be characteristic of 30 km altitude conditions. The uncertainty in both  $k_0$  and  $k_\infty$  was accounted for according to the intermediate regime equation recommended by DeMore et al., 1983. This analysis yielded a  $k(\text{max}) = 1.54k(\text{rec})$  and a  $k(\text{min}) = k(\text{rec})/1.59$ , and the  $f_i$  value of 1.56 is the square root of  $1.54 \times 1.59$ .

(d) The factor of 1.40 was applied to the effective photoabsorption cross section and thus affects both the atmospheric transmissivity as well as the oxygen photodissociation rate.

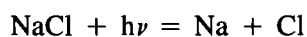
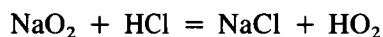
in either detailed laboratory verification of the proposed kinetic mechanisms and rate parameters or *in situ* measurements to establish sufficient levels of proposed stratospheric species prevent a solid case for their inclusion at this time. Of course, these same deficiencies also currently prevent a quantitative assessment of the uncertainty these unrepresented reaction classes pose.

Two reaction classes of potential, but as yet unproven, importance bear special notice. These are upper stratospheric reactions of meteor deposited sodium compounds and lower stratospheric heterogeneous reactions of reservoir species.

### Sodium Chemistry

Stratospheric sodium chemistry poses a striking picture with basic sodium compounds formed in the mesosphere from meteor ablated atomic sodium meeting acid compounds formed from  $\text{Cl}_x$ ,  $\text{NO}_x$ , and  $\text{CO}_2$  in the lower stratosphere to form salt and water in the upper stratosphere (Murad *et al.*, 1981). Model results predict that downward diffusing molecular sodium will be found in the form of  $\text{NaOH}$ ,  $\text{NaO}_2$ , and/or  $\text{NaO}$  (Liu and Reid, 1979; Sze *et al.*, 1982). Each of these gas phase compounds react at a gas kinetic rate with  $\text{HCl}$  and probably quite rapidly with other acid gases such as  $\text{HNO}_3$  (Silver *et al.*, 1984a; Silver and Kolb, 1985). If  $\text{NaCl}$  is formed by reaction with  $\text{HCl}$  during the day, it is quickly destroyed by photodissociation releasing atomic  $\text{Cl}$  (Rowland and Rogers, 1982).

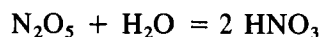
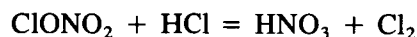
The rate of condensation of the mesospheric and upper stratospheric gaseous sodium compounds is unknown, and therefore their concentration is difficult to model; furthermore, no attempt has yet been made to measure them. However, if as little as one percent of the downward diffusing sodium reaches the 40 km level in molecular form, a significant amount of atomic chlorine could be liberated from  $\text{HCl}$  through catalytic reactions such as (Silver and Kolb, 1985):



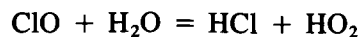
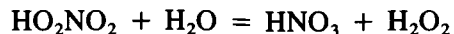
### Heterogeneous Reactions of Reservoir Species

The mid and lower stratosphere contain a persistent but highly variable layer of sulfuric acid aerosols. These aerosols are generally assumed to be composed primarily of supercooled liquid sulfuric acid and water in an approximately 75%  $\text{H}_2\text{SO}_4$ /25%  $\text{H}_2\text{O}$  weight ratio but they also contain significant impurities such as  $\text{Cl}^-$ ,  $\text{Br}^-$ , and  $\text{NH}_4^+$  (Cadle and Grams, 1975).

Model calculations have indicated that reactions which form or liberate  $\text{NO}_x$  and  $\text{Cl}_x$  from their reservoir species:  $\text{HNO}_3$ ,  $\text{HO}_2\text{NO}_2$ ,  $\text{ClONO}_2$ ,  $\text{HCl}$ , and  $\text{HOCl}$  can play a key role in  $\text{Cl}_x$  and  $\text{NO}_x$  stratospheric processes. A number of such reactions including:



## MODEL PREDICTIONS



have been demonstrated to be very slow in the gas phase but quite rapid on the surfaces of laboratory apparatuses. As discussed in Chapter 2, it is quite conceivable that such reactions may proceed at a significant rate as heterogeneous processes on stratospheric sulfuric acid aerosols. Definitive heterogeneous kinetic experiments are clearly needed to allow further assessment of their heterogeneous reservoir reactions.

### 13.2.4 Uncertainty of Model Predictions to Choice of Boundary Conditions

For some species, especially nitrous oxide and methane, there is uncertainty as to whether to use constant concentration or constant flux boundary conditions in model calculations. To illustrate this point, the AER one-dimensional model was used to calculate the steady-state ozone reduction as a function of stratospheric  $\text{Cl}_x$  as the only perturbation; but one calculation was made assuming constant surface concentration of nitrous oxide as boundary condition and the other assuming constant surface flux (Figure 13-42). For small amounts of added  $\text{Cl}_x$ , the two different boundary conditions give essentially the same calculated ozone reductions, but for large  $\text{Cl}_x$  perturbations there is a substantial difference in the two calculated ozone reductions.

The reason for this difference can be illustrated by a simple mechanism, using A to represent nitrous oxide as the example:

Gross release from the surface, rate = P

Gross removal by the surface, rate =  $k[A]$

Stratospheric destruction = flux rate  $F = f[A]$

where  $f$  is a complicated function depending on the structure of the atmosphere between the surface and the upper stratosphere and the chemical and radiation field in the stratosphere. At steady state

$$P = k[A] + f[A], [A] = P / (k + f), \text{ and } F = P - k[A].$$

There are two limiting cases

(i)  $f \ll k$ , then  $[A] = P/k$ , an equilibrium constant, and the constant-concentration boundary condition is appropriate. If the stratospheric destruction coefficient  $f$  changes, the flux  $F$  changes, but the surface concentration remains constant.

(ii)  $f \gg k$ , then  $[A] = P/f$  is inversely proportional to  $f$ ,  $F = P =$  constant gross surface production rate, so that the constant flux boundary condition is appropriate. If the stratospheric destruction coefficient changes, the surface concentration changes but the flux remains constant.

For both nitrous oxide and methane, the production and destruction at the earth's surface (soils and waters) are complex, incompletely solved biological, geological, chemical problems. In the absence of good knowledge of the rates of surface sources and sinks, it is not obvious which type boundary conditions is better, some modelers use one and some use the other, and for large chlorine perturbations it makes a difference (for example, Figure 13-41).

### 13.2.5 Sensitivity to Trends of Trace Gas Species

Model calculations of the ozone distributions in future perturbed atmospheres are strongly dependent on the assumed rate of growth of trace gas species (for example, Figure 13-17; all cases in Sections 13.1 and 13.2 with mixed scenarios). Source strengths for several species (e.g. CFCs) are determined by technology and world-wide industrial growth. Emissions for others (e.g.  $N_2O$ ,  $CH_4$ ,  $CO_2$ ,  $CO$ ,  $NO_x$ ) are a mixture of industrial, agricultural, and natural processes (see Chapter 3). The resulting atmospheric concentrations depend on the rate of photochemical destruction within the atmosphere, on dynamical redistribution of the tracer (stratospheric-tropospheric exchange), and on surface losses. Major perturbations to stratospheric ozone are calculated to have a direct impact on the lifetimes of  $N_2O$ , CFC-11, CFC-12, and  $CCl_4$  (see, for example Table 13-9). These effects are based on the redistribution of stratospheric ozone and the ultraviolet radiation field, and they can be predicted with some confidence by 2-D, and probably even, 1-D models. The sources of some of these trace species involve the biosphere, soils, and the oceans; and thus the uncertainties of the biosphere, soils, and the oceans are part of the uncertainty of atmospheric models.

### 13.2.6 Ozone Changes Calculated to Occur in the Troposphere

Some models show calculated ozone changes in the troposphere, for example, Figures 13-1, 2, 3, 18, 19, 20. These portions of the calculated ozone-column change must be regarded as being especially uncertain. Present models are primarily designed for stratospheric simulations. Large uncertainties exist in connection with lack of knowledge of tropospheric  $NO_x$  distributions, heterogeneous processes, and non-methane hydrocarbons. Chapter 4 discusses tropospheric processes.

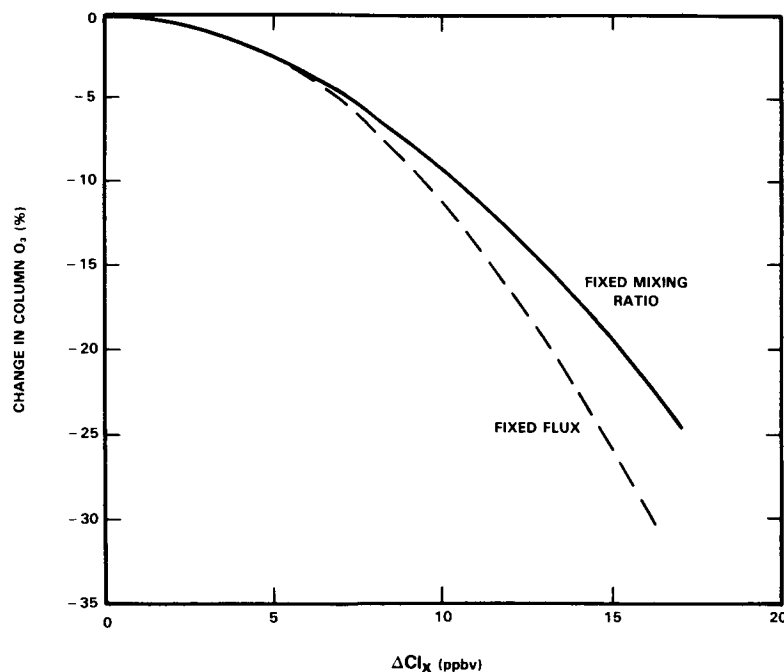


**Figure 13-41.** Comparison of use of fixed flux boundary condition and fixed surface concentration boundary condition for nitrous oxide in CFC perturbation calculations. Calculated ozone-column changes as a function of stratospheric  $Cl_x$  level with AER 1-D model.

## MODEL PREDICTIONS

### 13.2.7 Some Dynamical Uncertainties in Assessment Calculations

Ozone is jointly controlled by dynamics and photochemistry throughout the stratosphere. At high altitudes during daylight hours, photochemistry is fast, but the distribution of photochemically active trace species depend on longer-lived source molecules which are strongly influenced by atmospheric dynamics. At low altitudes in the stratosphere, dynamics moves and mixes ozone faster than it is formed from oxygen photolysis (Figure 13-25), but slow photochemical reactions operating over long ozone residence times significantly increase or decrease local ozone concentrations. This subsection discusses some recognized uncertainties and some recent insights in model treatment of atmospheric motions. (Fuller, more general discussions of these problems are given in Chapter 12).

In one-dimensional models, all transport is represented as vertical in direction and diffusive in nature, since transport is accomplished by an eddy diffusion coefficient function. In typical one-dimensional model studies, Northern Hemisphere mid-latitude tracer data have been used to parametrize empirically the eddy diffusion function to obtain agreement with observations of these species. Recently, a new suggestion has been put forward concerning eddy diffusion functions (Holton, 1985; Mahlman, 1985): a different eddy diffusion coefficient should be used for each species, depending on transport time scales (obtained from considerations of higher dimensional models) and the variation of its lifetime with height and latitude. This procedure is likely to affect perturbation calculations, since increasing chlorofluorocarbon abundances yield changes in photochemical lifetimes, and therefore associated changes in the lifetime-dependent eddy diffusion coefficients used in one-dimensional models. A detailed study of the possible importance of this procedure in one-dimensional perturbation calculations has not yet been performed.

To evaluate seasonal and latitudinal variations in the local ozone response, at least a two-dimensional (height-latitude) representation is required. In recent years a new insight has developed concerning the importance of using two-dimensional models for CFC perturbation calculations: if advection is sufficiently rapid, much larger ozone reductions are calculated at certain seasons for polar and temperate zones than the global average or for corresponding one-dimensional models (Pyle, 1980; Haigh and Pyle, 1982; Haigh, 1984; Garcia and Solomon, 1983; Solomon *et al.* 1985b). The discussion of this effect in terms of Garcia and Solomon's model is as follows. All current one- and two dimensional models calculate large ozone reductions by GFCs in the upper stratosphere near 40 km (Sections 13.1.2 and 13.1.3). The tropical lower stratosphere is characterized primarily by upward motion in the seasonal mean sense, so that the large ozone depletions occurring at 40 km are not transported downward to lower altitudes at those latitudes. At high latitudes, particularly in winter, the direction of net transport is downward in the zonal, seasonal average. The chemical lifetime of ozone in the middle and lower stratosphere at high latitudes is long in the winter because of the solar zenith angle and small fraction of sunlit hours in a day. Transport into the middle and high latitude lower stratosphere is dominated by vertical advection, bringing down strongly depleted ozone from the 35 to 40 km heights into lower altitudes. Large ozone depletions occur at high latitudes throughout the stratosphere relative to that found in the tropics. However, the ozone abundance at high latitudes in winter is influenced not only by vertical advection but also by horizontal mixing associated with breaking planetary waves (McIntyre and Palamer, 1983; Leovy *et al.*, 1985). An important topic for future research is to study the competition between these two different transport processes.

Different two-dimensional models, as discussed extensively in Chapter 12, use different treatments for advective transport and horizontal mixing. In this study there are representatives for each of two different approaches, one represented by the diabatic and residual Eulerian models of AER and GS, and the other by the classical Eulerian model of MPIC. The two types of model differ substantially in their prediction of  $\text{NO}_y$  in the lower stratosphere. Figure 13-31, but even so they give comparable predictions of global

ozone reduction. Tables 13-10 and 13-11. Both types of model show greater ozone-column reductions in polar regions than in tropical regions; but in general, the AER and GS models give a greater range to seasonal and latitudinal ozone changes than the MPIC model, as illustrated by Figure 13-24. These differences are important in terms of considerations of ozone depletions by CFCs, and the nature of two-dimensional atmosphere dynamics should be vigorously pursued.

Most of the ozone at middle and high latitudes lies below 20 km where it is likely to be subject to mixing and dispersion associated with stratosphere-troposphere exchange processes (Allam and Tuck, 1984b; Chapter 5). These processes are crudely parametrized in two-dimensional models. A great deal of further research into the transport processes occurring in the lowest part of the stratosphere and upper troposphere is needed to improve estimates of ozone column changes.

Comparison between the ozone changes calculated by the two-dimensional classical and residual Eulerian models and consideration of the important effects of changes occurring in the region below 20 km is determining the behavior of the ozone column at extra-tropical latitudes suggest that dynamical uncertainties associated with current two-dimensional models correspond to a factor of at least two in the uncertainty in the evaluation of the ozone column change.

### 13.2.8 A Recently Published Article

Farman *et al.* (1985) published an article entitled "Large losses of total ozone in Antarctica reveal seasonal  $\text{ClO}_x/\text{NO}_x$  interactions" in which they report seasonally variable 5 to 30% reduction of the south polar ozone column during 1980-84 relative to 1957-73. Current two-dimensional models (Figures 13-29 and 13-30) give 15 to 25% reduction of local ozone at 40 km at the poles, and the MPIC model shows between 2 and 3% reduction of the ozone column there. The results reported in the article give much larger ozone reductions in Antarctica than those given by the models. The article has not yet been assimilated by the modeling community, and it is premature for this report to do more than to note it with great interest and to recommend that it be given close attention in the near future.

### 13.2.9 Discussion of Total Uncertainty

When one looks at (i) the wide spread of model calculations of the ozone column change for the same assumed perturbations over the last ten years (Figure 13-37), (ii) the range of ozone column changes calculated by different one-dimensional models in 1985 for the same scenario (Table 13-2), and (iii) the large uncertainty implied by a study of the variation of individual rate coefficients over their assessed uncertainty range (Section 13.2.3.2; NRC, 1979), one gets the impression that the total uncertainty is very large and that the solution to this problem is still far away. This impression is probably correct, but a recent development indicates that the effect of the assessed uncertainty on photochemical coefficients is not as large as (iii) indicates. The Monte Carlo treatment of one-dimensional models, when it covers the range of assessed uncertainty in photochemical parameters and is screened by atmospheric observations of many species and at several altitudes (Stolarski and Douglass, 1985; Section 13.2.3.1), promises to be a powerful method of calculating the effect of chlorofluorocarbons on the ozone column for any given scenario for future changes of chlorofluorocarbons and other gases. After this method is carefully developed, it may be hoped that the uncertainty in calculating ozone changes due to the assessed uncertainty of rate coefficients will be no more than a factor of two.

Two-dimensional models supply information about seasonal and latitudinal ozone changes. This study used two-dimensional models representative of two substantially different treatments of atmospheric dy-

## MODEL PREDICTIONS

namics. For a given perturbation scenario, these two models gave satisfactory agreement concerning global-average ozone reduction (Table 13-8), but they give different latitude trends (Figure 13-24). Both models indicate that there is greater ozone reduction at temperate and polar latitudes than at tropical latitudes, but one model gives almost a factor of two greater ozone reduction at temperate zones during certain seasons than the other. It is estimated here (Section 13.2.7) that uncertainty in how to formulate atmospheric dynamics in the models contributes about a factor of two to the uncertainty of model predictions. This uncertainty factor is based on the judgment of experts in the field, and it is not a statistically derived number.

In terms of (i) the assessed uncertainties in photochemical parameters as reduced by constraints introduced by atmospheric observations and (ii) the recognized uncertainties in atmospheric dynamics, there may be as little as a factor of four uncertainty in model predictions of ozone changes, given a prescribed scenario for future changes of CFCs and other trace gases ( $\text{CH}_4$ ,  $\text{N}_2\text{O}$ ,  $\text{CO}_2$ , stratospheric  $\text{NO}_x$ , tropospheric  $\text{NO}_x$ ). In view of this range of recognized uncertainty, one should not be unduly surprised if a  $-7\%$  ozone change calculated in 1985 should be found to be  $-4\%$  or  $-12\%$  when calculated in 1988, for example.

The uncertainties due to unknown factors, such as unrecognized chemical species or unknown photochemical reaction rates, cannot be quantified.

Even if numerically accurate models were complete in photochemistry and satisfactorily approximated those aspects of atmospheric motions and other physical processes that strongly affect ozone, the models still could not predict future ozone changes due to increasing chlorofluorocarbons unless they were supplied with the future trends of other trace species. As the models continue to improve and as the body of field measurements continue to expand, the inability to predict future trends of the trace species may become the major source of uncertainty.

### 13.3 SUMMARY AND CONCLUSIONS

The calculations presented in this chapter were carried out by means of three two-dimensional and six one-dimensional models using prescribed scenarios for natural and anthropogenic perturbations (Tables 13-1, 7), prescribed values of insolation (Chapter 6), and a prescribed up-to-date set of chemical and photochemical parameters (Appendix A). Differences among results therefore reflect differences in the assumptions and methods of the models themselves (boundary values, eddy diffusion functions, diurnal averaging, numerical methods). The results are presented in terms of scenarios, which were selected to demonstrate the role of certain individual species and to illustrate possible future situations. The principal results of these model calculations of ozone changes are:

(i). The long-term release of chlorofluorocarbons at the 1980 rate would reduce the ozone vertical column by about 5% to 8% according to one-dimensional models (Scenario S1A of Table 13-2, relative to 1.3 ppbv  $\text{Cl}_x$  as background) and by a global average of about 9% according to two-dimensional models (Table 13-8), which involves a reduction of about 4% in the tropics, about 9% in temperate zones, and about 14% in polar regions (Figures 13-24, 33, 34). A major finding of recent years, which is emphasized in this report, is that two-dimensional models predict large seasonal and latitudinal variations in chlorine-induced ozone-column reductions, so that there are larger ozone reductions at some seasons in temperate and polar zones than that for the global average or that for one-dimensional models.

(ii). All models with all scenarios predict that this level of stratospheric chlorine (steady state produced by 1980 CFC flux) will reduce local ozone at 40 kilometers by a large amount, 60 to 80% (Table 13-3; Figures 13-18 - 21).

## MODEL PREDICTIONS

(iii). At about 80% of the present level of CFC release, coupled with doubling methane and increasing nitrous oxide by the factor of 1.2, one-dimensional models give ozone decreases of about 3% (Table 13-2, Scenario S2B), and a two-dimensional model gives an ozone decrease of about 4% (Table 13-8). If doubled carbon dioxide is added to the list of changes by other trace species, one-dimensional models predict ozone-column changes between +0.1 and -3.5% (Scenario S2C of Table 13-2). One-dimensional models predict that the magnitude and even the sign of the ozone-column changes due to increasing CFCs depend on the future trends of carbon dioxide, methane, and nitrous oxide.

(iv). If the release rate of CFCs should become twice the present level or if stratospheric  $\text{Cl}_x$  reaches 15 ppbv, the one-dimensional models predict that there will be 3% to 12% reduction of the ozone column, regardless of realistically expected increases in carbon dioxide, nitrous oxide, and methane (Table 13-2, Scenario S3C).

(v). The two-dimensional models calculate that between 1960 and 1985 there were large (about 20%) local percentage ozone reductions at 40 km in the polar stratosphere (Figures 13-29, 30). These calculations did not include the effects of increasing methane and carbon dioxide, which would tend to decrease the calculated ozone reduction.

(vi). For atmospheric perturbations considered one at a time, the one-dimensional models calculate the ozone steady-state vertical column to be increased by carbon monoxide, carbon dioxide, and methane; and they calculate it to be decreased by chlorofluorocarbons, nitrous oxide, and stratospheric aircraft (Table 13-4, Figures 13-7 to 12). These individual perturbations do not have an additive effect on ozone.

(vii). For *some* scenarios one-dimensional models predict an ozone reduction in the upper stratosphere and an ozone increase in the lower stratosphere or troposphere, to give an ozone column increase. Two-dimensional model results (Figures 13-18, 19, 20, 21) suggest that these particular one-dimensional results be interpreted as an ozone-column increase in tropical regions and an ozone-column decrease at temperate and polar regions; and even if there is a global average ozone increase, there might be significant ozone column decreases in the temperate zone.

(viii). Time-dependent scenarios were considered using one-dimensional models with CFC growth rates assumed to be 0%, 1.5%, and 3% per year. For a coupled scenario with increasing methane, carbon dioxide and nitrous oxide, the ozone column effects are relatively small for CFC increases at 0% and 1.5% (Figure 13-17, Scenarios T1B and T2B). At 3% CFC growth and the coupled scenario (Figure 13-17, Scenario T3B) the calculated ozone column decrease is 10% after 70 years and still rapidly decreasing.

(ix). Over the range 1 to 15 ppbv of stratospheric chlorine, one-dimensional models are strongly nonlinear in terms of ozone-column change as a function of added  $\text{Cl}_x$  (Figures 13-6, 41; Tables 13-10, 11), but the two-dimensional models are nearly linear (Tables 13-10, 11) over this range of added  $\text{Cl}_x$ . If  $\text{Cl}_x$  increases up to 21 ppbv are considered (see note at end of Section 13.1.4), a two-dimensional model shows the same pattern of nonlinearity as the one-dimensional models. The onset of the nonlinearity occurs close to the region where the  $\text{Cl}_x$  mixing ratio exceeds the background  $\text{NO}_y$  mixing ratio.

(x). The changes in model predictions during the last four years have been less than the record of the previous six years (Figure 13-37). Even so, there remain substantial recognized uncertainties in the field of stratospheric photochemical model predictions. Two investigators carried out Monte Carlo calculations over the full range of the assessed uncertainties (Appendix A) of photochemical parameters. In

## MODEL PREDICTIONS

one calculation, the ozone-column changes were calculated for an increase of 14 ppbv  $\text{Cl}_x$ , a doubling of methane, and a 20% increase of nitrous oxide. Within plus or minus one standard deviation of the unsymmetrical distribution of calculated ozone-column changes, the range was -1.9% to -13.5%, where the standard result was -7.7% (Table 13-14). The second Monte Carlo calculation considered only CFC perturbations, and varied the 1980 CFC flux by factors between 1 and 3.5 (Figure 13-40). Use of the recommended photochemical parameters with the current (1985) CFC release rate gave the calculated steady-state ozone-column change of -4.8%, and the Monte Carlo calculation over the full range of the assessed uncertainties of the photochemical parameters gave the average ozone-column changes of -5.7% and the (one standard deviation) range of -0.3% to -11.1%. A recent development by Stolarski and Douglass (1985) is that considering the atmospheric observations of many species and at several altitudes excludes many of the Monte Carlo cases. When this screening is carried out, the central value of calculated ozone change is the value most nearly consistent with atmospheric observations and the standard deviation of the calculated ozone changes is substantially reduced.

(xi). The past and future changes of the trace species, methane, nitrous oxide, and carbon dioxide, involve the biosphere and its great complexity. As stratospheric modeling matures during the next few years, the biggest uncertainty in making future predictions will probably be the uncertainty in formulating the scenarios for future changes in methane, nitrous oxide, and carbon dioxide.

### 13.3.1 Future Research

Regarding future research in model predictions, it is particularly important to encourage the development of two-dimensional models. Two-dimensional models have progressed to the point where they include sophisticated photochemistry, and further development requires continued deep study of atmospheric transport and dynamics. Two-dimensional models importantly give large latitudinal gradients in calculated ozone-column reductions, such that much larger ozone-column reductions are indicated in temperate and polar regions than the global average or the result of one-dimensional models.

One-dimensional models still play a vital role in rapidly surveying a wide range of scenarios, and in providing first approximations to many problems and to new ideas. The new Monte Carlo method that screens the results against atmospheric observations should be given top priority; it probably should become the standard tool for one-dimensional ozone-change assessment studies. As this method is developed and refined, it should be extended to two-dimensional models.

The value of both one-dimensional and two-dimensional models depends on the quality of the input photochemical and atmospheric data. Sensitivity studies carried out here show that model predictions are still strongly changed within the recognized uncertainty limits of the photochemical data and field measurements. To reduce this element of uncertainty, there should be continued support for research in photochemistry and in atmospheric measurement of trace species.